journal of the international meteor organization

WGN

49:4
august 2021

2021 Aurigid outburst analysis
Meteor shower and cluster catalog from SonotaCo
Orbital and physical properties of the Eta Virginids
Global network initiative for radio meteor observers

ISSN 1016-3115

WGN Vol. 49, No. 4, August 2021, pp. 73 – 112

Administrative

Ongoing Meteor Work

Radio Meteors

Front cover photo

Bright fireball captured on 2021 August 7 at $23^{h}20^{m}$ CEST ($21^{h}20^{m}$ UT) from Hohenhorn, Germany. For more information on this event visit: `https://fireballs.imo.net/members/imo_view/event/2021/4397`. Photo courtesy: Olaf Toepper.

Writing for WGN

This Journal welcomes papers submitted for publication. All papers are reviewed for scientific content, and edited for English and style. Instructions for authors can be found in WGN **45:1**, 1–5, and at `http://www.imo.net/docs/writingforwgn.pdf` .

Legal address

International Meteor Organization, Jozef Mattheessensstraat 60, 2540 Hove, Belgium.

Letter — Aurigid outburst on 2021 August 31

Jürgen Rendtel[1] *and Ralf Koschack*[2]

1 Introduction

Activity of the Aurigid meteor shower was first observed in 1935 (for a summary of the history see the IMO's Meteor Shower Workbook). The average shower maximum at $\lambda_\odot = 158\overset{\circ}{.}6$ (August 31 – September 1) is in a period which usually is little covered by observations. From the period 1935 – 1986, no reports of significant activity are known. In 1994 enhanced rates have been noted and in 2007 an outburst was predicted which occurred exactly at the calculated position (Rendtel, 2007). A slightly enhanced rate observed in 2019 gave rise to a detailed look at the assumed stream and possible encounters (Rendtel et al., 2020). For the 2021 IMO Meteor Shower Calendar, there were three model predictions available:

Sato: $\lambda_\odot = 158\overset{\circ}{.}383$, 2021 August 31, $21^\mathrm{h}17^\mathrm{m}$ UT,
Lyytinen: $\lambda_\odot = 158\overset{\circ}{.}395$, 2021 August 31, $21^\mathrm{h}35^\mathrm{m}$ UT,
Vaubaillon: $\lambda_\odot = 158\overset{\circ}{.}396$, 2021 August 31, $21^\mathrm{h}35^\mathrm{m}$ UT.

2 Observations

The Aurigid radiant at $\alpha = 91°$, $\delta = +39°$ is far north, but is quite low in the sky until about 01^h local time. At mid-northern latitudes (50° N), the radiant is only about 10° above the horizon at 22^h local time. So the most favourable region to observe the event extends from Asia westwards into the northeastern part of Europe. The morning hours were lit by a waning Moon (two days after last quarter) placed in northeastern Taurus not too far from the radiant. Both a reduced limiting magnitude and low radiant elevation will reduce the number of visible Aurigids. In fact, we received reports from many observers across Europe. This means that we have to deal with data collected at low radiant elevation. This implies that we have grazing meteors with peculiar appearance: apart from meteors close to the radiant, Aurigids appeared rather "slow" with often long trails if close to the horizon or very fast at higher elevation (especially near zenith). A radiant elevation of 6° (which was typical for central European locations around 20^h UT) has a geometrical zenith correction factor of 10, i.e. only a tenth of the meteors becomes visible and the error margins are very large. Around the peak time, the radiant is still below or near 15° in the northeastern sky. Nevertheless, our search for a short lived peak requires short count intervals. Consequently, individual count intervals may easily contain zero Aurigids, but are valuable samples. Like in 2007, the magnitude distribution of the 2021 Aurigids were different from the average Aurigid shower – outbursts are composed of larger meteoroids.

For our analysis we have observation reports from 36 observers worldwide (the list can be seen on the IMO's VMDB Meteor Shower Visual Campaigns page). The total sample for the peak night contains just 129 Aurigids, of which about 90 were recorded close to the peak. Some observers provided us with data for shorter intervals than stored in the VMDB.

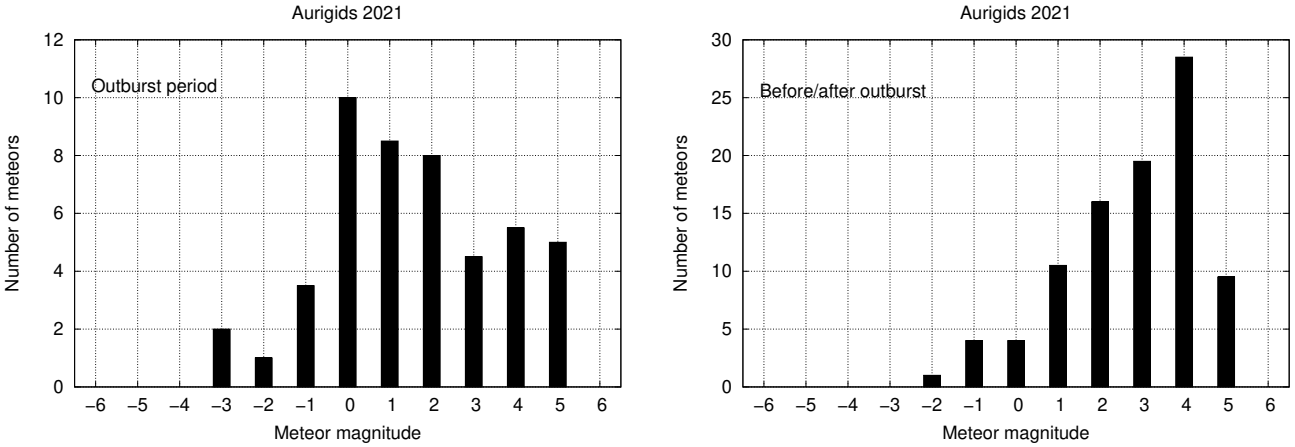

Figure 1 – Magnitude distributions of the Aurigids 2021 for the immediate peak period (left) and the neighbouring periods (right).

[1] Eschenweg 16, 14476 Potsdam, Germany. Email: jrendtel@web.de
[2] Hauptstraße 35, 18469 Velgast, Germany.

3 Analysis and results

First, we analysed the magnitude data of sessions with limiting magnitudes lm of at least +5.5. We calculated the population index r applying the regression method as well as the difference between lm and the average meteor magnitude m_{avg} (described in detail in the new edition of the IMO Meteor Observer Handbook which will be available in September 2021). The results of r from both methods are in very close agreement and we find for the Aurigids:

August 31, $21^{\mathrm{h}}00^{\mathrm{m}}$–$22^{\mathrm{h}}00^{\mathrm{m}}$ UT (peak) $r = 1.65$,

August 31 – September 02 (except August, 31 21^{h}–22^{h} UT) $r = 2.20$.

The magnitude distributions of the Aurigids in the peak period and the adjacent activity period are shown in Figure 1 (left and right, respectively). The population index in the peak period is remarkably low and close to the 2007 value ($r = 1.74$; Rendtel, 2007). The small sample does not allow us to determine a profile across the peak.

The peak is very short (Figure 2) and if we intend to detect the position of the highest ZHR and possible structures in the ascent and descent, we used intervals of 10 minutes duration or less for the immediate peak period. For the adjacent intervals we allowed also intervals up to 25 minutes length. In order to avoid systematic effects of the r-correction, we included only intervals with lm of at least +5.7. Since we do not have a r-profile at hand (only a fixed value for the peak period), we cannot derive any information about a possible mass sorting across the encounter (which would have an effect on the precise position of the maximum number density for different masses). In Figure 3 we show the profile of the number density for meteoroids causing meteors of at least +6.5 mag. Obviously, the outburst was composed mainly of much brighter meteors, but the small numbers do to allow us to derive a valuable number density profile for certain mass ranges.

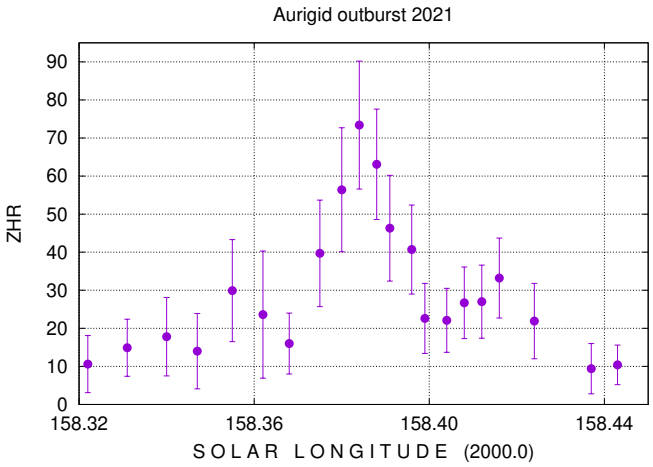

Figure 2 – ZHR profile of the 2021 Aurigids from visual observations submitted to the VMDB. Some observers provided data of shorter intervals than stored in the VMDB on request.

Of course, the ZHR (and later the number density) depends on the value of r for the respective section of a stream. Another very strong effect is present in the Aurigid shower: if the stream has only a slightly increasing number density towards the core but is combined with a significantly lower r as found in the Aurigids 2021 (and also 2007), an obvious ZHR peak becomes visible. Reducing r from 2.20 to 1.65 implies that the total conversion factor from the ZHR into the ND($\leq$ 6.5 mag) is 5 times lower. In other words, the stream of the same number density will appear as a 5 times higher ZHR. Although we do not have detailed numbers for the peak, the encountered meteoroid stream trail or filament has no density which exceeds the surrounding stream by orders of magnitude but only by a factor 5–10.

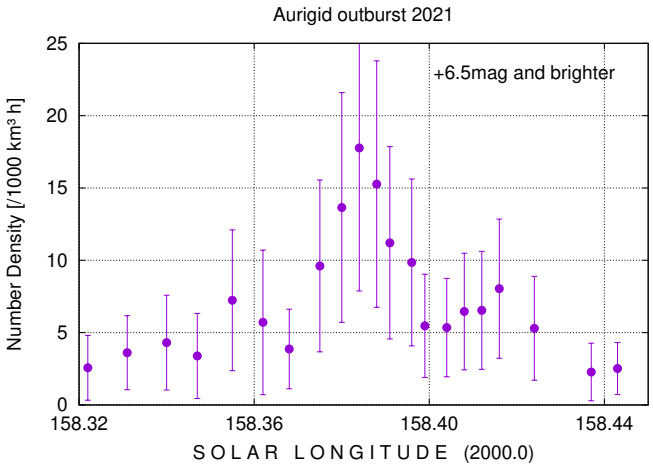

Figure 3 – Number density (meteoroids causing meteors of at least +6.5 mag within a cube of 1000 km edge length) of the Aurigids during the 2021 peak.

The peak positions of the ZHR (73 ± 17) is found at $\lambda_{\odot} = 158\overset{\circ}{.}384$, i.e. 2021 August 31, $21^{\mathrm{h}}18^{\mathrm{m}}$ UT. The neighbouring values are from 6 minutes before and after this moment and are quite similar (indicating a roughly symmetric profile). The maximum ZHR calculated here reached about half the value of the 2007 encounter and was of a similar particle size distribution. However, such a comparison must be taken with great care because of the very different circumstances. In 2007, the observations were made with a high radiant position while the 2021 peak occurred with a radiant very low in the sky. For the geometric correction, we assumed a zenith exponent of $\gamma = 1.0$. If the zenith correction has a value of 6, $\gamma = 1.2$ causes a 50% increase of the ZHR; $\gamma = 1.4$ would double it. Another effect on the ZHR may be introduced by the bright skies in the 2007 data which perhaps has reduced the ZHR. In both cases, there are large uncertainties.

The major conclusions from the 2021 Aurigid observations are:

1. The parameters used for modelling the Aurigid stream are obviously correct (congratulations to all three authors – remembering especially Esko Lyytinen who also provided an explanation after analysing the 2019 return; he certainly would be very happy to see the results).

2. Each observer's sample is way too small for any analysis. This is only possible by an international campaign with participants from many locations. Thanks to all observers who submitted their reports regardless of the sample size.

References

Rendtel J. (2007). "Visual observations of the Aurigid peak on 2007 September 1". *WGN, Journal of the IMO*, **35:5**, 108–112.

Rendtel J., Lyytinen E., and Vaubaillon J. (2020). "Enhanced activity of the Aurigids 2019 and predictions for 2021". *WGN, Journal of the IMO*, **48:5**, 158–162.

IMO bibcode WGN-494-rendtel-letter NASA-ADS bibcode 2021JIMO...49L..73R

Who is interested in old WGN issues?

Dear members of the IMO. I have a big pile of WGNs from 1985 until 2020. Who is interested in (part of) the collection? They are free of charge, I only ask for the shipping costs.
Please contact me at `e.van.ballegoij@gmail.com`.

Kind regards,
Erwin van Ballegoij

Ongoing Meteor Work

J14: A Meteor Shower and Cluster Catalog

SonotaCo[1], *S. Uehara, T. Sekiguchi, Y. Fujiwara, K. Maeda, M. Ueda*

A new meteor shower catalog (J14) with short interval meteor clusters data has been derived from constant video meteor observations during 2007–2020. J14 was clustered from 128 228 meteors that have better than 1.0° accuracy of radiant direction and 5% accuracy of geocentric velocity, selected from 353 231 meteors of 14 years SonotaCo Network video meteor observations (SNMv3). As the first stage, automated clustering on each subset that contains meteors in 1° interval of solar longitude was done. The purpose of this stage was to solve the radiant drift problem on the clustering and find exceptional drift other than 1° movement along with the ecliptic plane. In this clustering, a new numerical measure that express the statistical significance of a cluster concentration (Sig) was newly introduced. Sig enabled the mathematical evaluation of cluster concentration, independently from human bias. As the result of this process 1 104 clusters on 1° solar longitude interval (1LsCluser) were determined for a whole year. All 1LsClusters information is included in J14 catalog. They contain information about velocity and the radiant distribution radius for each solar longitude, something that was not involved in past shower catalogs. By connecting the 1lsClusters, a set of 136 meteor showers were determined. There are 17 showers that have been allocated new IAU meteor shower names (IAU #1111 to #1127). Owing to the accuracy and the homogenous aspects of original orbit dataset, and despite it having the geographical restriction of the observation network in middle latitude area of northern hemisphere, J14 becomes a cyclopedic and precise catalog of active meteor showers in recent years.

Received 2021 July 26

1 Introduction

A cyclopedic and precise meteor shower catalog is essential for meteor researchers in order to recognize the irregular appearance of the Earth colliding objects, and to identify any parent body which could possibly be hazardous to us.

In 2009 the first uniformed meteor shower catalog obtained from simultaneous video observation was built (J4; SonotaCo, 2009). It was derived from 39 208 meteors obtained in 2 years of 2007–2008 by SonotaCo Network (SonotaCo, 2009–2021). It contained 34 showers that have a clear concentration of orbits. However, in order to identify weaker showers with clear evidence, it was thought that the number of observed meteors was not enough, and the observations were continued.

Since then, video meteor observation networks have been set up in multiple regions in the world, and the reports of new meteor showers have rapidly increased. At the end of 2020, the number of registered meteor showers listed by the IAU Meteor Data Center (Jopek & Kaňuchová, 2017) reached 1049. However, the variation in the reliability of records is not small, and there can be many shower candidates that should be unified with others or deleted. At the present we cannot decide on which catalog we rely.

Given this situation, the SonotaCo Network observation has been constantly continued up to 2020. The number of the stacked orbit data has reached 353 231. The error computation and reducing method for SonotaCo Network data has been developed by SonotaCo (SonotaCo, 2016; SonotaCo, 2017).

[1]SonotaCo Network, Toru Kanamori 2-11-6 Daizawa Setagaya-ku Tokyo 1550032 Japan. Email: admin@sonotaco.jp.

IMO bibcode WGN-494-sonotaco-catalog
NASA-ADS bibcode 2021JIMO...49...76S

Here we planned to make a new meteor shower catalog, and made an error-managed 14 years meteor orbits set named SNMv3 (SonotaCo et al., 2021).

However, there are multiple unsettled issues regarding the determination of meteor showers. We aimed to build mathematically re-confirmable procedures of shower determination. In this paper, we formulate the issues, and propose one method for each, and report the resulting new meteor shower catalog named J14.

2 Orbit data set for clustering

In general, the accuracy of each meteor orbit is widely dispersed even it is obtained from same hardware in same network. It is very difficult to distinguish observational error from the natural deviation of shower meteors. Therefore, the selection of meteors before clustering based on the observational accuracy is very important.

As is written in the SNMv3 paper, on SNMv3 (SonotaCo et al., 2021), the effect of the selection of meteors based on their accuracy is clear. It increases the accuracy of each shower parameter, and possibly reveals the compact concentrations that have a small number of meteors in the noisy background. But the decrease of the number of instances, results in the decrease of the statistical significance of clusters, and makes it difficult to find vague and weak concentrations.

As the preliminary trial, we made an experimental automated clustering software and tested subsets listed in Table 1. Larger sets brought larger number of shower candidates. But most of the additional candidates are not clear ones, and this makes it difficult to determine the objective threshold for a shower. As the result of preliminary trials, we decided to use the single subset Er1Ev5 for further processing. It showed a better bal-

Table 1 – Tested subsets of meteors on SNMv3.

name	Er condition	Ev condition	number of orbits
ALL	—	—	353 231
E5	$Er \leq 5.0°$	—	303 076
E3	$Er \leq 3.0°$	—	268 418
E1	$Er \leq 1.0°$	—	156 426
Er1	$Er_{org} \leq 1.0°$	—	140 878
E05	$Er \leq 0.5°$	—	84 910
Ev5	—	$Ev < 5.0\%$	286 866
Ev1	—	$Ev < 1.0\%$	126 196
E1Ev5	$Er \leq 1.0°$	$Ev < 5.0\%$	142 123
Er1Ev5	$Er_{org} \leq 1.0°$	$Ev < 5.0\%$	128 228

Er: Standard deviation of radiant direction error (center angle on equatorial coordinates).
Er_{org}: Er before observation combination selection (SonotaCo, 2017).
Ev: Percentage of error on geocentric velocity (Vg).

ance of accuracy and the number of shower candidates. The use of the combination of multiple subsets or making each result from each subset were considered, but it was not tried on this occasion.

3 Introducing of short interval cluster

In the formulation of issues, we firstly tried to separate the shower drift problem from others.

The drift is the issue that shower parameters change depending on the solar longitude of the observation. It affects clustering methods and the coordinates of evaluation space.

To decrease the effect of the drift, Sun centered ecliptic coordinates (SCEC) have been often used in meteor shower analysis. SCEC cancels the +1.0° drift in solar longitude that is in parallel with ecliptic plane. But as is shown in Figure 1, there are a variety of drift directions that are not in parallel with ecliptic plane. SCEC does not solve the problem for them.

Here, for the purpose of handling the variety of drifts on an even condition, and to separate the drift problem from the clustering process, we tried clustering on a short interval of solar longitude, where effect of drifts can be ignored as it is within the observational accuracy. Therefore, we do not need to care about the difference of solar longitude and we can use any coordinates and criteria for clustering. Showers can be determined in the post stage as the composed sequence of clusters.

In comparison with the radiant direction accuracy of Er1Ev5 set, we select 1° of solar longitude interval for clustering on this paper. We named the cluster obtained from a set of meteors in 1° of solar longitude as 1LsCluster.

As the clustering result of 1LsClusters we will get the information about Vg, cluster radius, and the intensity of appearance on each solar longitude of the shower, information that was not included in past shower catalogs. Here, we decided to publish all 1LsCluster information as a table with the shower data.

4 Criterion of orbit similarity

In an objective meteor shower clustering, a criterion regarding the similarity of orbits is necessary.

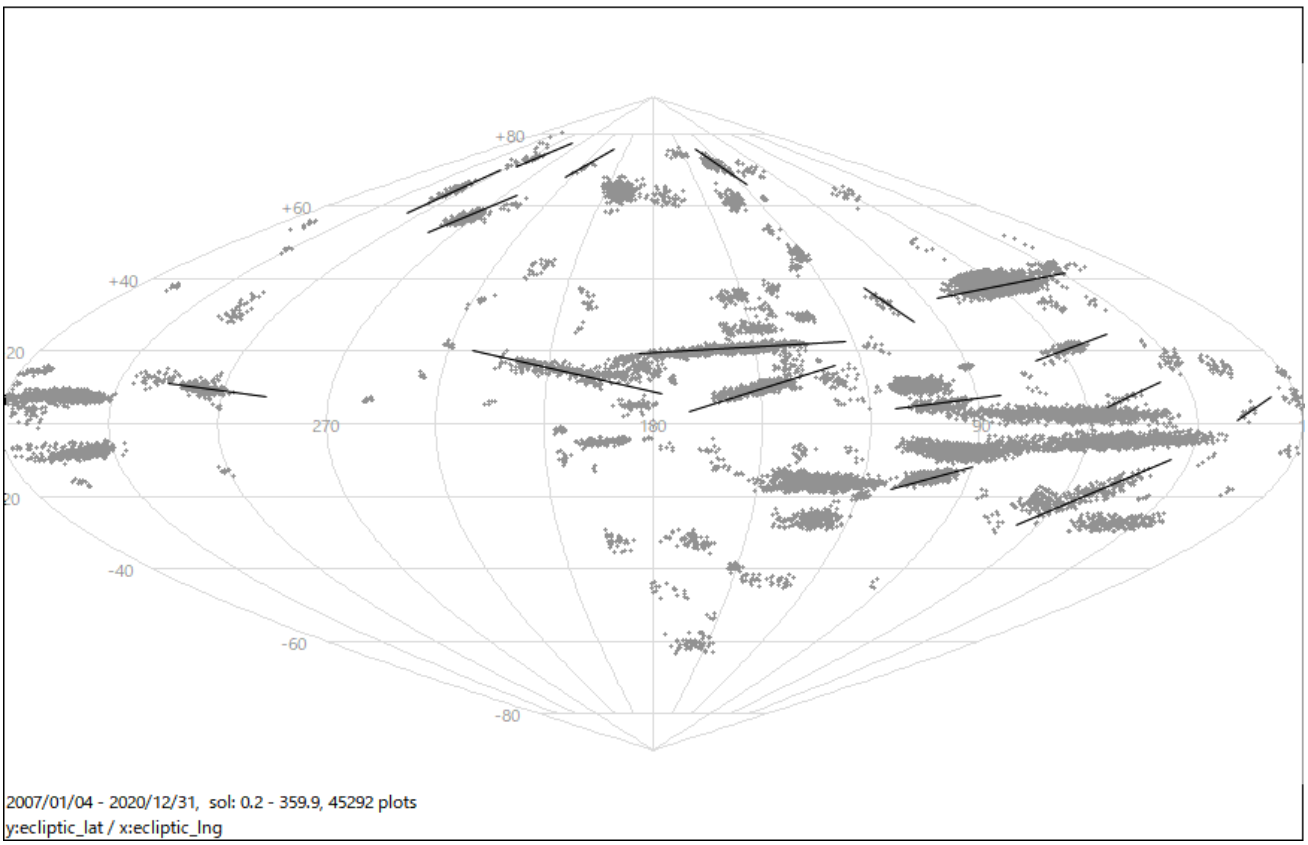

Figure 1 – Plot of shower meteor radiant on ecliptic coordinates. Black line shows the shower drift not in parallel with ecliptic plane (horizontal direction is in parallel with ecliptic plane).

D' criterion (Drummond, 1979) has been often used as the criterion of orbit similarity. D' is the modified criterion of D criterion (Southworth & Hawkins, 1963) that is a combined value using fixed coefficients for the difference of heliocentric orbit elements. D' express the similarity of orbits by one value and can be used in the comparison of a meteor orbit and an asteroid orbit that does not collide to the earth.

While for the earth colliding objects, the differences in the radiant parameters were widely used for the comparison of their orbits. Radiant parameter is a set of solar longitude of occurrence time (Ls), radiant direction (a pair of right ascension (Ra), and declination (De), or their values in ecliptic coordinate), and geocentric velocity (Vg).

By ignoring the difference of the Earth's position in each year, (Ls, Ra, De, Vg) can be converted to heliocentric orbit elements. It means there is essentially no difference between D' and radiant parameter comparison. The difference is that D' is one value that used fixed weights of elements, while the radiant parameter comparison can be weighted freely depending on the natural dispersion of each component. It is apparent that the D or D' value is small among orbits that are concentrated sharply on the radiant parameters. But the reverse is not correct. Figure 2 shows the distribution of radiant direction of selected orbits using two methods. The mother set, and the centered orbit are the same. The clustering threshold is tuned to result in the same number of selected orbits. It shows the results obtained from D' selection contain many orbits that have big differences of radiant direction. This means that it is better to use multiple thresholds on radiant parameter components rather than using a composed single D' value. As for meteors, D' can be used on orbits at different solar longitudes, but it is not recommended because there is the drift problem.

From this point, we decided to use the differences in radiant direction and Vg as the criterion of orbit similarity in the orbit clustering on 1° solar longitude interval.

As the difference of radiant direction, we have been using the center angle between two radiant directions on the equatorial coordinates (R). Because there is no reason to use the difference on SCEC or other measures on the short interval observations.

As the criterion of the difference of Vg, we use the absolute difference of Vg (dVg) or the percentage of dVg/Vg on this research.

Figure 2 is the selection result by $D' < 0.091$, lower figure uses $R < 3.0°$ and $dVg < 8$ km/s. of the orbits in range of solar longitude 282.°2–283.°2. Threshold value is tuned to select the same number of orbits. R is the difference of radiant direction from a center, dVg is the difference of geocentric velocity. All coordinates used in this paper use J2000.

5 Drift computation

The 1LsCluster table can be used as the reference of drifted values. However, the drift computation method is still is necessary, because they are used for daily observation when the past observation might not exist.

As for the drift of radiant direction, we use the same computation method as on J4 (SonotaCo, 2009). It expresses the radiant drifting direction and the speed (center angle par day) at the peak of the shower as a 2 dimensional vector (dra, dde). The drift is computed as the movement on the great circle of celestial sphere. The sample of the drift computation for the Perseids (PER) is shown in Figure 3. By this method, even in the high declination area where the Ra–De plane is not isotopic, it can compute precise positions. It can also compute the curved drift on the equatorial coordinates that is required for long term showers like Taurids or Perseids.

Vg has been used with radiant direction for classification of meteors, but the drift of Vg has not been

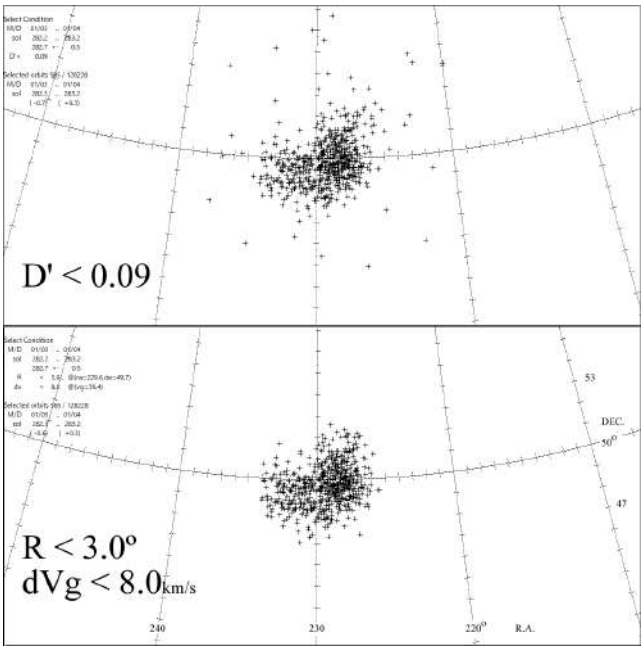

Figure 2 – Selection of orbits by two similarity criteria.

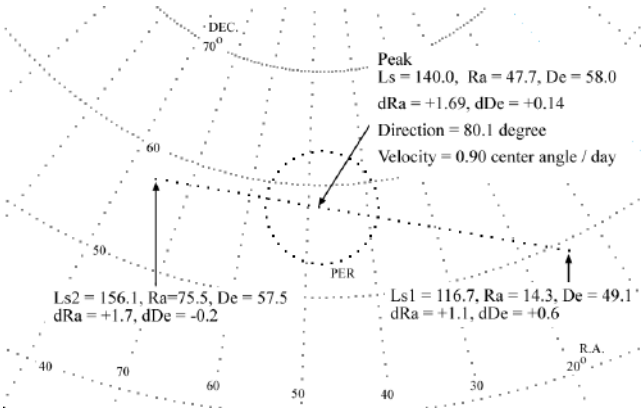

Figure 3 – Constant velocity drift computation on a great circle. This figure shows radiant direction drift computation results of PER. This plot uses gnomonic (center) projection whereby a great circle is expressed in a straight line. The computation uses the law of cosines and the law of sines of spherical trigonometry. This method enables the drift computation of any direction at any position, where the differences per day are not constant on equatorial coordinates.

involved in past shower catalogs. In J14, we compute and include the Vg drift as dVg (km/s/day).

6 Handling of natural deviation

In a set of one shower meteor orbits, there is a natural deviation of orbit parameters. In meteor shower analysis, there are two processes that are affected by the natural deviation. One is clustering of showers, and the other is the shower classification of a meteor. The clustering is the determination process of shower parameters, that computes the natural deviation from observed meteor samples. The classification is a determination of the assigned shower for a meteor using the cataloged values of natural deviation.

Because there are differences of natural deviation depending on the shower, we must use a different threshold for each shower. For example, as is shown in Figure 4, we must use far looser threshold for classification of Geminids (GEM) meteors compared with compact shower such as October Camelopardalids (OCT). The handling of this natural deviation has not been formulated. The problem is how to express the natural deviations in the shower catalog, and how to use them in the meteor shower classification.

Here, we propose a common statistical method that records the standard deviation (SD) of a parameter on the catalog, and use multiplying factor n-sigma threshold depending on the purpose of classification. In this method, the computation of the probability of the appearance becomes possible by assuming the shape of the distribution.

In the meteor shower classification, using the criterion written in Section 3, SD of R (SDR), and SD of Vg (SDV) is necessary on the catalog. And n-sigma for R (Nr), and for Vg (Nv) should be decided depending on the observation accuracy and the purpose of classification. Figures 4 and 5 show the sample of relation between SD and the classification condition using Nr, Nv.

7 Measurement of concentration significance

The establishment of the numerical criterion on concentration degree of shower meteors is the subject that we have not solved yet.

As the criterion regarding the strength or the intensity of a shower, stream to background (S/B) ratio (Jenniskens et al., 2016), intensity (ratio of shower meteor number against all or sporadic meteor number in the same interval), shower meteor count, or hourly rate has been used. These are reliable for strong showers, that have a sufficient number of samples, but it was difficult to use these criterions for the determination of weak showers.

Here we tried to compute the statistical significance of a meteor shower cluster based on the statistical null hypothesis testing method using p-value. It computes the mathematical probability of an event by coincidental random activity, and compares it to a threshold called p-value. In the social sciences, 5% or 1% of p-value is often used, and in the physics, as the probability of not coincidental events, $Q = 1.0 - p$ such as 99.7% or 99.9999% is often used as "believable reliability". By using the relationship between the factor of standard deviation and the probability on the standard distribution, the Q can be expressed by the factor n of n-sigma. By this expression 3.0 sigma corresponds to $Q = 99.7\%$ and 5.0 sigma corresponds to $Q = 99.9999\%$. Here we call the n that corresponds to the "probability of a cluster is not happened by the coincidence of sporadic meteors" as the statistical significance of the meteor cluster concentration (Sig).

Q can be computed by Equation 1, using the number of all instances (N), number of instances in the cluster (n) and the probability that one random instance becomes inside of the cluster (P_1).

$$Q_{Nn} = 1 - \sum_{x=n}^{N} \binom{N}{n} P_1^x (1 - P_1)^{N-x} \qquad (1)$$

As for P_1, the ratio of radiant distribution area size can be used. As the simplest example shown in Figure 6, assuming concentric two circles of radiant area those radii are R and $2R$, and N is the number of radiants in $2R$, n is the number of radiants in R. In this case, P_1 is 0.25.

Figure 6 shows samples of cluster that have $Sig > 3.0$ ($Q > 0.9997$), and Figure 7 shows samples of $Sig < 3.0$ concentrations. For most of the major showers, Sig of their 1LsClusers became more than 5.0 ($Q > 0.999999$). As the result of a preliminary trial, though there are several exceptions, it seems $Sig > 3.0$ can be a fair threshold of being a shower on Er1Ev5 set.

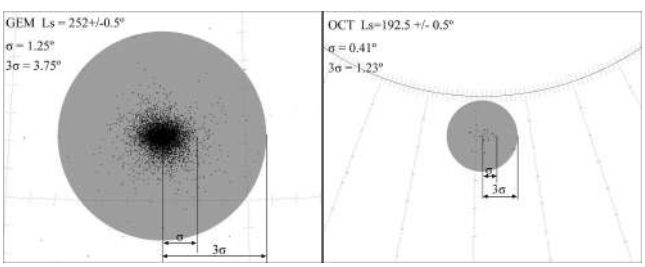

Figure 4 – Radiant direction plots of shower meteors of GEM, OCT on its shower peak. σ: Standard deviation of the radiant direction deviation from the center of the cluster. 3σ: Radius of classification circle as the shower ($Nr = 3.0$).

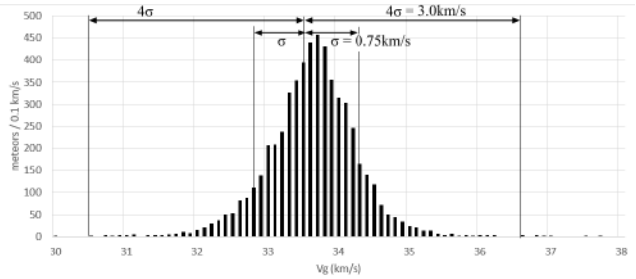

Figure 5 – Vg distribution of GEM (5652 meteor in Ls: $262\,^{\circ}0 \pm 0\,^{\circ}5$, $R < 3.75°$). σ: standard deviation of Vg measured on 1LsCluster of GEM at $Ls = 262°$. 4σ: clustering range of Vg ($Nv = 4.0$).

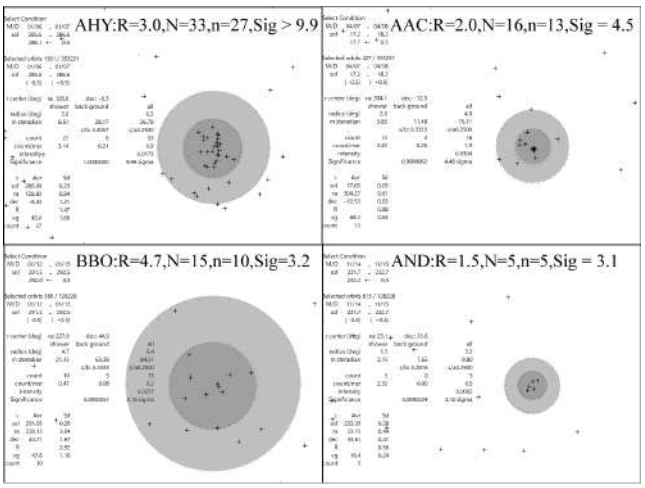

Figure 6 – Sample of statistical significance of 1LsClusters. Inner dark gray circle is the shower area of which the radius is R. Outer light gray circle is the background area of which the radius is $2R$. AHY: Alpha Hydrids, AAC: April alpha Capricornids, BBO: beta Bootids, AND: Andromedids Annual.

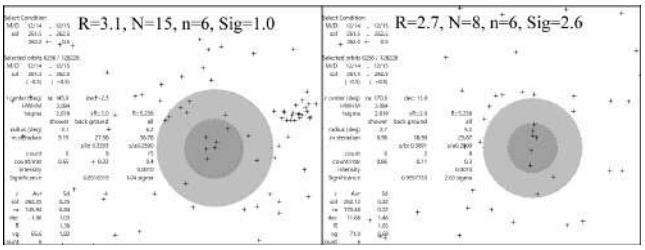

Figure 7 – Concentrations that does not have enough significance.

As is shown in Figure 8, Sig changes depending on R. By finding a value of R that gives maximum Sig, we can determine the radiant distribution radius as Rm. Rm can be used for the determination of the set of meteors in the cluster that is used for the computation of cluster parameter such as center radiant direction of the cluster, SDR, or SDV.

In the numerical computation of Sig on computers, there is a limitation of double precision values. Limits are $0.25^{501} = 2.2\text{E-}308$ and factorial of $171 = 7.3\text{E+}306$. On J14, an approximate computation using a precomputed table was used for large number of N. And $Sig > 9.0$ was not computed, because it is apparently significant.

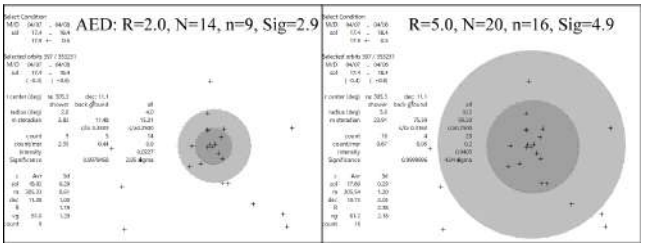

Figure 8 – Sample of Sigs on different Rs. As for possible April epsilon Delphinids (AED), $R = 5.0°$ gives the largest $Sig = 4.9$.

8 Automated clustering method

As the first stage, an automated clustering on each subset of SNMv3 Er1Ev5 that contains meteor orbits in 1° interval of solar longitude was carried out. The clustering was processed as follows.

1. Assume a concentric two circles of which the radiuses are $R = 3.0°$, and $6.0°$, for each radiant direction in the subset.
2. Compute Sig on (1).
3. Find a radiant that gives the largest Sig in the subset. And set it as the initial center direction of the cluster.
4. Find the Rm that gives largest Sig on the center direction.
5. Compute average direction of orbits that is inside of Rm, and set it to the center direction of the cluster.
6. Repeat (4) to (5) while the cluster is changing.
7. Register the cluster as the new one and compute cluster parameters, such as SDR, SDV.
8. Remove the element of the registered cluster form orbits set and repeat (1) to (7) until the largest Sig becomes under 1.0.

In this clustering, only the condition about radiant direction was used, and the condition about Vg was not used, because the deviation of Vg is very small in a small radiant area at the same solar longitude.

9 Clustering result

As the result of automated clustering on 360 subsets of 1° interval of solar longitude, in range of $Sig > 1.0$, 1256 1LsCluster are detected. Figure 9 shows the number of clusters for each solar longitude.

All clusters obtained by automated process were manually checked. 80% of the resulted clusters had $Sig > 3.0$ and seemed well concentrated clusters. There were, however, the issues described below.

1. There are faint clusters that have $Sig < 3.0$, which are obviously recognizable as a cluster. Especially for the clusters that have small N, Sig cannot be large, because the significance depends on the total number of instances. For example, as is shown in AND in Figure 6. To be $Sig > 3.0$, at

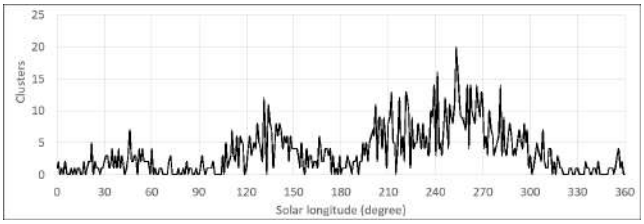

Figure 9 – Number of clusters on each solar longitude obtained by automated process.

$P_1 = 0.25$, there must at least 5 instances, even if all instances are inside of the cluster. For this reason, we checked all clusters that have small N by human eye. As an example, a cluster of a new shower December alpha Lyncids (LAD) listed in Section 13 is added. Though it has only 4 meteors in 14 years and Sig was 2.7, it is the Sun grazing meteors and is outstanding in low-density area.

2. The large areas around the apex, anti-helion, or inhomogeneous distributions were recognized as the significant cluster. To exclude those that can be thought as "not a shower (a gathering that have other reason)", we set the upper limit $Rm < 10°$. Through this limitation, many large clusters around the apex were rejected, and some other clusters that have ambiguous limits were manually deleted.

3. For some clusters, the automated determination of the center of the cluster or the best Rm could not find the global optimum, but selected an inappropriate local optimum. For each of those clusters, the center direction and R were settled manually.

As the result of manual checks, 1104 clusters shown in Table 2 were determined. Figure 10 shows the change of Sig, before and after the manual check. Figure 11 shows the position of 1104 clusters.

10 Shower composition from clusters

In this paper, we define a meteor shower as follows and tried to compose a shower from 1LsClusters,

1. Topologically connected concentration of meteor radiant on 4-dimensional space of (Ls, Ra, De, Vg).

2. The center of the concentration can be computed by the drift computation with small error compared with its natural deviation.

By finding and connecting nearby clusters one by one, a shower candidate can be determined as a set of 1LsClusters. The automated shower composition was done using conditions below.

1. The difference of Ls (dLs) between the cluster and the shower candidate is less than 3.0°.

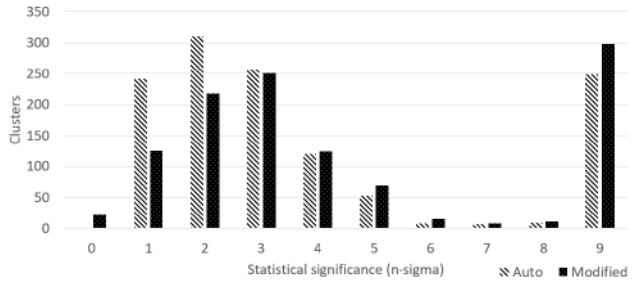

Figure 10 – The distribution of statistical significance of 1LsClusters before and after the manual modification.

2. The center angle of the radiant direction from estimated position using drift (dR/dLs) is less than 2.0.

3. The difference of Vg from the computed value using drift (dVg/dLs) is less than 5%.

After the automated process, shower candidates were manually checked. Below are the major problems found.

1. Northern Taurids (NTA) and Southern Taurids (STA) were connected, and there appeared isolated two 1LsClusters at the same solar longitude. dR/dLs threshold changed to 1.9, and the showers were separated.

2. November Orionids (NOO) and December Monocerotids (MON) were connected. $dR/dLs < 1.2$ was required for the separation.

3. PER and zeta Cassiopeiids (ZCS) were merged. They were separated into two spans of (ZCS: 107°–116°) and (PER: 116°–156°), because the drift parameters are not constant.

As the result of modification, 136 sets of 1LsClusters are determined as the candidates of showers. Figure 12 shows a sample of 1LsClusters sequence of a shower.

11 Shower parameter determination

Shower parameters are determined from the set of 1Lscluster parameters as below.

1. Find the cluster that has the largest meteor count, and set its average solar longitude as peak solar longitude of the shower (Lsp).

2. Set the shower parameter values equal to the peak cluster values for Ra, De, Vg, Sig.

3. Compute the average value in all clusters for SDR, SDV, and set them as the shower parameters.

4. Re-count the number of meteors of the shower and set the shower intensity (IP), and number of meteors (ns).

5. Search drift direction around the peak of (Ra, De) that gives minimum error by (6).

6. Compute the radiant drifting velocity by least square method that gives minimum error of radiant direction for all clusters.

7. Compute the unit vector of (dra, dde) form (5), (6), and set them as shower parameters.

8. Compute the dVg by least square method over all clusters and set it as shower parameter.

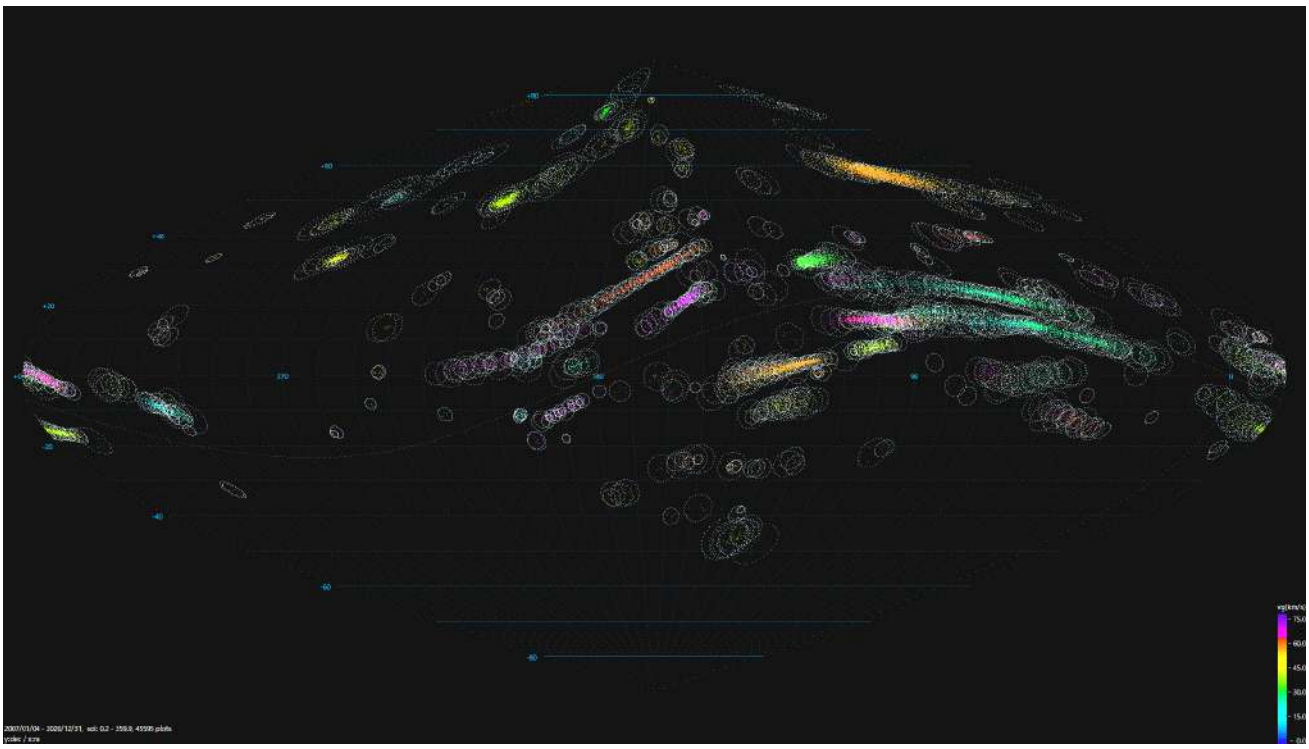

Figure 11 – 1104 Clusters and radiant direction of clustered meteors. White circle is showing double of standard deviation of radiant direction on the cluster ($Nr = 2.0$).

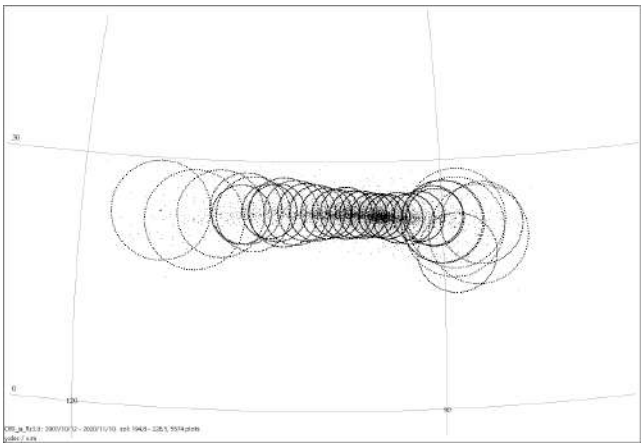

Figure 12 – 1LsClusters sequence of Orionids (ORI). The radius of circle is 2.0 * SDR of each cluster.

12 Shower identification

Derived shower candidates were compared with showers in the existing catalog and shower names and codes were identified. For this comparison, J4 and the IAU MDC `streamfulldata.csv` at 2021/01/01 (1785 records) were used. J4 contains major showers with precise information of drift and the span of solar longitude, and was preferred. Because MDC records do not have solar longitude span, SDR, SDV, they were assumed as ±5°, 1°, 5 km/s.

Initially, all meteors in SNMv3 Er1EV5 were independently classified by three catalogs (J14 shower candidates, J4, and MDC records) with the classification condition $Nr = 3.0$, $Nv = 5.0$. In addition, the cross counts of showers were made. The cross count is the number of shower meteors in other catalogs. Table 3 shows an example of J14 STA cross count on MDC showers. The cross count also shows duplication of showers in the compared catalog.

By selecting the shower that had largest number of common meteors, 119 sets of 136 sets were identified as known showers. 17 sets are considered to be new showers, and newly registered in IAU MDC shower list as the numbers of #1111 to #1127.

As a result, the 136 meteor shower catalog J14 was compiled. Table 4 shows J14 all shower parameters. All shower parameters are newly derived by the formulized process described in Section 11.

13 Outline of new showers

Table 5 shows the full name and relationship with nearby showers for the 17 new showers. Parameters of these showers are included in Table 3. Figures 13 to 29 show the radiant distribution of all meteors in the same solar longitude span of the shower. Gray circle is showing the new shower radiant area.

14 Classification using shower parameters

Figure 30 shows 48 754 shower meteors in SNMV3 Er1Ev5 128 228 meteors classified by J14 shower parameters, using $Nr = 3.0$, $Nv = 4.0$. Figure 31 shows 79 474 sporadic meteors reduced from it. There is no clear hole nor ghost of shower concentrations. This result means the shower clustering and the drift computation on J14 is fairly successful. The ratio of shower meteors was 38.0%.

When an accuracy-unmanaged set of SNMv3 (353 231 meteors) $Nr = 6.0$, $Nv = 8.0$ was used to reduce the ghosts of showers, it classified 142 570 shower

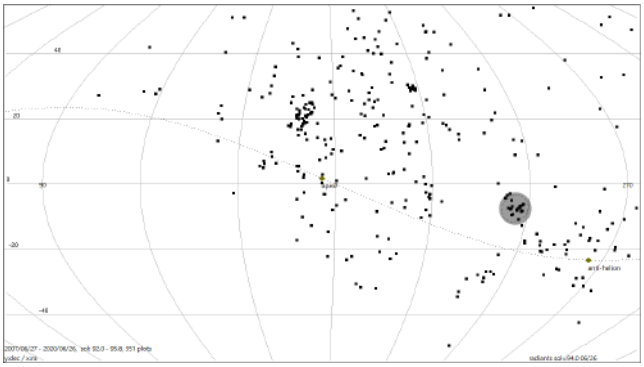

Figure 13 – #1111 (AQI) Aquilids.

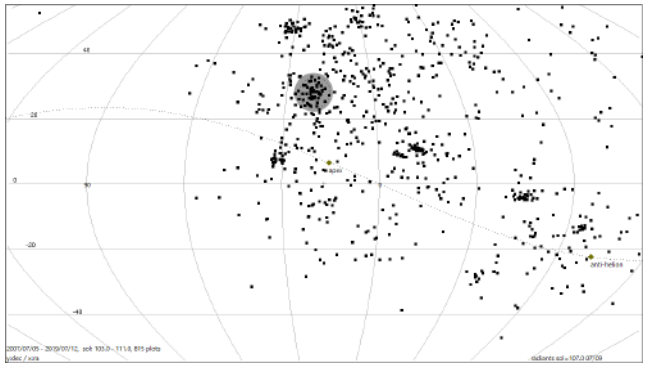

Figure 14 – #1112 (UPI) upsilon Piscids.

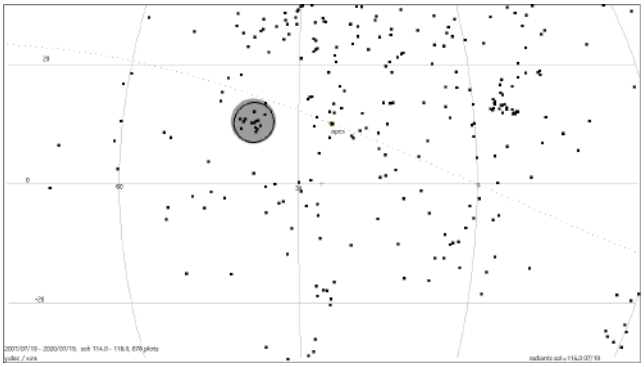

Figure 15 – #1113 (SJA) Southern July xi Arietids.

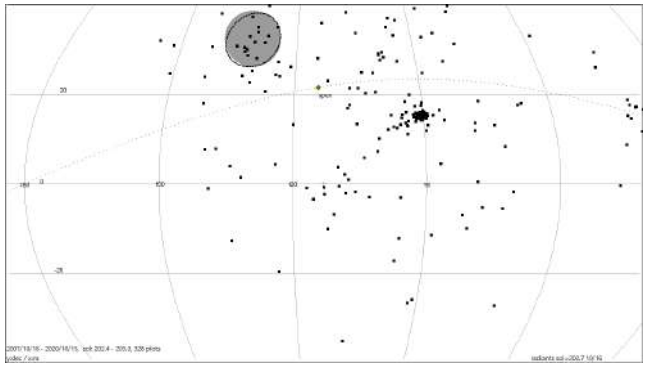

Figure 16 – #1114 (SGC) sigma1 Cancrids.

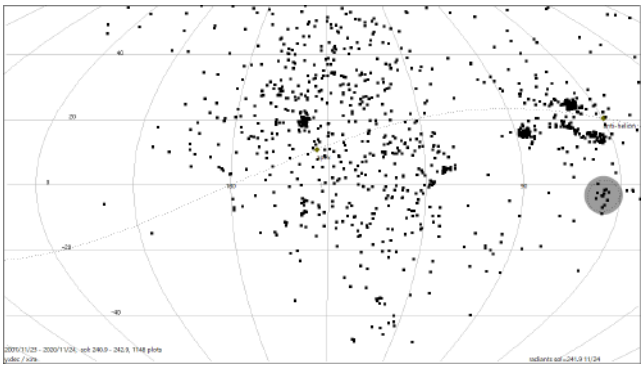

Figure 17 – #1115 (NXE) November xi Eridanids.

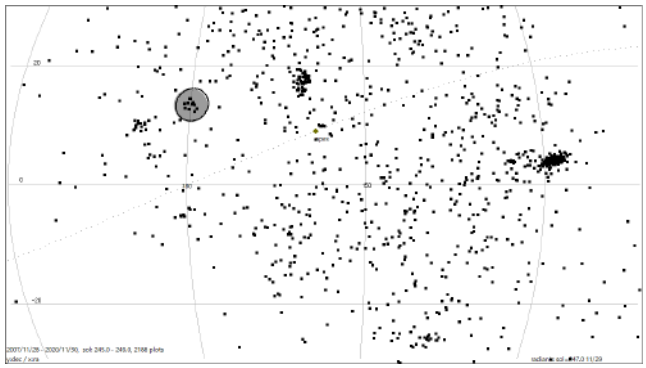

Figure 18 – #1116 (NFL) 95 Leonids.

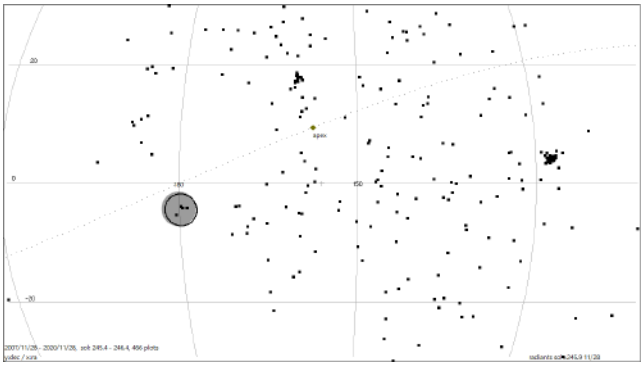

Figure 19 – #1117 (NEV) November eta Virginids.

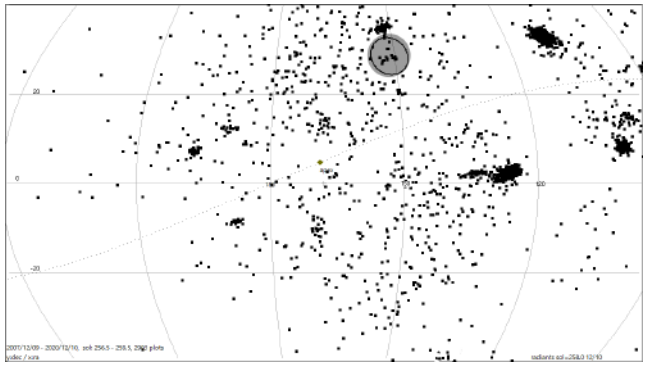

Figure 20 – #1118 (MLT) 24 Leonis Minorids.

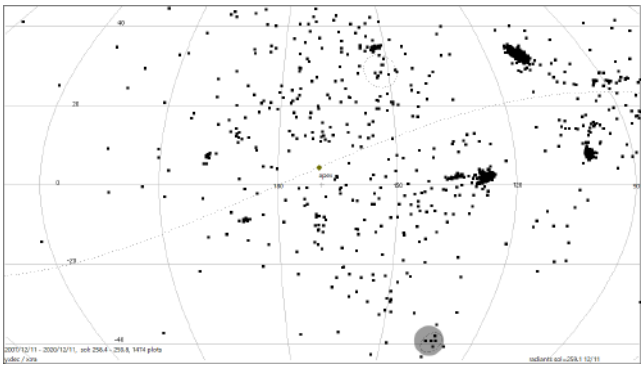

Figure 21 – #1119 (LAV) lambda Velorumids.

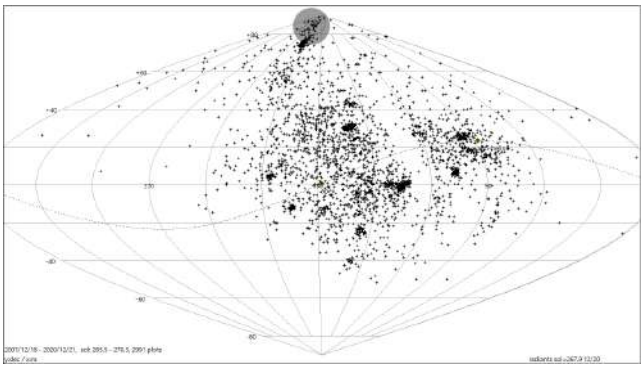

Figure 22 – #1120 (DUM) delta Ursae Minorids.

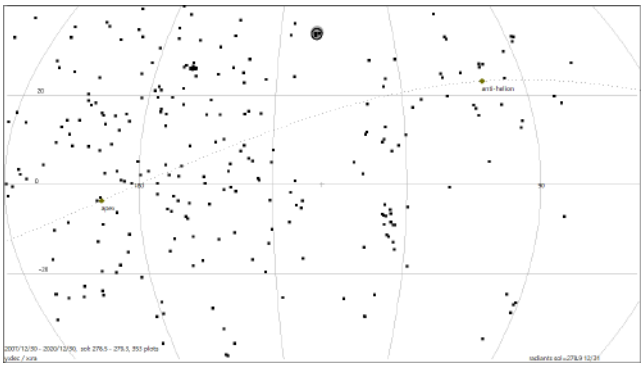

Figure 23 – #1121 (LAD) December alpha Lyncids.

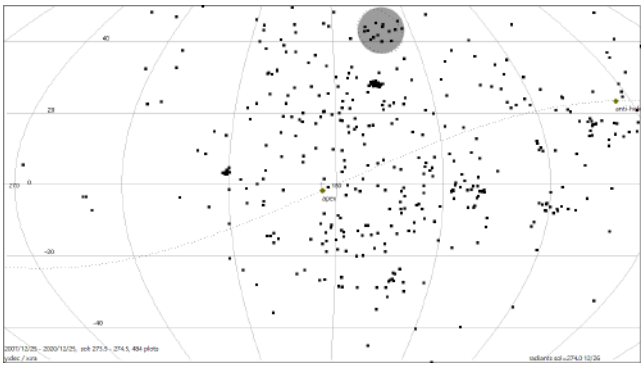

Figure 24 – #1122 (UMN) Northern December omega Ursae Majorids.

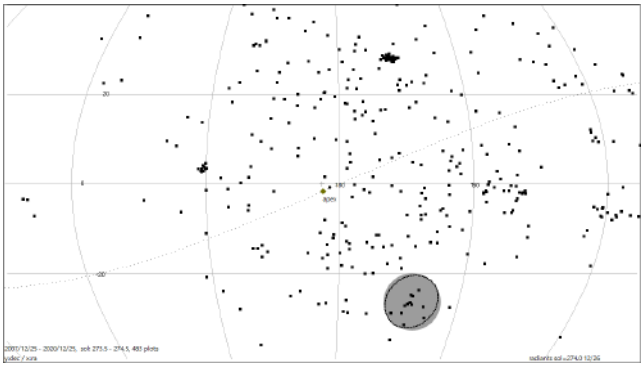

Figure 25 – #1123 (FFH) 44 Hydrids.

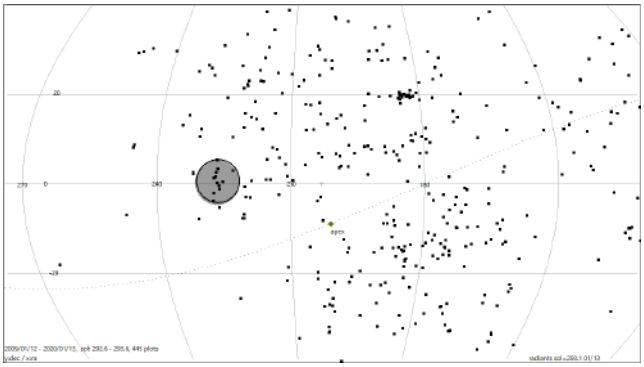

Figure 26 – #1124 (HTV) 110 Virginids.

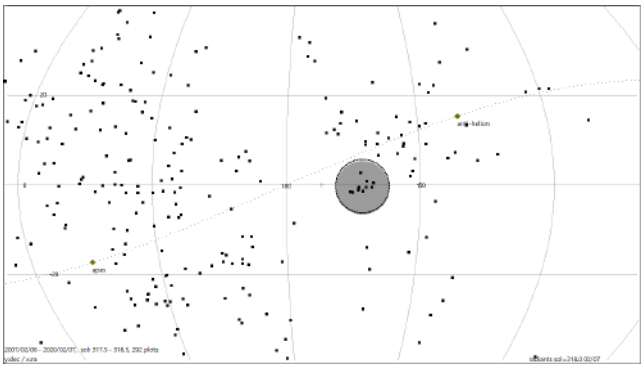

Figure 27 – #1125 (FFL) 55 Leonids.

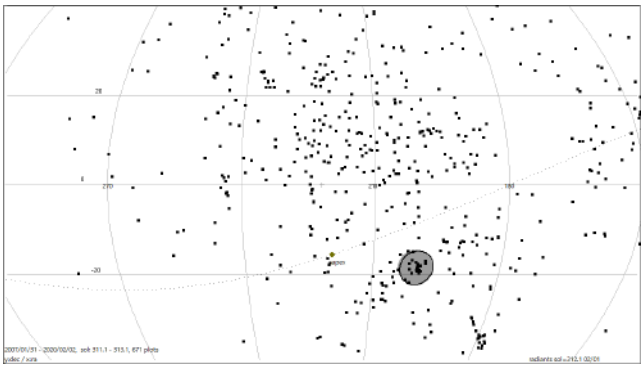

Figure 28 – #1126 (SOV) 61 Virginids.

Table 3 – Sample of cross count of common meteors. Code: MDC shower code and the "adno" as the suffix. Count: the number of meteors that were classified as the shower in 3560 meteors that were classified as J14_"m5fd" shower candidate. From this count, the candidate "m5fd" was identified as STA.

code	count	code	count
ATS.1	1	NTA.8	4
ATS.2	1	ORS.1	20
ATU.1	1	ORS.2	28
DAT.1	3	ORS.3	39
DAT.2	3	ORS.4	63
DZT.1	41	ORS.5	55
DZT.2	39	SOA.1	140
FTA.2	106	SOA.2	151
FTA.3	86	SOA.3	183
FTR.1	473	SPI.1	23
FTR.2	537	SPI.2	6
GTA.1	155	SPI.3	4
LCT.1	338	SSA.1	3
LCT.2	209	STA.1	64
LTA.1	352	STA.2	196
LTA.2	309	STA.3	129
MTA.1	86	STA.4	682
MTA.2	56	STA.5	131
NET.1	1	STA.6	337
NET.2	1	STA.7	132
NOA.2	3	STS.1	631
NOA.3	1	STS.2	620
NPS.1	34	TAR.1	1
NPS.2	41	TAR.2	2
NTA.3	3	TEA.1	10
NTA.4	4	XAR.1	261
NTA.6	20	XAR.2	215
NTA.7	1		

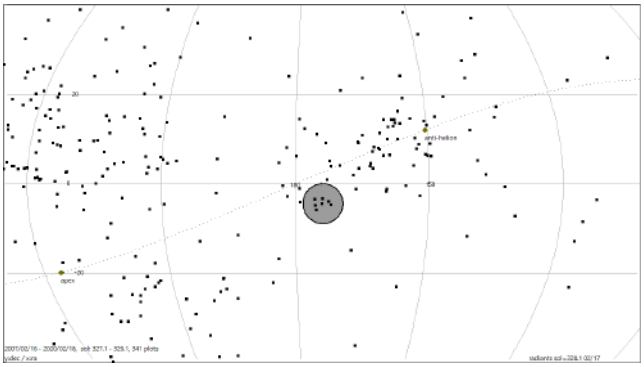

Figure 29 – #1127 (ESL) 87 Leonids.

meteors and 210 661 sporadic meteors. The ratio of shower meteors was 40.4%, and low density areas of sporadic meteors appeared near shower positions.

15 A new gap in a stream

Two low-density areas on the radiant distribution were known. One is around (220°,0°) on SCEC caused by the Sun grazing meteors (SonotaCo, 2009; Figure 6). The other is the very low inclination orbits area around the ecliptic plane, caused by the gravitational effect of the planets. It appears as a gap in one dust stream, like the intermediate area between NTA and STA.

As is written in Section 10, on the composition of showers, exceptional thresholds were required on the separation of NTA–STA and NOO–MON. It means that Ls, Ra, De, Vg values of NOO and MON were very close. NOO and MON are believed to have the same parent body comet C/1917 F1 Mellish (Vereš et al., 2011).

From these points, the low-density area between NOO and MON, shown in Figure 32, can be a gap in one stream. The appearance of this gap is very similar to the gap between NTA and STA, but intriguingly, the gap is not parallel to current ecliptic plane. Instead, it is parallel to some other shower's drift direction, and the position is shifted towards the south from current ecliptic plane. No clear explanation for this gap is currently available. Further research about the evolution of this stream is expected.

16 Conclusion

J14 has the features listed below.

1. Based on 14 years continuous observation.
2. Observation error of all orbits was managed to below 1.0° of radiant direction and 5% of geocentric velocity.
3. Difference of radiant direction and geocentric velocity was used as the criterion of the orbit similarity.
4. Clustering was carried out on 1.0° intervals of solar longitude, and 1104 clusters were determined.
5. Radiant drift was computed as moving on the great circle.
6. Drift of geocentric velocity was introduced.
7. Natural deviations of radiant direction and the geocentric velocity were measured and expressed as standard deviation.
8. Threshold on the shower classification is formulized as the n-sigma of standard deviation.
9. Statistical significance that computes the probability that a cluster is not a chance concentration was introduced. The concentration degree and optimum radius became computable.

As the result, all meteor orbits concentrations that are observable form northern hemisphere are arranged into 136 showers. J14 becomes the first catalog that have all information for each solar longitude.

The probability of not coincidental occurrence 99.97% (3.0 sigma) seemed a fair threshold for a clear concentration of statistical significance.

There were many weak concentrations that seemed like a shower but their *Sig* is less than 3.0. This means that the number of observations is still not enough for the mathematical determination, and the continuation

Table 5 – New Showers. Remark notes the relation with nearby showers. For example, Ls of AQI 92.°6–96.°1 is differed more than 5° from any of registered Ls of NZC 86.°0, 101.°5, 108.°1, 101.°0, 107.°3.

iauno	code	name	relation to nearby showers
#1111	AQI	Aquilids	Ls differs from NZC
#1112	UPI	upsilon Piscids	Ls differs from PPS
#1113	SJA	Southern July xi Arietids	Ls differs from JXA
#1114	SGC	sigma1 Cancrids	Ra differs from TCA
#1115	NXE	November xi Eridanids	-
#1116	NFL	95 Leonids	-
#1117	NEV	November eta Virginids	-
#1118	MLT	24 Leonis Minorids	De differs from COM,DLM
#1119	LAV	lambda Velorumids	-
#1120	DUM	delta Ursae Minorids	-
#1121	LAD	December alpha Lyncids	Ls differs from ALY
#1122	UMN	Northern December omega Ursae Majorids	Ls differs from DOU
#1123	FFH	44 Hydrids	Ls differs from TPY
#1124	HTV	110 Virginids	-
#1125	FFL	55 Leonids	-
#1126	SOV	61 Virginids	-
#1127	ESL	87 Leonids	-

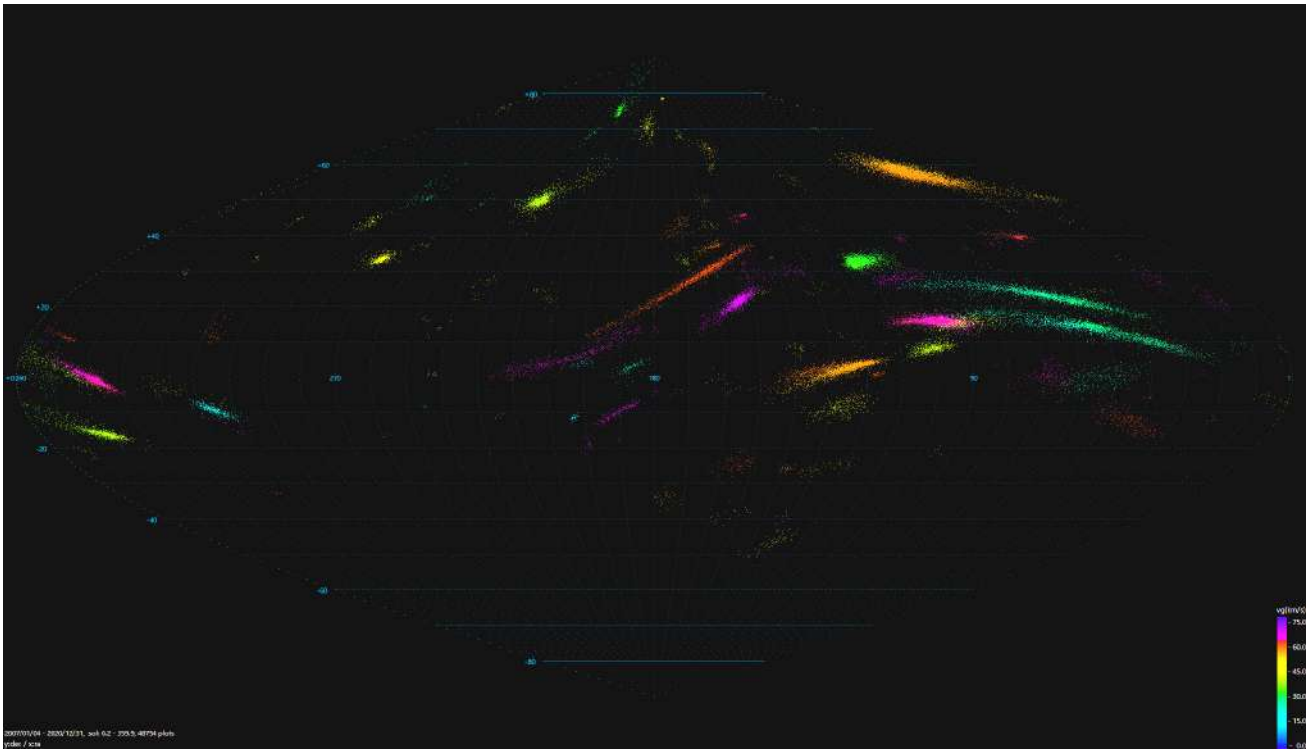

Figure 30 – J14 shower meteors in SNMv3 Er1Ev5 ($Nr = 3.0$, $Nv = 4.0$, 48 754/128 228 Orbits).

of observations for the next update of the catalog is required.

As for the analysis of showers in southern hemisphere, and the research on the annual activity, the combination of the data from multiple regions in the world will be required.

Regarding video observations, in addition to the orbital information, the material information, such as spectrum or the fragmentation type classification has started being added to the network. They are expected to be utilized in the meteor shower clustering in the future.

After 14 years of observation, we have reached not a goal, but the starting line.

Acknowledgements

J14 is one of the fruits of continuous efforts by all observers of SonotaCo Network. T. Masuzawa and all members listed in SNMv3 paper who observed the tremendous number of meteors with high accuracy for 14 years must be acknowledged at first. At last, we thank Yasuo Shiba, who checked J14 new showers and found a duplication of showers.

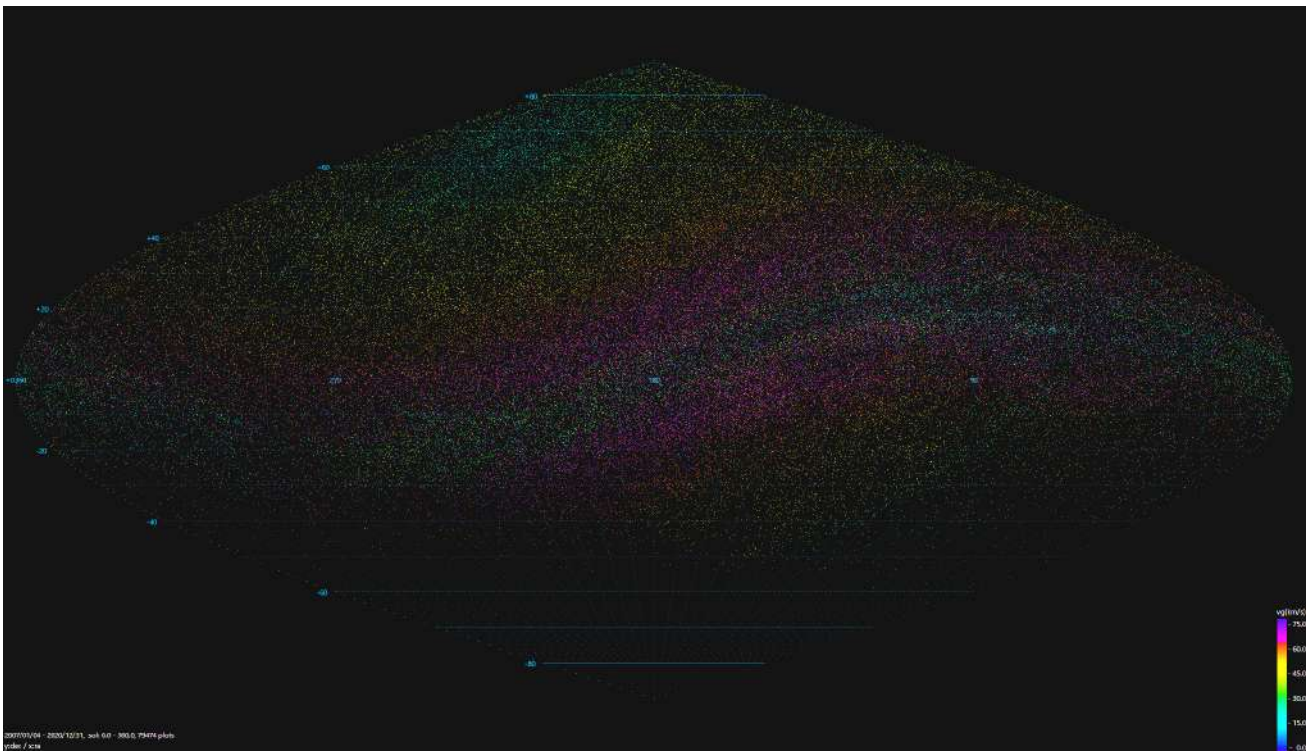

Figure 31 – J14 sporadic meteors in SNMv3 Er1Ev5 ($Nr = 3.0$, $Nv = 4.0$, 79 474/128 228 Orbits).

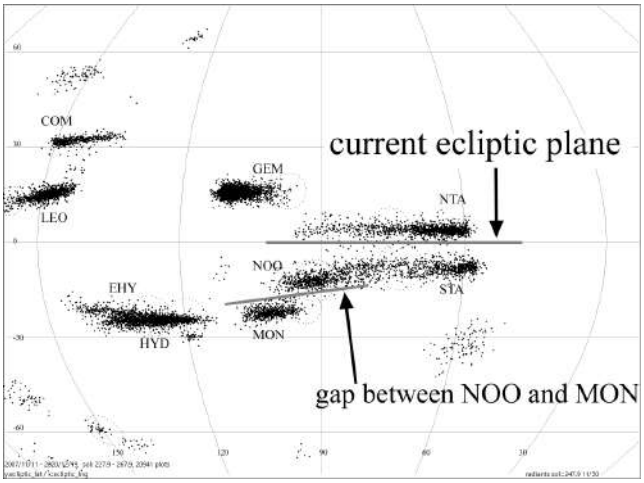

Figure 32 – Gap between NOO and MON.

References

Drummond J. D. (1979). "On the meteor/comet orbital discriminant D". *Proceedings of the Southwest Regional Conference for Astronomy and Astrophysics*, **5**, 83–86.

Jenniskens P., Nenon Q., Albers J., Gural P. S., Haberman B., Holman D., Grigsby B. J., Samuels D., and Johannink C. (2016). "The established meteor showers as observed by CAMS". *Icarus*, **266**, 331–354.

Jopek T. J. and Kaňuchová Z. (2017). "IAU Meteor Data Center-the shower database: A status report". *Planetary and Space Science*, **143**, 3–6.

SonotaCo (2009). "A meteor shower catalog based on video observations in 2007 - 2008". *WGN, Journal of the IMO*, **37:2**, 55–62.

SonotaCo (2009-2021). "SonotaCo Network Simultaneously Observed Meteor Data Sets (SNM20xx)". `https://sonotaco.jp/doc/SNM/index.html` .

SonotaCo (2016). "Observation error propagation on video meteor orbit determination". *WGN, Journal of the IMO*, **44:2**, 42–45.

SonotaCo (2017). "Exhaustive error computation on 3 or more simultaneous meteor observations". *WGN, Journal of the IMO*, **45:5**, 95–97.

SonotaCo, Masuzawa T., Sekiguchi T., Miyoshi T., Fujiwara Y., Maeda K., and Uehara S. (2021). "SNMv3: A Meteor Data Set for Meteor Shower Analysis". *WGN, Journal of the IMO*, **49:3**, 64–70.

Southworth R. B. and Hawkins G. S. (1963). "Statistics of meteor streams". *Smithsonian Contributions to Astrophysics*, **7**, 261–285.

Vereš P., Kornoš L., and Tóth J. (2011). "Meteor showers of comet C/1917 F1 Mellish". *Monthly Notices of the Royal Astronomical Society*, **412:1**, 511–521.

Handling Editor: Javor Kac

Table 2 – J14 Clusters List.

code	lsp	ra	de	vg	sdr	sdv	sig	ns
AAC	17.7	304.1	−12.5	69.2	0.7	0.6	4.8	10
ACB	308.1	231.7	27.5	57.9	0.9	0.6	3.0	8
ACB	309.0	233.2	26.3	58.9	1.1	1.5	3.4	7
ACB	312.1	235.3	23.4	58.6	1.6	1.5	4.2	8
AED	17.9	305.3	11.1	60.9	1.4	1.2	3.3	8
AED	19.0	306.9	10.8	60.9	1.1	1.0	3.7	8
AED	20.9	308.1	12.2	60.6	1.1	0.6	3.1	5
AED	22.1	309.5	13.4	60.2	1.2	1.1	3.4	7
AGC	155.3	353.1	75.7	43.9	0.8	0.8	3.1	5
AGC	155.9	356	77.3	43.2	2.0	1.4	4.3	10
AGC	157.1	358.6	76.8	44.6	0.5	0.4	1.6	3
AGC	158.0	5.5	76.3	45.2	1.7	0.7	1.6	3
AGC	159.1	3.1	78.9	44.3	1.7	0.5	1.9	5
AGC	160.1	16.8	79.3	45.5	1.6	0.4	2.2	4
AHY	272.0	119.9	−7.3	45.1	2.0	2.1	3.0	7
AHY	274.2	117.5	−7.0	42.5	1.7	1.6	1.0	6
AHY	275.0	121.3	−8.5	44.6	2.1	1.6	5.3	15
AHY	276.1	122.4	−6.2	44.2	1.5	0.8	2.0	7
AHY	277.1	122.4	−7.5	44.0	2.0	1.6	4.5	16
AHY	278.0	124.0	−7.4	44.4	1.3	1.3	3.3	8
AHY	278.9	123.7	−7.7	43.8	2.0	1.4	4.0	13
AHY	280.0	124.7	−7.9	43.5	2.0	1.8	10.0	19
AHY	281.0	125.7	−7.5	43.7	1.8	1.4	5.8	15
AHY	282.0	126.1	−8.9	43.3	2.0	1.3	6.8	18
AHY	283.0	126.9	−9.2	43.6	1.7	1.7	4.6	11
AHY	284.0	127.1	−8.3	43.5	1.0	0.8	5.1	13
AHY	284.9	127.6	−8.3	43.5	2.0	1.2	4.2	11
AHY	286.1	128.8	−8.3	43.1	1.4	1.2	5.7	20
AHY	287.0	128.1	−9.3	42.0	1.5	1.4	4.8	10
AHY	287.9	130.3	−9.6	43.1	1.7	0.8	3.1	5
AHY	288.9	129.3	−9.2	42.4	1.7	0.6	4.0	9
AHY	289.9	131.2	−9.2	43.1	1.5	0.7	4.5	9
AHY	291.0	132.1	−9.8	43.1	1.3	0.5	2.2	5
AHY	292.9	133.1	−10.4	42.7	1.0	1.2	3.0	6
AHY	294.1	133.5	−10.2	42.9	1.4	1.2	2.6	5
AHY	295.1	133.3	−11.3	41.3	1.0	0.5	2.2	3
AHY	296.0	135.8	−11.1	42.7	2.0	1.0	2.6	6
AHY	296.8	135.5	−11.8	42.4	1.0	0.7	2.7	4
AIC	154.1	1.1	−7.7	35.8	2.0	1.2	0.7	3
ALA	106.2	352.0	53.3	52.2	1.4	1.7	1.8	4
ALO	13.0	242.5	0.9	55.9	1.0	0.7	3.7	9
ALO	14.2	242.8	1.0	56.4	0.9	0.4	2.6	5
AMO	238.0	116.0	1.0	61.6	1.2	1.0	3.0	11
AMO	239.1	117.0	0.8	62.2	0.7	1.4	2.0	7
AMO	240.0	117.5	0.9	61.8	0.6	1.1	7.4	17
AMO	240.9	118.2	0.5	61.4	0.7	1.3	4.2	12
AND	232.2	23.1	33.6	16.6	0.6	0.1	2.7	4
AOC	135.2	26.7	0.5	66.7	1.7	0.9	1.7	5
AQI	92.9	303.3	−7.8	39.7	2.0	3.3	3.0	7
AQI	95.2	303.9	−7.6	40.6	1.2	1.4	2.6	6
AQI	95.8	306.5	−6.7	39.8	0.9	0.6	1.0	2
ARI	70.8	39.1	22.3	40.6	1.5	0.5	1.5	2
ARI	71.8	39.7	24.5	39.0	1.5	0.5	1.5	2
ARI	72.7	41.3	22.8	38.8	1.5	0.5	1.5	2
ARI	73.9	41.3	24.2	40.7	1.5	0.5	2.2	3
ARI	74.8	41.7	24.4	41.3	1.5	0.5	0.7	1
ARI	75.5	43.7	24.7	40.1	1.5	0.5	0.7	1
ARI	77.2	43.7	24.2	40.6	0.6	1.0	2.7	4
ARI	78.9	45.1	24.3	41.8	1.5	0.5	2.2	3
ARI	80.0	46.1	24.7	42.1	1.5	0.5	0.7	1
ARI	80.9	46.6	24.1	41.9	0.6	0.9	2.7	4
ARI	83.9	48.8	27.6	45.1	1.5	0.5	0.7	1
ARI	83.0	49.2	26.2	41.3	1.5	0.5	1.5	2
AUR	156.1	88.8	39.4	65.1	0.8	0.5	2.7	4
AUR	158.2	90.7	39.0	65.9	0.6	0.7	4.5	9
AUR	158.9	91.1	39.2	65.7	0.9	1.1	3.7	8
AUR	160.2	93.1	39.2	64.7	1.7	1.6	1.8	6
AVB	21.9	198.0	4.2	20.2	1.0	0.3	2.6	6
AVB	23.9	198.3	4.4	19.7	1.0	0.5	1.5	4
AVB	25.1	200.4	2.5	19.6	2.2	0.3	1.6	3
AVB	25.8	200.1	3.2	19.2	1.1	0.1	1.6	3
AVB	26.8	200.8	4.9	19.7	1.5	1.1	2.7	4
AVB	28.0	202.4	3.8	20.5	1.4	1.8	2.7	4
AVB	29.0	201.4	3.8	18.6	1.0	0.7	3.8	7
AVB	30.8	203.2	4.0	18.6	0.9	0.5	3.1	5
AVB	32.4	203.4	3.3	18.3	1.8	0.5	1.0	3
BBO	292.0	227.9	44.9	47.6	1.6	0.9	1.8	6
BPI	128.9	336.6	−3.5	41.0	0.7	1.6	3.0	6
BPI	130.0	336.6	−2.5	39.6	2.0	0.7	0.8	4
BPI	131.1	338.2	−3.0	40.1	2.0	1.4	2.1	6
BPI	132.0	339.4	−1.7	40.3	1.1	0.7	2.2	9
BPI	132.7	340.6	−1.9	40.0	1.1	0.6	1.8	4
BPI	134.3	341.5	−1.0	39.5	1.3	0.9	2.3	8
BPI	134.9	341.1	−1.5	39.5	1.5	0.9	2.2	10
BPI	136.0	342.7	−0.5	40.1	1.2	0.9	3.3	8
BPI	136.8	343.2	−0.2	39.6	1.1	1.0	4.9	12
BPI	138.2	344.8	1.1	39.6	1.4	2.5	5.5	17
BPI	139.0	344.7	0.4	39.5	1.8	1.0	4.0	12
BPI	139.9	344.8	1.1	39.3	1.2	1.2	3.2	11
BPI	141.0	345.3	1.7	38.2	2.0	1.0	3.4	10
BPI	142.0	347.8	1.6	39.1	2.0	1.0	3.8	14
BPI	142.9	349.3	3.4	37.1	2.0	2.6	3.4	9
BPI	144.0	350.1	3.0	38.0	1.7	4.9	3.3	14
BPI	144.9	349.3	2.8	37.8	1.6	1.1	2.0	7
BPI	146.0	351.0	4.1	38.9	1.9	2.5	3.2	10
BPI	147.0	353.0	4.0	38.4	1.7	1.1	3.1	9
BPI	147.9	351.7	3.5	35.7	2.0	4.9	2.4	9
BPI	148.9	354.0	4.6	38.7	1.7	1.0	3.2	10
BPI	149.9	355.5	5.1	37.4	1.9	1.7	3.2	10
BPI	151.1	354.9	5.5	37.2	1.4	1.0	0.7	6
BPI	152.0	356.6	4.9	37.6	1.5	1.0	2.9	9
BPI	152.9	356.8	6.9	38.5	2.0	3.1	3.2	10
BPI	154.0	357.3	6.7	38.4	2.0	2.7	3.4	13
BPI	155.0	358.9	6.7	38.7	1.5	1.6	3.8	7
BPI	156.1	357.8	8.1	36.6	1.0	6.7	3.0	6
BPI	158.6	1.3	8.9	37.3	1.3	1.7	2.2	4
CAN	108.8	31.3	48.3	57.1	1.3	1.0	2.2	4
CAN	109.8	33.2	47.6	57.4	1.6	0.7	3.1	5
CAN	110.9	34.2	49.1	56.9	1.4	0.8	3.7	9
CAN	112.0	34.1	48.7	56.1	2.0	1.8	2.6	5
CAN	113.0	37.3	49.7	56.1	1.5	1.7	1.6	3
CAP	114.0	299.9	−12.2	24.8	0.4	0.5	3.1	5
CAP	114.9	299.1	−12.4	24.3	2.0	1.3	3.2	10
CAP	117.0	301.6	−11.5	24.5	1.5	0.8	5.6	16
CAP	117.9	302.5	−11.5	24.3	1.3	0.7	3.4	7
CAP	118.8	302.7	−11.0	24.2	2.0	1.2	5.4	14
CAP	120.1	303.4	−11.0	24.2	2.0	1.2	4.8	10
CAP	121.2	303.1	−10.7	23.3	1.3	0.6	10.0	18
CAP	122.1	303.5	−10.6	23.2	1.3	0.8	10.0	23
CAP	123.1	303.7	−10.4	22.7	0.9	0.3	3.7	10
CAP	124.0	303.7	−10.3	22.4	1.1	0.6	7.2	15
CAP	125.1	304.7	−9.8	22.3	0.6	0.4	7.4	17
CAP	126.0	305.2	−9.5	22.4	0.8	0.9	10.0	40
CAP	127.0	305.9	−9.4	21.9	1.0	0.6	10.0	31
CAP	127.8	306.6	−9.0	21.9	1.1	0.5	10.0	42
CAP	128.9	307.0	−9.0	21.7	1.1	0.5	10.0	46
CAP	129.9	307.2	−8.4	21.7	1.1	0.4	10.0	30
CAP	131.0	308.0	−8.4	21.3	1.2	0.6	10.0	37
CAP	131.9	308.5	−8.0	21.0	1.3	0.6	5.4	18
CAP	132.9	309.6	−7.8	20.9	1.4	1.0	6.0	17
CAP	134.0	309.4	−7.3	20.6	1.2	0.5	4.6	11
CAP	135.0	310.4	−7.1	20.8	1.2	0.9	4.0	9
COM	252.0	145.9	37.0	62.7	0.9	1.1	3.4	11
COM	253.2	147.6	37.1	62.8	0.8	1.5	2.8	8
COM	253.7	148.3	36.6	62.9	1.3	0.5	3.7	8
COM	254.9	149.3	36.2	63.2	0.9	1.0	10.0	20
COM	256.0	150.1	35.7	63.4	0.8	1.0	7.5	20
COM	256.9	151.1	35.3	63.2	1.2	0.9	10.0	19
COM	258.0	152.5	34.8	62.9	1.0	0.9	10.0	27
COM	259.0	153.0	34.5	63.6	1.0	0.8	10.0	31
COM	260.1	154.2	34.0	63.2	0.8	0.6	10.0	26
COM	261.0	155.1	33.7	63.1	0.8	1.2	10.0	33

Table 2 – J14 Clusters List — continued.

code	lsp	ra	de	vg	sdr	sdv	sig	ns
COM	262.0	156.0	33.2	63.2	0.8	0.9	10.0	34
COM	263.0	156.7	32.7	63.1	1.0	0.7	10.0	33
COM	264.0	157.7	32.3	63.2	0.8	1.0	10.0	45
COM	265.0	158.6	31.9	63.3	0.8	0.8	10.0	60
COM	266.1	159.4	31.5	63.3	0.7	1.1	10.0	80
COM	267.0	160.5	31.1	63.3	0.9	1.0	10.0	65
COM	268.0	161.3	30.7	63.3	0.8	1.3	10.0	74
COM	268.9	162.0	30.3	63.2	0.9	0.8	10.0	78
COM	270.0	163.2	29.8	63.2	0.9	1.4	10.0	60
COM	271.0	164.0	29.3	63.0	1.0	1.9	10.0	69
COM	272.1	164.7	28.9	63.1	0.9	1.1	10.0	54
COM	273.0	166.3	28.5	63.7	0.8	0.7	10.0	26
COM	274.0	166.8	28.1	63.5	0.9	0.6	10.0	47
COM	275.1	167.7	27.5	63.6	0.9	1.1	10.0	48
COM	276.0	168.4	27.2	63.3	1.0	1.3	10.0	45
COM	277.0	169.3	26.9	62.9	1.2	1.3	10.0	46
COM	278.0	170.2	26.4	63.5	0.8	1.0	10.0	32
COM	279.0	171.3	26.0	63.2	0.9	0.9	10.0	24
COM	280.0	172.3	25.4	63.2	1.0	1.3	10.0	36
COM	281.0	172.8	25.0	63.2	1.1	1.0	10.0	32
COM	281.8	173.5	24.5	63.1	1.1	1.4	10.0	25
COM	283.0	174.4	24.1	63.6	1.1	0.9	5.4	21
COM	284.1	175.4	23.7	63.2	0.9	0.8	10.0	20
COM	285.0	176.4	23.2	63.1	1.2	1.3	10.0	34
COM	286.0	177.8	23.1	63.2	1.2	1.1	5.2	19
COM	287.1	178.1	22.3	63.3	0.7	1.2	10.0	22
COM	287.8	178.7	22.0	63.6	1.4	0.9	5.6	16
COM	289.0	179.8	21.2	63.2	1.4	1.0	5.2	19
COM	290.0	180.1	21.2	63.0	1.4	0.7	10.0	22
COM	291.0	180.6	20.3	62.6	1.1	1.9	4.2	12
COM	292.1	182.3	19.7	63.6	1.3	0.5	3.3	8
COM	292.9	182.8	19.5	62.9	1.6	1.0	5.8	19
COM	293.9	183.7	19.6	63.4	1.0	1.3	3.1	9
COM	295.2	185.5	18.4	62.8	1.1	0.5	2.7	7
COM	296.1	184.9	18.2	63.4	1.6	0.8	1.1	7
COM	296.9	186.3	17.9	63.5	1.7	0.6	2.9	12
COM	297.8	186.2	17.8	62.5	2.0	1.6	1.2	11
COM	300.0	189.2	17.3	63.4	1.6	1.0	2.7	7
COM	300.9	188.6	16.1	62.4	2.0	1.5	1.2	7
COM	302.3	190.2	14.1	63.8	2.0	1.4	2.9	10
COM	303.8	191.7	15.3	62.5	1.1	1.4	3.7	11
COM	306.0	193.0	14.4	62.4	1.1	2.8	4.1	15
COM	307.0	195.8	14.1	62.8	0.9	2.1	2.6	5
COM	308.2	194.7	13.1	62.9	1.3	1.1	1.7	5
COM	308.9	197.0	13.2	63.4	1.8	1.2	4.2	12
COM	310.0	196.9	12.2	63.9	1.2	0.8	2.6	6
COM	311.1	197.8	12.2	61.8	1.7	2.1	3.4	7
COM	311.9	196.9	12.0	61.8	1.5	0.4	2.6	6
COM	313.2	199.9	10.9	63.0	2.0	0.9	1.9	10
CTA	222.9	69.6	31.1	44.4	1.4	1.3	1.8	4
DAB	262.9	211.3	21.6	59.9	1.5	1.1	4.0	10
DAB	263.9	212.4	22.1	59.2	1.0	0.3	3.1	5
DAB	265.0	213.8	22.6	60.0	0.9	0.9	2.7	4
DAD	254.9	209.2	58.4	40.9	2.0	2.1	3.0	17
DAD	254.7	200.7	66.4	41.6	2.0	2.6	1.7	8
DAD	255.7	213.6	57.9	40.6	1.9	1.8	1.1	8
DAD	257.1	208.1	60.9	40.1	2.0	2.6	3.0	16
DAD	258.0	216.1	55.9	41.0	2.0	1.8	1.6	6
DAD	259.1	197.7	65.3	43.0	1.6	2.3	1.4	6
DAD	260.1	214.3	54.7	41.8	2.0	2.3	2.9	10
DAD	260.2	201.2	65.1	40.7	2.0	2.5	1.0	6
DAD	264.0	213.8	59.0	39.6	2.0	1.2	1.1	7
DAD	265.0	216.2	53.6	42.2	2.0	3.4	3.4	11
DAD	267.0	214.0	57.4	41.9	2.0	2.6	2.4	10
DAD	275.2	218.0	59.5	39.4	2.0	4.1	2.5	8
DAD	277.9	220.5	57.4	40.0	0.9	2.0	1.9	5
DAD	279.0	221.5	55.2	39.2	1.4	0.8	0.8	5
DBC	276.0	124.7	11.0	39.3	2.0	2.9	4.2	12
DEV	275.0	196.5	10.8	69.6	0.9	0.9	1.8	6
DEX	268.0	158.9	−4.0	68.5	1.4	1.6	2.9	9
DMH	262.1	149.7	−23.8	62.3	2.0	1.6	2.5	10
DMH	263.1	150.4	−23.8	62.7	0.7	0.4	2.2	5
DMH	264.1	151.9	−23.9	61.9	2.0	2.9	3.3	12
DMH	266.2	153.3	−25.0	63.1	0.9	1.2	2.7	7
DMH	267.9	155.4	−23.9	63.6	1.1	0.8	3.0	6
DMH	269.0	155.8	−25.3	62.5	2.0	2.0	3.4	11
DMH	270.0	157.2	−24.8	62.7	1.2	2.9	2.7	7
DOU	268.9	158.0	42.9	56.4	1.4	0.7	5.3	12
DOU	270.1	160.3	42.8	56.8	1.1	0.5	2.5	8
DRV	252.0	184.3	13.6	68.2	1.2	1.0	2.8	11
DRV	253.0	185.3	13.3	68.2	1.3	1.4	4.2	12
DRV	253.8	185.2	10.9	68.3	2.0	1.7	3.4	9
DRV	256.0	187.6	13.3	68.3	0.8	1.0	2.7	7
DRV	257.0	189.5	13.1	68.5	1.6	1.0	2.3	8
DRV	259.0	190.4	12.1	68.2	1.5	1.3	2.7	7
DRV	260.0	190.6	12.1	68.5	2.0	0.8	3.2	11
DRV	261.2	191.9	11.5	68.4	0.6	0.7	2.6	5
DRV	263.1	194.4	12.4	67.6	1.3	1.1	3.4	7
DRV	264.3	195.8	13.3	67.9	0.6	0.5	2.2	4
DSX	188.8	158.0	−2.3	32.5	1.9	1.3	2.7	4
DSX	189.9	158.2	−3.5	32.2	2.0	1.0	2.2	3
DUM	267.9	219.1	84.3	29.6	1.6	0.6	3.3	8
DUM	272.3	214.8	82.4	29.8	2.0	0.9	1.0	3
ECV	300.8	190.4	−17.9	66.9	0.6	1.0	1.8	4
EGE	197.1	94.9	29.0	69.7	2.0	1.4	2.4	13
EGE	200.7	95.8	29.5	69.4	1.3	1.3	2.2	7
EGE	201.9	99.4	28.1	69.4	1.5	1.4	2.2	9
EGE	204.1	99.3	29.1	68.7	2.0	1.1	3.7	18
EGE	205.9	101.8	28.1	68.6	1.6	1.3	3.9	11
EGE	207.1	103.3	27.7	69.5	1.4	1.3	3.7	17
EGE	208.0	104.2	28.4	68.2	2.0	1.8	3.8	21
EGE	208.8	104.4	27.5	68.4	1.3	0.9	2.3	6
EGE	210.0	104.7	27.3	68.5	1.1	0.8	1.7	5
EGE	210.9	106.1	27.1	69.0	0.8	0.5	3.4	10
EGE	212.0	106.7	27.6	69.7	1.5	1.7	3.4	10
EGE	212.9	108.0	27.3	69.2	1.0	0.6	1.8	7
EGE	214.0	107.5	26.1	68.5	1.7	1.6	3.9	15
EGE	215.9	109.8	26.6	68.6	1.2	1.3	2.8	8
EHY	246.2	123.4	0.9	62.0	1.6	0.9	1.6	6
EHY	249.1	126.0	3.4	62.7	1.4	1.2	3.7	12
EHY	250.0	127.8	2.8	63.3	1.5	0.5	1.8	7
EHY	251.0	127.5	3.1	59.2	1.6	12.5	3.4	11
EHY	252.1	129.8	3.3	63.0	1.4	0.7	3.9	15
EHY	253.0	130.3	2.8	62.4	1.3	2.0	4.9	18
EHY	254.0	129.0	2.8	61.3	2.0	2.3	4.3	19
EHY	254.9	131.5	2.3	62.6	1.1	0.9	4.5	12
EHY	256.0	132.1	2.5	62.5	1.4	1.5	5.4	21
EHY	257.1	132.8	2.3	62.4	1.5	0.8	4.7	16
EHY	258.0	134.1	2.2	62.8	0.9	1.0	4.2	12
EHY	259.0	135.1	2.0	62.7	1.6	1.6	4.0	17
EHY	259.9	135.5	1.9	62.6	1.1	0.7	4.5	12
EHY	261.0	136.5	1.9	62.3	1.3	1.1	4.3	10
EHY	261.9	136.9	1.4	62.3	1.4	1.0	6.9	23
EHY	263.1	137.6	1.3	61.9	1.2	0.7	5.4	14
EHY	263.9	138.5	0.7	62.0	1.2	1.6	10.0	20
EHY	264.8	139.4	0.8	62.3	1.4	1.3	3.0	11
EHY	266.1	140.7	0.4	62.3	1.2	0.6	2.3	8
EHY	267.1	141.1	1.3	61.6	1.9	1.2	4.7	14
EHY	268.0	141.6	0.9	61.7	1.4	1.1	4.0	9
EHY	269.0	142.8	−0.2	61.9	1.5	1.0	3.7	11
ELY	47.0	293.8	43.6	44.7	2.0	1.3	2.4	10
ELY	48.0	292.3	42.5	44.9	2.0	1.2	3.7	9
ELY	49.1	290.6	43.4	44.1	1.7	0.9	4.2	13
ELY	50.0	291.0	43.4	44.5	1.6	1.1	10.0	29
ELY	51.1	290.9	43.8	44.1	1.1	0.7	3.7	12
ELY	52.1	291.6	44.7	43.7	1.3	1.0	4.2	11
EOP	355.1	258.2	−16.1	70.8	0.9	0.5	2.6	5
EOP	356.2	259.2	−16.6	70.9	0.6	0.4	2.7	4
EPV	247.8	188.9	10.0	65.9	0.8	0.7	2.6	6
EPV	248.9	190.0	9.3	66.3	0.7	0.5	2.7	4
EPV	251.9	192.5	9.5	66.1	0.8	1.7	3.0	7
EPV	253.1	193.1	8.6	65.8	1.0	0.7	3.8	7

Table 2 – J14 Clusters List — continued.

code	lsp	ra	de	vg	sdr	sdv	sig	ns
EPV	255.0	195.0	7.7	66.0	1.2	0.9	3.7	11
EPV	255.9	194.8	7.5	66.4	2.0	1.3	2.0	11
EPV	257.2	197.0	7.1	66.2	0.9	1.1	3.9	11
EPV	258.1	197.3	7.2	66.2	1.1	0.7	3.4	10
EPV	259.1	197.9	7.2	66.2	1.1	0.7	4.5	9
EPV	259.9	198.5	6.9	66.5	1.0	0.5	3.7	9
EPV	261.0	199.6	6.4	66.1	1.4	0.7	3.3	8
EPV	263.0	201.5	6.0	66.3	1.0	0.6	4.2	12
EPV	264.1	201.8	5.4	65.7	1.4	0.6	2.4	7
EPV	266.1	204.1	5.1	66.5	0.5	0.4	2.6	5
EPV	267.1	204.8	4.7	66.6	0.9	0.8	3.7	11
EPV	268.0	205.2	5.1	66.6	0.8	1.6	3.7	10
EPV	269.1	206.1	4.3	66.1	1.0	1.5	4.5	12
EPV	270.2	207.8	4.8	66.2	1.5	1.1	3.9	11
EPV	272.2	208.8	4.2	66.8	1.4	0.5	3.7	11
EPV	272.9	208.3	2.8	66.9	2.0	0.9	4.5	9
EPV	274.0	210.6	3.6	66.1	1.0	1.3	4.5	12
EPV	275.1	211.3	3.4	67.1	0.8	0.9	4.3	10
EPV	275.9	212.2	3.7	66.0	1.5	1.4	5.3	12
EPV	276.9	212.7	2.9	66.3	1.5	1.4	5.2	16
EPV	278.0	213.6	3.3	66.4	1.3	1.1	4.2	11
EPV	279.9	215.2	2.3	66.7	1.5	1.1	2.9	12
EPV	281.1	215.5	1.4	66.4	2.0	1.3	3.9	11
EPV	281.8	217.5	2.9	65.4	2.0	1.8	2.2	10
EPV	282.9	217.7	2.5	66.9	1.1	1.9	3.1	9
EPV	284.0	217.6	2.2	66.7	1.7	1.1	1.4	8
EPV	285.0	219.9	1.0	66.4	1.3	0.8	3.7	10
EPV	286.1	220.6	1.3	66.0	1.6	2.2	3.3	8
EPV	286.8	221.2	1.8	66.0	1.5	1.9	4.5	12
EPV	287.9	222.3	0.7	65.7	2.0	1.4	4.3	15
ERI	123.1	31.6	−15.7	64.7	1.1	0.4	1.8	4
ERI	126.2	34.4	−15.4	64.5	1.5	0.6	4.2	8
ERI	127.1	34.7	−15.5	64.2	1.1	1.2	3.7	8
ERI	127.9	35.2	−14.6	64.0	1.4	1.3	3.4	9
ERI	128.9	36.6	−14.7	64.4	1.4	0.4	3.7	8
ERI	130.9	38.8	−14.5	64.0	1.6	0.8	5.3	15
ERI	131.9	39.2	−13.2	64.6	2.0	0.8	4.7	15
ERI	132.8	40.7	−14.1	64.1	1.1	0.7	2.7	7
ERI	134.2	40.5	−12.6	64.1	1.1	1.0	5.6	16
ERI	134.9	42.1	−13.1	63.6	1.8	0.8	5.8	15
ERI	135.9	42.7	−12.5	64.0	1.7	0.9	2.3	8
ERI	136.9	43.4	−11.9	64.0	1.1	0.9	5.0	15
ERI	137.9	44.1	−12.3	64.2	1.2	0.9	4.8	13
ERI	138.9	45.3	−11.3	64.4	1.4	1.0	5.0	11
ERI	139.9	46.0	−12.1	64.2	2.0	0.5	4.6	11
ERI	141.2	47.3	−11.0	64.4	2.0	1.1	3.4	14
ERI	142.2	48.1	−10.7	63.8	1.2	0.4	3.0	7
ERI	143.0	48.8	−10.0	64.1	1.6	1.0	2.8	8
ERI	144.0	50.3	−11.8	63.2	2.0	1.8	2.4	7
ERI	144.9	49.3	−8.3	64.8	2.0	1.5	3.1	14
ERI	146.9	51.9	−8.9	64.2	2.0	1.3	4.9	16
ERI	148.1	53.5	−9.2	61.7	2.0	3.6	1.2	9
ESL	328.1	173.8	−4.4	40.4	1.5	2.0	2.6	6
ETA	34.2	330.6	−4.8	64.5	1.1	0.9	3.5	6
ETA	35.0	331.0	−4.5	64.9	0.7	1.7	3.4	7
ETA	35.9	331.6	−3.9	64.3	1.1	1.0	3.1	5
ETA	37.2	332.5	−3.8	65.1	1.0	0.9	6.8	18
ETA	38.2	333.2	−3.5	64.9	0.9	1.2	10.0	19
ETA	39.0	333.7	−3.2	65.1	0.9	1.0	10.0	38
ETA	39.9	334.2	−2.8	65.2	0.7	0.8	10.0	35
ETA	41.0	334.8	−2.5	65.3	0.7	0.8	10.0	65
ETA	42.0	335.6	−2.1	65.2	0.7	0.8	10.0	72
ETA	43.0	336.2	−1.8	65.4	0.8	1.1	10.0	96
ETA	44.1	336.9	−1.4	65.5	0.8	1.2	10.0	241
ETA	45.1	337.5	−1.1	65.5	0.7	2.0	10.0	306
ETA	46.2	338.3	−0.7	65.8	0.8	1.1	10.0	185
ETA	47.0	338.8	−0.4	65.5	0.8	1.3	10.0	238
ETA	48.0	339.4	−0.1	65.7	0.9	1.1	10.0	114
ETA	48.9	340.0	0.2	65.9	0.9	0.9	10.0	92
ETA	49.9	340.6	0.5	65.8	0.9	1.1	10.0	88
ETA	51.0	341.6	0.8	65.8	0.9	1.3	10.0	73
ETA	52.2	342.5	1.2	65.9	0.9	1.2	10.0	46
ETA	53.1	343.2	1.7	66.2	1.0	1.3	10.0	50
ETA	54.0	343.7	1.9	65.9	1.1	1.0	10.0	33
ETA	55.0	344.1	2.5	65.8	0.6	0.7	2.6	5
ETA	56.0	345.0	2.4	66.0	0.8	0.5	7.4	17
ETA	56.8	345.3	3.0	65.8	0.8	0.9	10.0	19
ETA	57.9	346.4	3.2	65.4	1.1	0.9	10.0	20
ETA	58.8	347.0	3.9	66.1	1.0	1.0	4.5	12
ETA	60.2	348.1	3.8	66.5	1.2	1.3	5.3	12
ETA	60.7	349.1	4.2	66.5	1.5	0.7	2.6	5
ETA	62.1	349.4	4.8	66.4	1.0	0.6	3.3	8
ETA	63.1	349.8	5.8	66.9	2.0	1.3	3.0	7
ETA	63.9	351.2	5.4	66.6	0.8	0.5	2.2	3
ETA	65.1	352.7	5.4	65.8	1.1	0.6	3.1	5
EVE	246.2	121.0	−48.0	38.1	2.8	1.0	2.3	11
EVE	247.0	127.6	−44.8	42.2	1.8	0.9	2.6	5
EVE	247.8	135.3	−46.4	43.6	3.1	2.7	2.6	6
EVE	249.0	129.2	−46.0	41.6	2.6	0.9	8.1	26
EVE	249.7	131.0	−45.3	43.1	2.3	0.8	5.3	24
EVE	250.8	127.8	−44.1	42.6	2.1	1.2	5.8	26
EVE	252.1	131.4	−46.6	41.7	2.1	1.3	6.3	27
EVE	253.1	132.5	−46.9	42.1	2.6	1.6	10.0	31
EVE	253.8	133.4	−46.5	42.5	2.6	1.7	10.0	30
EVE	254.9	131.9	−46.1	42.9	2.7	2.0	5.4	27
EVE	257.1	135.4	−46.4	44.1	3.0	2.2	2.8	18
EVI	1.9	188.7	2.7	26.1	2.0	2.2	3.6	14
EVI	354.0	183.4	4.1	27.8	1.6	1.7	4.2	13
EVI	355.1	183.5	3.7	26.7	1.9	1.0	2.2	9
EVI	355.9	185.8	3.0	27.4	1.4	0.8	4.0	12
EVI	356.9	186.0	3.0	27.9	1.7	1.9	3.7	18
EVI	358.0	187.3	2.5	27.3	1.2	0.9	4.0	12
EVI	358.9	187.6	2.5	26.7	1.2	1.1	5.4	14
EVI	360.0	190.0	0.4	27.8	2.0	1.5	1.9	9
FAQ	107.9	314.8	−3.6	37.7	1.3	1.5	2.6	5
FAQ	109.0	315.2	−4.2	38.0	1.7	1.9	2.6	6
FAQ	111.0	317.2	−3.1	37.2	1.6	0.7	2.6	6
FAQ	112.0	318.5	−2.3	37.4	1.6	0.9	1.8	4
FAQ	112.8	319.7	−3.5	38.2	1.8	1.4	2.1	6
FAQ	114.0	320.6	−2.0	38.8	2.0	3.9	3.1	5
FAQ	114.9	320.3	−3.5	40.4	2.0	1.4	1.3	3
FAQ	115.9	322.1	−1.3	37.1	1.7	1.8	2.3	6
FFH	274.0	161.7	−26.3	63.7	2.0	1.1	3.7	10
FFL	318.0	163.0	−0.3	40.3	2.0	1.9	4.0	10
GAQ	51.0	307.1	16.7	61.6	1.7	0.8	3.4	9
GAQ	52.1	308.5	15.0	63.3	0.9	0.9	2.2	4
GEM	247.1	98.1	34.0	32.4	1.1	0.5	2.3	6
GEM	249.1	101.5	34.9	33.0	1.5	2.0	3.4	10
GEM	249.9	100.1	33.6	34.4	2.0	3.2	9.4	21
GEM	251.0	102.5	34.1	33.1	2.0	2.0	5.2	17
GEM	251.9	103.5	33.6	32.6	1.6	1.7	10.0	37
GEM	253.0	103.8	33.4	32.7	1.4	1.0	10.0	30
GEM	253.9	105.0	33.4	33.3	1.2	1.6	10.0	33
GEM	254.9	106.2	33.3	32.8	1.2	1.1	10.0	98
GEM	256.0	107.3	33.1	33.0	1.3	1.0	10.0	114
GEM	257.0	108.4	33.0	33.1	1.1	1.0	10.0	138
GEM	258.1	109.5	32.9	33.2	1.0	0.9	10.0	225
GEM	259.0	110.4	32.8	33.3	1.0	0.8	10.0	341
GEM	260.1	111.5	32.7	33.4	0.8	0.7	10.0	681
GEM	261.0	112.5	32.5	33.5	0.7	0.7	10.0	1897
GEM	262.0	113.5	32.3	33.6	0.6	0.8	10.0	5566
GEM	262.8	114.2	32.1	33.7	0.6	0.7	10.0	1560
GEM	262.7	114.4	31.9	34.2	2.0	2.2	10.0	38
GEM	263.8	115.3	31.7	33.5	0.8	0.7	10.0	86
GEM	264.9	116.6	31.6	33.1	0.6	0.6	4.3	15
GLI	35.9	224.7	−11.1	28.2	1.0	0.5	3.0	6
GUM	298.0	228.1	68.9	28.2	1.2	0.6	3.7	8
GUM	299.0	227.9	68.5	28.7	1.3	0.7	5.0	11
GUM	300.1	229.8	67.3	28.7	1.3	0.8	3.0	7
HTV	293.1	226.3	0.6	65.9	1.6	0.9	3.0	11
HVI	36.8	203.0	−11.1	18.7	0.7	0.8	3.0	6
HVI	37.9	202.5	−11.0	18.8	0.8	0.4	3.1	5

Table 2 – J14 Clusters List — continued.

code	lsp	ra	de	vg	sdr	sdv	sig	ns
HVI	39.3	202.9	−11.0	18.4	0.9	0.3	3.8	7
HVI	40.0	203.3	−11.6	18.1	0.8	0.4	5.7	13
HVI	42.0	203.7	−12.0	17.4	0.7	0.4	3.1	5
HYD	241.9	113.5	4.9	59.7	0.9	0.7	4.0	9
HYD	243.1	115.2	4.5	59.4	1.7	0.9	2.5	11
HYD	243.9	115.3	4.9	59.6	1.0	1.2	5.0	15
HYD	245.1	116.7	4.4	59.8	1.0	0.9	7.2	15
HYD	246.2	117.4	4.3	59.3	1.0	1.2	10.0	33
HYD	247.0	118.2	4.0	59.4	1.0	1.0	10.0	47
HYD	248.0	118.6	4.1	59.4	0.8	0.9	10.0	51
HYD	249.1	119.5	3.9	59.3	1.0	1.1	10.0	100
HYD	249.9	120.2	3.8	59.3	1.0	1.0	10.0	87
HYD	250.9	121.0	3.6	59.2	0.9	0.9	10.0	117
HYD	252.0	121.7	3.5	59.1	0.9	0.9	10.0	180
HYD	253.0	122.6	3.2	58.9	1.0	1.0	10.0	165
HYD	253.8	123.2	3.1	58.8	1.0	1.0	10.0	97
HYD	254.9	124.1	2.8	58.7	1.1	0.9	10.0	206
HYD	256.0	124.9	2.7	58.7	1.1	0.9	10.0	175
HYD	257.0	125.9	2.5	58.6	1.2	1.1	10.0	161
HYD	258.1	126.8	2.2	58.7	1.4	1.1	10.0	127
HYD	259.0	127.6	2.1	58.5	1.2	0.9	10.0	126
HYD	260.0	128.5	1.8	58.6	1.3	1.0	10.0	91
HYD	260.9	129.3	1.4	58.5	1.4	1.0	10.0	92
HYD	262.0	129.9	1.5	58.5	1.3	0.9	10.0	95
HYD	262.9	130.9	1.1	58.1	1.4	1.1	10.0	63
HYD	264.0	131.9	0.6	58.7	1.7	1.5	10.0	40
HYD	265.0	132.6	0.7	58.3	1.5	1.0	10.0	59
HYD	266.0	133.1	0.7	57.9	1.6	1.3	10.0	38
HYD	266.9	134.3	−0.1	58.4	1.6	1.1	10.0	35
HYD	268.0	134.8	−0.2	57.9	1.2	1.1	5.4	22
HYD	269.0	135.6	−0.6	58.0	1.6	1.5	5.8	25
HYD	270.0	137.5	−1.4	58.5	2.0	1.5	5.1	23
HYD	271.0	138.6	−1.2	57.9	2.0	2.3	10.0	35
HYD	271.9	138.2	−1.5	58.4	2.0	1.3	3.8	13
HYD	273.0	139.4	−1.7	57.8	1.3	1.7	3.0	11
HYD	274.0	141.1	−2.2	58.7	2.0	1.2	3.5	17
HYD	275.1	142.0	−2.8	58.0	2.0	1.4	3.5	17
HYD	276.0	141.9	−2.0	57.4	1.9	1.3	4.3	15
HYD	277.0	142.7	−3.8	57.5	2.0	1.7	2.4	12
HYD	277.8	142.9	−4.9	57.1	1.5	0.7	1.0	4
HYD	280.0	146.4	−3.9	58.1	2.0	1.0	2.6	9
HYD	282.1	147.8	−6.0	57.7	2.0	2.0	3.4	13
JEC	82.2	314.6	33.5	52.7	0.6	0.5	4.0	9
JEO	92.8	245.7	−8.1	13.0	0.8	0.3	3.5	6
JIP	93.8	331.5	29.3	58.6	0.4	0.6	4.5	9
JIP	95.1	333.1	29.6	59.1	0.7	0.8	2.7	4
JLE	279.3	145.1	24.4	53.3	1.5	0.5	2.2	3
JLE	281.8	147.2	24.0	52.5	1.3	0.7	4.2	8
JLE	282.8	147.9	23.8	51.5	1.5	0.5	1.5	2
JLE	283.9	148.6	23.8	52.4	1.5	0.5	1.6	3
JLE	285.8	150.0	23.3	50.9	1.5	0.5	1.0	2
JLE	286.7	150.4	22.7	51.1	1.5	0.5	0.7	1
JPE	107.1	346.7	10.9	64.3	0.9	0.7	3.7	8
JPE	108.0	347.5	10.6	64.2	0.5	0.8	5.7	13
JPE	108.9	348.3	11.0	64.7	0.7	0.7	3.4	9
JPE	110.0	348.8	10.8	64.7	0.7	1.5	2.2	4
JPE	110.8	349.6	11.4	63.9	1.1	1.0	4.3	10
JPE	111.9	350.4	11.7	64.2	1.1	0.9	3.7	9
JPE	114.1	352.4	11.6	64.0	1.3	0.4	3.0	6
JPE	115.0	353.0	12.1	64.4	1.8	0.5	1.0	3
JPE	116.0	354.6	12.9	64.0	1.3	0.4	1.8	4
JPE	117.0	354.5	15.0	64.2	2.0	1.0	2.9	9
JPE	118.0	355.5	13.1	63.9	1.1	0.8	3.0	6
JRC	84.2	320.6	43.9	49.9	0.9	0.7	3.0	6
JRC	85.2	321.4	44.6	50.1	0.9	0.7	3.5	6
JSP	108.8	354.3	9.5	65.8	0.6	1.6	2.2	4
JUG	124.1	279.7	50.6	27.0	1.1	0.3	2.6	5
JUG	125.2	280.3	50.3	27.4	0.6	0.4	5.7	13
JUG	125.8	280.1	50.9	27.4	0.7	0.3	4.5	9
JXA	105.0	29.6	7.6	68.7	1.0	0.5	3.0	6
JXA	107.2	31.4	7.7	68.7	1.3	0.2	2.2	5
KCA	289.1	137.9	8.7	44.6	1.3	2.5	3.0	8
KCA	291.9	139.4	6.9	41.6	1.7	4.1	4.2	8
KCG	136.6	283.4	50.2	22.2	3.4	1.9	5.1	13
KCG	138.0	285.7	49.7	22.5	1.6	0.8	2.7	4
KCG	139.2	285.2	48.5	21.3	2.0	0.4	3.7	8
KCG	140.2	276.9	53.1	20.2	2.0	0.6	0.8	4
KCG	141.1	277.0	51.4	19.5	2.0	1.4	1.7	8
KCG	143.0	276.1	54.3	20.0	1.9	0.7	1.6	7
KCG	145.4	288.1	54.1	23.1	1.4	0.3	3.5	6
KCG	145.4	275.9	58.6	21.3	1.2	0.9	1.5	4
KCG	146.3	290.0	53.5	23.4	1.5	0.7	3.3	8
KCG	146.5	275.1	61.0	22.2	2.0	0.3	0.7	6
KCG	147.8	276.1	60.8	22.0	1.3	0.6	1.5	4
KCG	148.9	268.6	62.1	21.5	0.8	0.2	1.3	3
KCG	150.2	268.9	62.0	21.7	2.0	0.9	1.9	5
KDR	250.0	184.1	71.7	43.1	2.0	1.2	10.0	29
KDR	250.9	184.8	70.5	43.9	2.0	1.5	10.0	51
KDR	251.9	187.2	70.4	43.4	1.5	1.0	10.0	37
KDR	252.9	190.0	70.9	42.4	1.9	1.6	2.1	8
KUM	222.1	143.4	45.7	65.2	0.7	1.2	10.0	23
KUM	222.9	144.3	45.7	65.1	0.6	1.1	10.0	32
KUM	223.9	146.2	45.6	64.8	1.2	2.0	4.2	13
KUM	226.0	148.5	44.4	65.1	0.8	0.9	2.6	9
KUM	227.1	148.0	43.6	64.7	0.4	0.6	1.2	4
KUM	227.9	150.1	44.4	64.6	1.5	0.9	2.6	5
LAD	278.9	140.5	33.7	49.6	0.4	0.5	2.7	4
LAV	258.1	132.7	−38.3	51.2	0.5	0.2	0.6	2
LAV	259.1	133.4	−39.5	49.6	1.2	0.8	1.5	4
LEO	225.9	147.7	25.0	69.9	0.8	1.3	4.8	13
LEO	227.1	148.5	24.6	70.1	1.1	0.8	3.0	8
LEO	227.8	149.4	24.9	70.0	1.0	1.1	4.2	14
LEO	229.1	150.3	24.4	69.9	1.1	1.0	5.8	19
LEO	229.9	150.2	23.7	70.2	0.8	1.2	8.5	23
LEO	230.9	150.9	23.2	69.9	1.0	0.9	10.0	37
LEO	232.0	151.9	23.3	70.1	0.9	1.0	10.0	51
LEO	233.0	152.3	22.8	70.4	0.9	1.4	10.0	82
LEO	234.0	153.0	22.3	70.2	0.8	1.0	10.0	172
LEO	234.9	153.6	22.1	70.2	0.7	1.4	10.0	192
LEO	236.0	154.2	21.7	70.3	0.7	0.9	10.0	249
LEO	237.0	154.9	21.1	70.5	0.8	1.1	10.0	202
LEO	238.0	155.4	20.8	70.4	0.8	1.1	10.0	229
LEO	239.9	156.6	19.9	70.6	0.8	1.1	10.0	64
LEO	241.1	157.5	19.6	70.3	0.8	1.2	10.0	38
LEO	242.0	158.0	19.2	70.4	1.0	0.7	10.0	34
LEO	242.9	158.7	19.0	70.9	1.1	1.2	10.0	26
LEO	243.8	159.1	18.2	70.3	0.8	0.8	5.2	19
LEO	245.0	159.9	18.1	71.0	0.6	1.0	5.2	17
LEO	246.1	160.4	17.4	70.5	0.9	1.8	4.3	15
LEO	247.1	161.5	17.7	70.7	1.7	1.2	4.9	17
LEO	249.9	163.2	16.1	70.8	1.4	1.5	2.9	10
LEO	252.0	164.3	15.5	70.5	1.8	1.2	4.3	16
LEO	254.8	166.0	14.3	71.4	1.8	0.8	2.2	11
LEO	255.9	165.7	14.5	68.8	1.1	1.4	1.6	6
LEO	256.9	167.1	13.5	71.1	1.1	0.5	3.0	7
LMI	205.0	154.3	37.6	61.9	1.6	1.2	2.1	6
LMI	205.9	156.7	37.4	61.5	0.3	0.2	2.7	4
LMI	207.0	157.6	37.4	61.6	0.7	0.8	10.0	25
LMI	207.9	158.7	37.3	61.4	0.8	0.7	10.0	29
LMI	208.9	160.0	37.0	61.3	0.8	0.6	6.3	16
LMI	209.9	160.6	36.3	62.0	0.5	0.7	4.8	10
LMI	210.9	161.8	36.3	61.2	1.0	0.7	5.3	12
LMI	211.8	163.1	35.8	60.9	1.0	0.8	4.7	14
LMI	212.8	164.0	35.7	61.3	1.4	0.8	4.8	13
LMI	213.9	165.5	35.5	60.9	1.4	1.1	4.3	10
LMI	214.8	166.0	35.1	60.6	1.0	1.5	4.0	9
LUM	213.0	156.9	50.7	60.2	0.9	0.6	2.2	5
LUM	213.9	157.4	49.9	61.0	0.9	0.7	2.6	5
LUM	214.9	158.5	49.5	60.3	1.4	1.2	3.4	9
LUM	215.8	160.0	50.0	58.8	1.8	2.0	3.0	6
LYR	28.2	269.9	34.9	44.5	2.3	2.6	1.0	4
LYR	29.1	269.1	34.3	46.0	1.4	1.3	2.6	6

Table 2 – J14 Clusters List — continued.

code	lsp	ra	de	vg	sdr	sdv	sig	ns
LYR	30.0	269.9	33.7	46.2	1.4	1.3	4.2	12
LYR	31.1	270.7	33.8	46.2	1.2	0.7	10.0	71
LYR	32.1	272.0	33.4	46.7	1.0	0.7	10.0	246
LYR	32.8	272.8	33.3	46.9	1.1	0.8	10.0	154
LYR	32.9	278.3	30.4	49.0	1.5	1.5	2.2	5
LYR	33.9	273.9	33.0	47.2	1.5	1.0	10.0	32
LYR	34.7	275.7	32.7	47.5	2.0	0.6	2.2	7
LYR	35.7	277.7	33.4	46.9	1.7	1.3	2.2	5
MBC	54.1	301.6	−15.6	65.9	0.8	0.9	3.8	7
MCB	237.0	96.7	−22.0	45.6	2.0	1.2	1.8	4
MCB	238.0	94.0	−20.7	44.0	1.2	0.7	2.7	4
MLT	256.9	150.6	28.3	64.7	0.9	1.1	1.5	4
MLT	258.9	152.2	28.7	65.3	1.9	1.2	2.4	9
MON	247.9	93.8	9.9	43.1	1.4	1.0	3.3	8
MON	249.0	94.9	9.3	43.2	1.1	0.7	3.0	7
MON	249.7	95.5	8.4	41.9	0.8	1.1	3.8	7
MON	250.9	95.7	8.6	41.6	0.8	1.1	3.7	11
MON	252.0	96.3	9.0	42.3	1.0	1.0	10.0	28
MON	253.1	96.8	9.1	42.2	1.0	0.9	10.0	21
MON	253.9	97.3	8.9	42.0	1.2	1.5	5.4	21
MON	254.9	98.2	8.5	41.7	1.1	0.7	10.0	56
MON	255.9	98.9	8.6	41.4	1.2	1.1	10.0	58
MON	257.0	99.7	8.3	41.4	0.9	0.8	10.0	74
MON	258.0	100.4	8.3	41.3	0.8	1.0	10.0	58
MON	258.9	100.9	8.0	40.9	0.8	0.8	10.0	64
MON	260.0	101.7	7.9	40.7	0.9	0.8	10.0	54
MON	260.9	102.4	7.7	40.8	1.0	0.7	10.0	56
MON	262.0	103.0	7.8	40.7	1.1	0.7	10.0	51
MON	263.0	103.7	7.5	40.6	1.3	1.1	10.0	38
MON	264.0	104.1	7.6	40.0	1.2	0.8	10.0	34
MON	264.9	104.9	7.5	40.0	0.9	0.7	10.0	22
MON	266.0	105.8	7.1	39.7	1.3	1.0	5.3	24
MON	266.9	106.2	6.9	39.2	1.2	0.7	6.8	18
MON	267.9	106.8	6.8	38.9	0.5	0.9	3.0	6
MON	268.9	107.5	6.7	38.9	1.0	0.5	4.5	9
MON	272.0	109.6	5.3	38.8	2.0	1.3	2.1	8
MVE	264.1	148.3	−37.7	54.4	1.9	1.6	3.0	6
MVE	269.0	157.9	−40.0	56.7	1.2	0.8	2.6	5
NEV	245.9	179.8	−4.5	66.8	0.9	0.5	3.1	5
NFL	247.1	179.8	13.4	68.2	0.8	1.8	2.7	7
NFL	248.1	180.1	13.5	68.1	1.0	0.6	1.5	4
NHD	226.1	123.4	−4.3	65.3	1.7	0.4	1.8	7
NHE	35.0	260.7	37.3	40.1	1.1	0.9	3.5	6
NHE	35.8	263.0	37.0	40.7	1.6	0.8	4.3	10
NIA	150.7	351.2	−0.3	31.8	1.9	2.7	1.6	6
NIA	151.9	350.5	−2.5	31.9	2.0	2.8	1.0	9
NIA	153.8	350.4	−1.6	28.5	2.0	4.4	2.7	7
NIA	155.0	351.4	−0.1	30.5	1.2	2.2	0.6	5
NIA	158.3	355.1	2.1	29.5	1.0	1.6	1.7	5
NID	223.0	191.9	69.2	42.1	2.0	1.7	2.2	7
NOO	229.1	77.8	15.2	41.3	1.5	5.2	2.6	5
NOO	232.1	78.0	14.9	40.4	2.0	3.3	2.1	9
NOO	232.8	80.1	15.9	43.4	1.1	2.2	3.4	9
NOO	234.0	81.4	16.1	43.6	1.4	2.2	3.4	10
NOO	234.9	79.9	14.8	41.8	1.9	3.4	3.4	7
NOO	235.9	82.0	16.4	42.8	1.7	2.5	2.3	11
NOO	236.9	82.7	14.7	41.9	1.8	2.6	1.4	8
NOO	238.0	83.6	15.5	43.3	1.9	1.8	5.5	24
NOO	239.2	85.4	14.8	42.7	2.0	2.0	4.0	13
NOO	240.0	86.1	16.2	43.4	1.4	1.4	4.9	17
NOO	241.0	86.0	16.0	42.6	1.6	2.6	10.0	25
NOO	242.0	86.9	16.2	43.6	1.4	0.7	10.0	20
NOO	242.9	88.1	15.7	43.3	1.4	1.3	8.3	24
NOO	243.9	88.8	15.5	42.9	1.3	0.9	10.0	26
NOO	245.0	89.4	15.3	43.3	1.1	0.7	10.0	29
NOO	246.1	90.2	15.5	43.1	1.1	1.2	10.0	56
NOO	247.0	91.0	15.4	42.6	1.2	1.6	10.0	54
NOO	247.9	91.4	15.3	42.4	1.2	1.4	10.0	58
NOO	249.0	92.2	15.2	42.3	1.2	0.9	10.0	50
NOO	249.8	93.1	15.4	42.3	1.2	1.3	10.0	33
NOO	250.9	93.5	15.1	42.0	1.1	0.7	10.0	41
NOO	252.0	94.1	15.2	41.2	1.5	2.0	10.0	38
NOO	252.9	94.7	14.8	41.2	1.3	1.9	8.2	27
NOO	254.0	95.4	14.4	41.4	1.1	0.6	4.5	14
NOO	254.9	96.1	14.9	40.7	1.6	1.7	10.0	35
NOO	256.0	96.6	14.8	40.6	1.5	0.9	6.9	24
NOO	257.0	98.6	13.9	39.9	2.0	2.7	5.0	21
NOO	257.9	97.7	14.5	39.1	1.0	2.8	2.3	8
NOO	259.0	98.2	14.8	39.5	1.6	1.6	2.7	10
NOO	260.1	99.9	14.7	39.5	1.7	2.3	3.1	9
NPI	182.1	12.7	9.2	28.1	1.4	3.1	1.8	7
NPI	184.0	11.8	9.5	25.8	1.9	1.5	1.4	5
NSU	241.0	147.5	59.8	55.3	0.8	0.7	3.4	9
NSU	241.7	148.5	59.4	55.1	1.4	1.1	3.3	8
NSU	242.8	149.7	58.3	55.1	0.8	1.0	2.3	6
NTA	200.0	31.7	16.4	29.5	1.5	1.9	2.4	7
NTA	200.8	36.9	17.3	31.5	1.5	2.8	3.0	7
NTA	202.0	40.1	17.5	33.6	1.3	1.4	2.1	8
NTA	202.8	39.7	16.9	33.3	1.8	1.4	8.4	35
NTA	203.9	35.3	17.6	28.1	1.0	1.1	2.1	6
NTA	205.0	38.9	17.7	30.5	1.7	2.0	4.3	15
NTA	205.9	35.4	17.2	28.7	1.0	1.8	3.0	7
NTA	206.1	43.0	18.3	33.8	0.9	0.6	3.8	7
NTA	207.1	40.7	17.4	30.2	2.0	2.4	1.5	29
NTA	208.0	43.9	18.8	31.7	1.3	1.6	3.0	11
NTA	208.9	39.1	17.7	28.2	2.0	0.7	1.4	5
NTA	210.4	40.2	18.0	27.8	1.5	1.3	3.0	6
NTA	211.1	44.8	19.4	30.4	1.9	1.8	10.0	25
NTA	212.1	45.3	19.5	30.7	2.0	3.9	4.8	19
NTA	213.0	44.6	18.4	28.9	2.0	1.8	3.3	30
NTA	214.1	46.2	19.5	29.7	2.0	1.8	10.0	29
NTA	214.8	46.9	20.2	28.9	1.4	2.0	10.0	26
NTA	216.0	47.4	20.1	28.7	1.7	1.5	5.4	22
NTA	217.0	44.2	20.6	27.0	0.7	0.7	3.1	5
NTA	217.2	49.2	20.4	29.5	1.4	1.3	10.0	33
NTA	217.8	49.7	20.8	29.2	1.5	1.4	10.0	39
NTA	219.0	49.7	20.8	28.6	1.9	1.7	10.0	63
NTA	220.0	51.6	21.2	28.9	1.5	1.3	10.0	25
NTA	221.0	52.0	21.2	28.8	1.3	1.1	10.0	96
NTA	222.0	52.6	21.4	28.5	1.3	1.1	10.0	106
NTA	223.1	53.4	21.6	28.3	1.2	1.1	10.0	100
NTA	223.9	54.0	21.8	28.3	1.5	1.6	10.0	68
NTA	225.1	55.2	21.9	28.3	1.3	1.3	10.0	74
NTA	226.0	55.8	22.0	28.2	1.4	1.1	10.0	58
NTA	227.1	56.3	22.3	27.7	1.3	1.2	10.0	52
NTA	228.0	57.2	22.6	27.5	1.3	1.2	10.0	71
NTA	229.0	57.9	22.6	27.4	1.3	1.1	10.0	78
NTA	230.1	58.9	22.8	27.6	1.2	1.0	10.0	87
NTA	231.0	59.6	22.9	27.4	1.1	1.1	10.0	77
NTA	232.0	60.4	23.1	27.4	1.2	1.3	10.0	129
NTA	232.9	60.9	23.3	27.0	1.2	1.0	10.0	111
NTA	234.0	61.8	23.3	27.0	1.4	1.3	10.0	70
NTA	234.9	62.2	23.5	26.6	1.3	0.8	10.0	55
NTA	236.0	63.3	23.8	26.4	1.3	0.9	10.0	64
NTA	237.0	64.5	23.9	26.5	1.2	0.7	10.0	41
NTA	238.0	64.9	24.0	26.2	1.3	0.9	10.0	63
NTA	239.0	65.7	24.2	26.1	1.3	0.7	10.0	58
NTA	239.9	66.3	24.3	25.6	1.3	0.9	10.0	46
NTA	241.1	67.7	24.5	26.2	1.2	0.9	10.0	39
NTA	242.0	68.1	24.5	25.6	1.4	1.2	10.0	38
NTA	242.9	69.0	24.6	25.6	1.3	0.8	10.0	29
NTA	244.0	69.3	24.8	25.3	1.3	1.0	5.4	20
NTA	245.1	71.1	25.3	25.4	1.1	0.6	5.4	20
NTA	246.2	71.9	25.1	24.8	1.3	0.6	4.8	20
NTA	247.0	72.7	25.4	24.9	1.4	1.0	6.1	23
NTA	248.0	73.5	25.2	24.8	1.2	0.8	5.4	18
NTA	249.2	74.3	25.2	24.8	1.6	1.0	5.7	21
NTA	249.8	75.2	25.8	24.9	1.3	1.4	10.0	20
NTA	250.9	75.5	25.3	24.4	1.3	0.5	5.7	21
NTA	252.0	76.2	24.6	24.4	2.0	2.3	1.2	19
NTA	253.0	78.1	26.0	24.8	1.8	1.2	3.7	15
NTA	253.8	77.9	25.6	24.2	1.1	1.0	3.2	10

Table 2 – J14 Clusters List — continued.

code	lsp	ra	de	vg	sdr	sdv	sig	ns
NTA	254.8	79.7	25.6	24.5	2.0	1.4	6.2	22
NTA	256.0	80.6	25.9	23.5	1.5	1.4	5.7	21
NTA	257.0	82.5	25.2	24.5	1.6	1.1	3.1	12
NTA	258.2	87.0	25.9	26.0	1.8	1.4	3.4	11
NTA	258.9	82.1	26.5	23.3	1.8	1.1	1.6	8
NTA	258.9	90.1	25.5	28.2	1.6	2.5	1.7	8
NTA	260.0	89.4	26.3	26.5	2.0	1.9	2.9	12
NTA	260.9	88.7	26.1	25.5	2.0	1.2	1.3	8
NTA	262.0	90.8	25.7	26.4	0.9	1.1	1.6	9
NTA	263.0	89.6	26.2	25.2	2.0	2.2	2.6	16
NTA	263.9	88.0	27.1	24.2	2.0	2.0	2.2	12
NTA	265.1	94.8	24.2	28.1	2.0	2.6	1.4	13
NTA	265.9	94.6	25.5	26.5	1.9	1.2	4.4	18
NTA	267.0	95.6	25.8	26.0	1.4	0.9	3.0	11
NTA	267.9	97.0	25.4	26.4	1.5	1.2	1.7	9
NTA	270.9	94.4	26.2	23.5	1.8	1.5	1.8	7
NTA	272.1	98.4	25.2	25.2	2.0	2.4	2.6	18
NTA	273.0	99.6	26.6	25.3	2.0	3.5	2.5	11
NTA	275.0	100.7	25.9	23.9	2.0	3.9	3.3	24
NTA	276.1	104.0	24.7	25.3	1.7	1.4	1.2	6
NUE	160.9	62.6	−2.0	66.4	1.2	0.9	1.5	4
NUE	163.0	64.2	0.0	65.9	2.0	0.9	2.1	6
NUE	164.7	66.3	−0.3	65.1	2.0	1.5	2.8	15
NUE	166.3	66.8	−0.1	65.6	2.0	1.9	4.0	22
NUE	167.0	67.5	0.4	65.9	2.0	2.1	4.1	19
NUE	168.0	69.0	0.8	65.8	2.0	1.8	4.4	31
NUE	169.1	69.3	1.0	66.4	1.7	1.2	3.8	13
NUE	171.1	71.2	1.2	66.2	2.0	1.1	2.6	13
NXE	241.9	65.2	−3.3	26.1	2.0	1.0	2.0	7
NXE	242.9	65.8	−4.0	25.6	2.0	0.8	3.0	7
OAG	207.0	70.8	35.9	56.7	0.9	0.5	2.2	4
OAG	207.6	71.4	36.1	57.8	0.3	0.0	1.0	2
OAG	209.1	71.8	33.3	54.4	0.8	0.9	2.2	3
OCP	190.9	45.7	69.0	48.8	2.0	2.2	2.6	9
OCT	192.6	168.8	78.5	45.5	0.4	0.9	10.0	22
OCU	201.3	144.3	64.7	55.3	1.4	0.8	3.4	7
OCU	202.0	144.0	64.5	55.6	1.2	0.9	10.0	28
OCU	202.8	146.8	64.5	55.3	1.5	0.8	10.0	22
OCU	204.1	148.3	63.2	55.7	1.8	1.4	2.9	9
OER	211.1	44.8	0.9	30.8	2.0	1.0	4.2	11
OER	212.8	45.1	1.4	29.7	2.0	2.2	2.5	8
OER	214.0	46.4	0.6	29.9	2.0	1.1	2.1	8
OER	216.0	48.3	0.6	30.7	1.5	1.1	2.6	6
OER	217.9	48.7	0.0	29.4	1.9	1.1	4.0	13
OER	218.9	51.4	0.3	29.8	1.9	0.9	2.2	7
OER	221.0	51.5	0.1	29.4	1.5	0.9	2.3	6
OER	222.1	52.3	2.2	29.4	1.6	0.5	0.2	4
OER	222.9	53.0	0.3	29.1	2.0	0.9	4.5	16
OER	224.0	54.0	0.1	28.9	1.5	0.8	1.4	5
OER	225.0	55.0	0.8	29.4	1.6	1.0	2.3	8
OER	225.8	53.2	0.1	27.7	1.3	0.9	1.8	4
OER	226.9	55.3	−0.9	27.7	2.0	1.6	3.7	10
OER	228.0	55.6	−0.5	27.6	2.0	1.4	3.7	10
OER	229.1	57.3	−0.7	27.6	2.0	1.3	2.5	10
OER	230.0	58.6	−1.2	28.1	2.0	1.1	3.7	9
OER	231.1	60.1	0.0	29.2	2.0	1.7	2.6	5
OER	232.1	58.8	−3.1	26.7	1.6	0.5	3.0	8
OER	233.0	59.9	−1.4	27.5	2.0	1.4	5.2	17
OER	234.0	61.1	−1.9	26.6	2.0	2.1	2.3	8
OER	237.1	62.7	−1.2	26.8	2.0	1.5	4.2	14
OHY	307.0	173.5	−33.3	58.4	1.8	0.8	2.7	7
OHY	307.9	175.3	−34.0	57.4	1.6	1.2	2.6	6
OHY	311.2	178.3	−33.8	59.4	1.7	1.3	2.7	7
OHY	312.1	178.8	−34.7	58.3	1.2	1.6	3.7	8
OMC	56.9	306.6	−32.4	64.6	1.0	1.0	2.2	4
OMC	58.0	306.5	−32.8	64.3	1.0	0.9	3.5	6
OMI	152.9	40.1	−5.8	62.1	1.0	1.2	2.7	7
OML	217.3	146.8	29.4	67.6	1.5	0.7	2.4	9
OML	221.0	150.7	30.8	67.4	2.0	1.2	2.5	8
ORI	195.0	88.9	12.5	67.9	1.6	0.8	1.8	12
ORI	196.1	87.1	13.9	67.2	2.0	1.4	4.6	20
ORI	197.0	86.8	14.8	66.5	1.6	1.5	2.9	13
ORI	198.2	89.0	14.5	68.2	2.0	1.4	2.7	13
ORI	199.0	88.9	15.2	66.9	2.0	1.2	6.2	25
ORI	200.0	90.0	15.0	66.6	1.7	0.9	10.0	39
ORI	201.0	90.1	15.0	66.7	1.6	1.3	10.0	51
ORI	201.9	90.6	15.4	66.7	1.2	0.9	10.0	56
ORI	202.9	90.8	15.5	66.5	1.2	1.3	10.0	66
ORI	204.0	92.0	15.5	66.4	1.0	1.0	10.0	141
ORI	205.0	92.8	15.3	66.4	1.0	1.2	10.0	207
ORI	206.1	93.7	15.4	66.4	1.0	1.4	10.0	268
ORI	207.0	94.6	15.5	66.3	0.9	1.5	10.0	732
ORI	207.9	95.2	15.6	66.3	0.9	1.1	10.0	864
ORI	208.9	95.8	15.7	66.3	0.9	1.2	10.0	417
ORI	210.0	96.6	15.7	66.0	0.9	1.5	10.0	231
ORI	211.0	97.4	15.8	66.0	0.9	1.2	10.0	431
ORI	211.9	98.0	15.9	65.8	1.0	1.2	10.0	373
ORI	213.0	98.8	15.9	65.9	1.0	1.1	10.0	295
ORI	214.0	99.6	15.9	65.9	1.0	1.2	10.0	250
ORI	214.9	100.4	15.9	65.7	1.1	1.0	10.0	225
ORI	216.0	101.3	16.0	65.7	1.2	1.3	10.0	80
ORI	217.1	102.2	15.9	65.4	1.3	1.2	10.0	96
ORI	217.9	103.2	15.9	65.6	1.4	1.2	10.0	98
ORI	218.9	103.8	15.9	65.3	1.2	1.0	10.0	67
ORI	219.8	104.4	16.0	65.2	1.1	1.4	10.0	39
ORI	221.0	105.7	15.7	65.5	1.5	1.0	10.0	44
ORI	222.0	106.4	16.2	65.0	1.4	1.4	10.0	55
ORI	222.9	106.7	15.7	64.8	1.2	2.0	10.0	48
ORI	223.9	108.4	15.7	65.4	1.8	1.5	10.0	31
ORI	225.0	110.6	15.1	65.7	2.0	1.1	8.3	29
ORI	228.0	113.4	15.7	65.2	2.0	1.6	3.7	23
PAN	72.1	355.3	46.5	50.9	1.1	0.1	2.6	5
PAU	131.2	351.0	−21.9	45.2	1.0	0.7	2.7	4
PAU	135.4	352.9	−20.2	44.2	0.9	1.3	2.7	4
PCE	158.1	6.0	−5.5	36.2	1.5	1.0	1.8	6
PCE	158.9	6.8	−5.2	37.0	0.9	0.7	2.2	5
PER	117.0	14.5	50.9	58.1	1.6	1.1	3.4	10
PER	118.2	16.1	51.9	58.0	1.6	1.3	3.7	10
PER	118.7	17.3	52.3	57.8	1.7	0.7	1.9	5
PER	121.2	21.1	53.8	57.8	2.0	1.5	5.2	17
PER	122.2	22.2	53.5	58.0	1.7	1.1	5.7	22
PER	123.1	23.5	54.2	57.8	2.0	1.6	8.8	22
PER	124.0	24.8	54.5	58.0	2.0	1.2	8.8	22
PER	125.2	26.6	54.2	58.9	1.2	0.8	4.7	17
PER	126.1	27.9	54.9	58.2	1.6	1.3	10.0	45
PER	127.0	29.6	55.1	58.2	1.8	1.6	10.0	42
PER	128.0	30.9	54.7	58.7	1.4	0.8	10.0	88
PER	128.9	32.2	55.2	58.6	1.6	1.3	10.0	126
PER	130.0	34.3	55.6	58.7	1.5	1.3	10.0	106
PER	131.0	35.6	55.8	58.8	1.7	1.2	10.0	191
PER	132.0	37.1	56.1	58.8	1.6	1.0	10.0	237
PER	132.9	38.3	56.4	58.8	1.6	1.4	10.0	244
PER	134.1	40.0	56.6	58.9	1.5	1.0	10.0	302
PER	135.0	41.5	56.8	58.9	1.6	1.0	10.0	367
PER	136.0	42.8	57.2	58.8	1.6	1.0	10.0	263
PER	137.0	44.1	57.4	58.9	1.6	1.1	10.0	465
PER	138.1	45.5	57.6	58.9	1.5	1.1	10.0	483
PER	139.1	46.6	57.8	59.0	1.3	1.3	10.0	896
PER	140.0	47.7	58.0	59.0	1.2	1.1	10.0	1819
PER	141.1	49.5	61.6	56.5	1.8	3.4	3.7	10
PER	141.0	49.8	58.2	59.0	1.3	1.0	10.0	988
PER	142.0	51.7	58.3	59.0	1.7	1.0	10.0	478
PER	143.0	54.1	58.6	58.9	1.7	0.9	10.0	175
PER	144.0	55.0	58.7	59.0	2.0	1.2	10.0	195
PER	144.9	56.2	58.6	59.0	2.0	1.4	10.0	118
PER	145.9	57.1	59.5	58.8	2.0	1.6	10.0	72
PER	146.9	59.3	59.1	59.2	2.0	1.4	10.0	56
PER	148.0	60.3	59.4	59.1	2.0	1.4	10.0	45
PER	149.2	59.7	59.6	59.0	1.0	1.0	3.9	15
PER	149.1	70.1	61.7	57.8	2.0	1.2	3.0	11
PER	149.9	64.7	60.3	58.3	2.0	1.7	10.0	28
PER	151.0	66.4	59.5	59.2	2.0	1.5	4.7	17

Table 2 – J14 Clusters List — continued.

code	lsp	ra	de	vg	sdr	sdv	sig	ns
PER	153.1	67.4	59.9	59.0	2.0	1.4	4.3	22
PER	155.8	70.1	59.8	59.7	1.4	1.0	2.3	8
PGE	275.2	129.9	23.0	40.5	1.6	1.8	1.7	5
PGE	275.9	126.6	25.4	39.6	2.0	1.7	2.2	7
PGE	277.1	132.4	23.8	41.2	1.0	1.0	2.6	5
PHC	188.8	121.7	29.9	66.1	0.8	0.3	1.8	4
PPS	92.0	8.6	20.0	66.9	1.4	0.5	4.0	9
PPS	92.9	8.0	22.6	66.4	1.7	1.9	3.7	9
PPS	93.8	10.2	20.8	66.6	1.8	0.5	3.0	7
PPS	95.2	11.8	23.6	66.1	2.0	0.7	2.9	9
PPS	96.3	11.2	21.5	66.4	0.9	0.1	2.2	3
PPS	96.9	11.9	23.1	66.2	1.6	0.7	3.2	10
PPS	98.0	13.5	22.4	67.7	1.4	0.2	2.2	3
PSO	161.2	74.3	−5.8	64.2	1.3	0.9	2.2	5
PSO	164.8	78.1	−2.9	65.3	1.5	0.9	1.7	5
PSR	25.0	242.3	13.6	45.4	2.0	1.7	5.3	12
PSR	25.8	244.1	13.5	46.4	2.0	0.8	5.0	11
PSU	251.0	167.3	44.5	61.5	1.0	0.6	3.4	10
PSU	252.0	169.3	44.0	61.4	1.3	0.8	5.2	16
PSU	253.1	169.8	43.6	60.2	1.4	1.6	3.1	9
PSU	253.8	170.9	43.1	61.4	0.6	0.9	2.7	4
PSU	255.9	172.1	41.3	61.5	1.7	1.1	3.0	11
PSU	257.1	175.1	40.7	61.9	1.6	0.6	4.3	10
PSU	260.0	165.3	43.3	60.2	2.0	1.5	2.8	11
PSU	260.8	167.9	43.0	60.3	0.8	0.8	3.0	7
QUA	280.0	222.4	53.3	40.3	2.0	1.5	4.1	19
QUA	281.0	226.0	51.8	40.7	2.0	2.2	10.0	37
QUA	282.2	229.4	49.2	40.6	2.0	1.2	10.0	50
QUA	283.1	229.8	49.7	40.3	1.6	0.9	10.0	868
QUA	283.7	230.9	49.7	40.2	1.4	1.3	10.0	119
QUA	285.0	229.9	50.7	39.9	2.0	2.6	10.0	40
QUA	286.0	229.7	50.4	40.0	1.9	1.2	10.0	31
QUA	287.0	232.3	49.6	39.8	2.0	1.6	5.6	31
QUA	287.8	232.1	48.9	40.7	1.9	2.2	3.5	17
QUA	288.8	235.0	50.5	38.3	2.0	1.0	4.0	14
ROR	183.9	84.0	3.7	65.7	1.2	0.9	1.6	6
RPU	221.3	119.6	−25.5	56.3	1.3	1.0	2.6	5
RPU	223.0	121.2	−23.5	58.2	1.6	0.9	2.2	5
RPU	223.8	122.5	−25.1	57.1	1.8	0.5	1.6	6
RPU	229.8	130.0	−26.5	57.5	1.4	0.8	3.0	6
RPU	231.0	131.6	−26.5	58.2	1.2	0.8	1.8	4
RPU	232.6	133.1	−26.4	58.1	1.2	0.8	3.5	6
SDA	118.9	332.6	−18.5	40.9	1.9	1.3	2.6	5
SDA	121.3	335.5	−16.8	41.3	1.0	0.5	3.5	6
SDA	122.0	335.8	−17.3	41.2	1.0	0.5	9.2	16
SDA	123.0	337.0	−17.1	41.2	1.0	0.8	10.0	38
SDA	124.1	337.7	−16.9	41.0	0.9	0.8	10.0	35
SDA	125.2	338.8	−16.8	40.7	0.9	0.9	10.0	50
SDA	126.0	339.5	−16.5	40.2	1.1	1.1	10.0	100
SDA	127.0	339.8	−16.3	40.3	0.9	0.8	10.0	82
SDA	127.9	340.6	−16.3	40.1	1.0	0.9	10.0	114
SDA	128.9	341.4	−16.0	39.9	1.1	0.9	10.0	108
SDA	129.9	342.1	−16.0	39.5	1.3	0.8	10.0	70
SDA	131.0	342.8	−15.7	39.6	1.2	0.8	10.0	75
SDA	131.9	343.6	−15.6	39.3	1.3	0.8	10.0	84
SDA	132.8	343.9	−15.4	38.8	1.2	0.8	10.0	43
SDA	134.1	345.4	−15.0	38.8	1.5	0.9	10.0	53
SDA	134.9	346.0	−14.7	38.4	2.0	1.1	10.0	27
SDA	136.1	347.2	−14.6	38.1	1.4	1.2	8.8	22
SDA	137.0	348.0	−14.6	37.9	2.0	1.3	5.4	19
SDA	138.1	349.0	−12.6	38.0	2.0	1.7	4.8	13
SDA	139.0	350.1	−13.7	38.0	2.0	1.6	5.2	20
SDA	140.0	350.6	−11.8	38.9	2.0	1.7	4.2	14
SDA	141.0	352.0	−12.3	38.6	2.0	1.7	2.9	9
SDA	142.1	353.6	−12.0	36.6	2.0	3.6	4.3	19
SDA	142.9	352.0	−14.3	36.9	1.6	0.6	1.3	3
SDA	144.0	354.2	−12.0	37.2	2.0	1.8	4.5	17
SDA	146.9	356.0	−10.8	37.4	2.0	2.1	4.5	15
SDA	148.9	357.2	−9.2	37.2	2.0	1.7	2.6	13
SDA	149.7	359.1	−7.3	38.6	1.5	2.0	1.5	4
SDA	150.8	360.0	−7.2	38.1	1.2	1.9	3.0	7
SDA	153.1	2.6	−7.0	36.0	2.0	3.8	2.6	9
SGC	202.7	131.7	32.1	67.7	2.0	1.0	2.6	12
SJA	114.9	36.8	10.1	68.9	1.1	0.4	3.1	5
SJA	118.0	39.0	10.6	68.2	1.2	0.9	3.1	5
SLD	221.1	160.0	68.9	48.7	1.2	1.0	3.0	7
SLD	221.9	161.0	67.7	49.0	1.0	0.7	4.6	11
SOV	311.1	199.4	−18.7	68.1	1.3	0.9	3.0	7
SOV	312.1	199.8	−18.6	68.0	1.2	0.6	2.4	9
SPE	163.2	42.8	39.4	64.5	0.8	1.4	2.2	5
SPE	164.0	44.0	39.5	63.9	0.8	1.0	10.0	20
SPE	165.0	45.3	39.6	64.1	0.8	1.1	10.0	19
SPE	166.1	46.5	39.6	64.3	0.7	1.1	10.0	54
SPE	167.1	47.5	39.4	64.3	0.6	1.0	10.0	69
SPE	167.9	48.4	39.4	64.2	1.1	1.2	10.0	27
SPE	169.1	50.7	39.9	64.2	1.0	0.8	5.4	14
SPE	171.0	52.5	40.1	64.0	1.6	0.8	4.0	12
SPE	173.0	54.1	39.9	64.3	1.0	0.3	3.0	7
SPE	173.7	55.8	39.4	64.5	1.4	1.3	3.1	9
SPE	174.9	59.0	39.3	65.5	2.0	1.0	2.8	12
SPE	175.7	59.2	39.6	65.9	2.0	1.2	1.9	9
SPE	177.2	60.9	39.8	65.4	1.9	0.9	1.4	5
SSA	204.1	48.8	23.7	42.9	0.9	2.0	2.7	4
SSX	269.0	152.3	-3.4	66.3	0.7	0.8	1.9	5
STA	182.0	20.1	4.1	30.0	2.0	2.1	1.7	9
STA	184.1	24.9	5.0	30.0	2.0	5.0	2.8	11
STA	184.9	21.6	4.8	29.1	1.8	2.0	2.7	7
STA	186.0	20.7	5.8	30.3	2.0	2.2	1.6	9
STA	188.1	24.1	6.1	28.6	1.7	1.5	3.2	10
STA	188.9	24.6	5.9	28.8	1.4	1.7	2.9	10
STA	189.9	30.5	8.2	28.9	1.6	2.6	1.9	5
STA	191.0	26.1	5.9	28.7	2.0	2.5	2.4	10
STA	192.0	28.2	7.7	29.9	2.0	2.2	4.2	12
STA	192.9	30.4	7.6	28.4	1.5	2.7	4.5	17
STA	193.9	30.7	7.8	29.5	2.0	2.2	10.0	33
STA	194.8	30.8	8.8	28.6	2.0	3.4	2.9	13
STA	196.0	31.8	8.4	28.8	1.7	1.6	10.0	28
STA	197.0	32.5	8.3	28.5	1.7	1.3	5.9	27
STA	198.2	34.6	9.1	28.7	1.7	1.7	10.0	27
STA	199.0	34.9	9.4	28.7	2.0	1.6	10.0	39
STA	200.0	35.6	9.4	28.4	1.5	1.2	10.0	47
STA	200.9	35.6	9.3	28.3	1.8	1.1	10.0	38
STA	202.1	37.0	9.9	28.8	1.5	2.2	10.0	45
STA	202.9	37.4	10.2	28.3	1.8	1.4	8.4	35
STA	204.0	37.8	10.0	27.9	2.0	1.5	10.0	40
STA	205.1	39.5	10.6	28.3	1.4	1.8	10.0	37
STA	206.1	39.8	10.7	28.0	1.7	1.9	10.0	33
STA	207.1	40.5	10.7	27.9	2.0	2.0	10.0	52
STA	207.9	41.2	11.2	27.9	1.6	1.8	10.0	40
STA	208.8	43.3	11.7	28.9	2.0	3.1	4.6	18
STA	210.0	42.6	11.4	28.4	1.2	2.2	3.8	13
STA	211.1	43.8	11.7	28.0	2.0	2.1	4.4	36
STA	212.0	45.3	12.6	28.7	2.0	2.2	10.0	58
STA	212.9	46.1	11.9	28.2	2.0	2.3	5.0	21
STA	214.0	46.3	12.5	27.7	1.5	1.5	6.6	30
STA	214.9	47.3	13.0	28.1	2.0	2.5	8.0	49
STA	216.1	48.5	13.2	28.5	2.0	1.8	5.7	45
STA	217.2	49.6	13.5	28.3	2.0	1.9	10.0	69
STA	217.9	50.1	13.6	28.2	1.5	1.6	10.0	79
STA	219.1	51.1	14.0	28.2	1.6	1.8	10.0	95
STA	219.8	51.7	14.1	28.4	1.2	1.3	10.0	56
STA	220.9	52.3	14.2	28.0	1.2	1.2	10.0	111
STA	221.9	53.0	14.3	27.9	1.2	1.1	10.0	122
STA	222.9	53.6	14.4	27.7	1.1	1.0	10.0	144
STA	223.9	54.2	14.4	27.4	1.3	1.4	10.0	66
STA	225.1	54.6	14.3	26.6	1.4	1.2	10.0	61
STA	225.9	54.7	14.2	26.3	1.6	1.3	10.0	33
STA	227.2	55.2	14.3	25.8	1.4	1.2	10.0	29
STA	228.0	56.4	14.7	26.1	1.2	1.1	10.0	57
STA	228.9	57.0	14.7	25.8	1.2	0.9	10.0	44
STA	230.1	57.8	14.9	25.6	1.2	0.7	10.0	36
STA	231.2	58.5	14.7	25.2	1.5	1.0	10.0	33

Table 2 – J14 Clusters List — continued.

code	lsp	ra	de	vg	sdr	sdv	sig	ns
STA	232.0	58.6	14.7	25.2	1.3	1.4	10.0	71
STA	232.9	58.8	14.7	24.5	1.3	0.9	10.0	62
STA	233.9	60.2	15.0	24.9	1.4	1.4	10.0	40
STA	235.0	60.0	14.6	23.8	1.5	0.9	10.0	26
STA	236.0	62.2	15.5	24.8	2.0	1.3	4.5	23
STA	237.1	68.6	17.0	28.4	1.1	0.8	2.3	8
STA	237.1	61.5	14.7	23.5	1.6	1.1	10.0	28
STA	238.0	63.1	15.5	24.0	1.6	1.0	10.0	40
STA	237.8	69.1	17.2	28.3	1.4	3.0	4.3	10
STA	238.9	63.2	15.1	23.3	2.0	1.2	10.0	34
STA	239.8	64.2	15.3	23.5	2.0	1.3	6.0	33
STA	239.9	71.7	18.7	29.0	2.0	1.8	1.7	8
STA	241.0	64.2	15.2	22.6	1.7	1.0	2.4	15
STA	241.1	71.3	17.4	27.4	1.3	1.0	3.7	11
STA	242.0	68.1	15.8	24.7	2.0	2.7	7.9	33
STA	243.0	66.3	14.8	22.8	2.0	1.2	6.3	35
STA	243.0	74.5	18.2	28.6	1.4	1.2	3.7	12
STA	243.8	65.7	14.2	22.0	1.8	1.0	2.3	12
STA	244.0	73.9	17.8	27.1	1.0	1.0	3.4	11
STA	244.9	67.8	15.6	22.7	2.0	2.2	3.3	28
STA	246.0	67.4	14.6	21.8	1.6	0.8	4.0	14
STA	246.1	76.2	18.2	27.5	1.1	0.7	3.2	11
STA	246.8	66.7	15.1	21.6	2.0	0.8	2.1	8
STA	247.2	77.0	18.3	27.1	1.3	1.2	5.4	19
STA	247.8	69.2	15.0	21.9	1.2	0.6	3.0	11
STA	248.0	77.1	17.9	26.2	1.5	1.2	4.9	16
STA	249.1	78.0	17.9	26.4	0.9	0.3	2.2	5
STA	249.0	70.2	14.9	21.6	1.4	0.8	3.8	14
STA	249.8	77.6	17.3	25.6	1.2	1.0	1.7	8
STA	250.9	79.7	18.3	26.4	1.0	0.8	3.1	14
STA	250.9	71.1	15.0	21.5	2.0	1.3	0.6	16
STA	252.0	73.3	15.1	21.6	2.0	1.3	2.3	18
STA	251.9	80.4	18.7	26.4	1.4	1.1	3.8	17
STA	252.9	80.4	17.9	26.0	1.4	0.6	6.8	18
STA	254.0	71.8	14.5	19.7	1.8	0.9	2.4	7
STA	254.1	82.0	18.1	26.0	1.3	0.7	3.7	12
STA	254.8	71.1	13.9	19.3	2.0	1.4	1.1	12
STA	254.8	82.6	17.8	25.9	1.9	1.1	5.4	30
STA	256.0	74.2	15.0	20.2	1.6	0.8	2.6	9
STA	256.2	84.4	18.0	26.1	1.0	0.7	4.0	13
STA	257.1	76.3	16.0	20.8	2.0	1.2	0.9	10
STA	256.8	84.8	18.0	25.1	0.8	2.7	3.7	11
STA	258.0	85.7	17.9	25.0	1.6	1.1	3.4	9
STA	258.8	84.4	17.9	24.9	2.0	1.5	1.3	13
STA	260.0	86.0	18.1	25.0	2.0	1.4	0.5	10
STA	260.9	85.8	17.7	24.2	2.0	1.5	2.5	8
STA	261.9	88.7	18.2	25.0	1.4	1.0	2.1	8
STA	264.0	92.4	18.1	26.3	2.0	2.4	2.9	12
STA	265.0	86.9	17.1	23.2	2.0	2.2	2.7	14
STA	266.1	84.6	15.6	20.8	2.0	2.2	1.7	11
STA	266.9	94.7	18.4	25.7	1.7	1.3	2.4	10
TCA	200.8	132.0	29.5	67.1	0.7	1.2	4.2	8
TCA	202.1	131.9	29.5	66.9	1.7	1.3	2.8	8
TCA	203.9	134.8	29.5	67.2	1.2	0.5	2.3	6
TCA	207.0	136.6	29.4	67.8	1.9	1.0	3.4	10
TCA	207.8	138.4	29.2	67.3	1.3	0.7	2.5	8
THC	132.0	19.2	−12.0	61.8	0.8	0.6	3.5	6
TLY	198.9	123.4	42.4	66.5	1.4	1.1	3.0	7
TOL	224.2	119.0	41.5	65.8	1.2	1.5	2.0	7
TPY	247.9	139.6	−25.8	59.0	2.0	0.6	1.7	9
TPY	249.0	138.2	−25.7	59.8	0.9	0.9	5.3	12
TPY	249.7	138.7	−26.0	60.1	1.0	1.3	3.3	8
TPY	250.8	140.1	−26.0	60.0	0.4	0.4	2.3	8
TSB	343.0	215.7	24.6	49.6	1.4	1.1	4.3	10
TTB	285.1	210.8	15.6	64.2	1.1	1.6	1.4	5
UAN	97.1	17.7	43.9	57.2	1.4	0.7	3.3	8
UMN	274.0	161.9	42.9	54.8	2.0	2.0	4.5	14
UPI	105.9	18.2	28.1	65.8	1.2	0.8	3.0	7
UPI	107.0	20.1	28.1	66.5	1.6	0.9	3.7	10
UPI	108.8	21.2	29.3	65.6	2.0	1.2	3.4	9
UPI	11.01	24.1	26.2	67.4	2.0	1.2	1.2	5
UPI	111.9	23.1	27.9	66.6	1.1	0.8	1.6	6
URS	264.0	211.2	79.0	32.8	2.0	1.3	2.4	7
URS	266.1	208.8	76.9	33.5	2.0	1.0	3.4	10
URS	269.0	214.4	75.4	33.7	1.5	0.7	3.7	9
URS	270.2	218.4	75.3	33.1	1.2	0.7	10.0	98
URS	270.7	219.3	75.4	33.0	1.0	0.7	10.0	100
UYL	167.9	110.0	55.5	58.9	2.0	1.1	4.8	13
UYL	170.2	113.5	55.1	59.3	1.7	0.7	3.0	6
UYL	171.0	115.6	56.3	58.4	1.4	1.3	3.1	5
XHE	351.1	254.4	48.6	34.5	1.1	0.4	2.3	6
XHE	351.9	253.5	48.9	35.8	1.6	2.7	4.2	8
XUM	298.1	169.1	33.0	41.0	1.0	0.6	4.5	12
XUM	299.0	169.7	32.5	41.0	1.4	0.9	10.0	30
XUM	299.8	170.6	32.8	40.6	1.2	0.8	4.2	8
XVI	253.0	184.6	−7.0	67.4	1.0	0.6	3.8	7
XVI	253.9	185.4	−7.6	68.0	0.4	0.8	3.1	5
XVI	254.9	185.9	−7.6	68.1	0.9	0.4	4.6	11
XVI	256.0	187.1	−7.8	68.1	1.0	0.8	10.0	20
XVI	257.1	187.2	−8.5	68.2	0.8	0.5	4.2	8
XVI	258.3	188.0	−8.7	68.3	0.4	0.9	4.2	8
XVI	259.1	188.7	−8.7	67.9	0.9	0.6	2.6	6
XVI	260.9	189.9	−10.2	67.9	1.2	1.0	10.0	17
XVI	262.0	190.8	−10.2	68.4	0.5	0.7	3.3	8
XVI	263.0	191.4	−10.1	69.0	0.9	2.0	4.9	12
XVI	264.0	191.9	−10.6	68.7	0.6	0.7	4.2	8
XVI	265.0	192.9	−11.3	67.7	0.8	1.4	4.5	9
XVI	265.9	193.5	−11.6	69.0	1.0	0.5	3.3	8
XVI	266.9	194.2	−11.6	68.7	0.8	1.3	4.9	12
XVI	268.1	194.6	−12.1	68.7	0.5	0.6	2.2	4
XVI	268.9	195.2	−13.0	68.2	0.9	1.7	4.0	10
XVI	270.1	196.9	−12.5	67.7	1.2	1.5	2.2	5
XVI	271.0	197.3	−13.4	68.2	1.3	1.1	3.4	7
ZCS	107.8	359.8	49.2	56.3	1.5	1.4	3.5	6
ZCS	111.0	3.3	50.8	56.5	1.0	0.6	3.5	6
ZCS	111.9	4.5	50.1	57.0	1.0	0.7	5.1	13
ZCS	113.1	6.5	50.3	57.7	1.1	0.8	5.8	15
ZCS	114.0	8.1	51.1	57	1.0	0.8	5.2	16
ZCS	115.0	9.7	51.6	57.4	1.3	0.7	4.6	11
ZCS	116.0	12.8	52.4	56.8	1.7	1.3	1.8	7

code: IAU MDC shower code
lsp: peak (or center) solar longitude (Ls) of the shower (or the cluster). Origin of dra, dde, dvg, degree, decimal
ra: right ascension of radiant, degree, decimal
de: declination of radiant, degree, decimal
vg: geocentric velocity, km/s, decimal
dra: ra component of 2 dimension moving vector of the radiant at Lsp, ra degree/day, decimal
dde: de component of 2 dimension moving vector of the radiant at Lsp, de degree/day, decimal
dvg: vg difference at lsp, km/s/day, decimal
sdr: standard deviation of the radiant direction distribution (1 sigma of cluster radius on the equatorial coordinate), degree, decimal
sdv: standard deviation of the geocentric velocity, km/s, decimal
sig: significance of the 3 sdr cluster against sporadic meteors, sigma, decimal (Peak cluster sig value for shower)
ns: number of the shower meteors in the period of ls1–ls2 (SNMv3Er1Ev5), integer

Table 4 – J14 shower catalog.

iauno	code	lsp	ls1	ls2	ra	de	vg	dra	ddec	dvg	sdr	sdv	sig	ip	ns
752	AAC	17.65	17.6	17.7	304.1	−12.5	69.2	0	0	0	0.7	0.6	4.8	29	10
429	ACB	308.07	307.5	312.5	231.7	27.5	57.9	1.12	−1.2	0.61	1.2	1.2	3	2.1	34
450	AED	17.94	17.5	22.4	305.3	11.1	60.9	1.03	0.55	−0.1	1.2	1	3.3	4.3	35
523	AGC	155.88	154.9	160.5	356	77.3	43.2	4.99	0.65	0.39	1.4	0.7	4.3	2.7	35
331	AHY	286.07	271.6	297.1	128.8	−8.3	43.1	0.71	−0.2	−0.2	1.6	1.2	5.7	2.2	301
505	AIC	154.07	154	154.1	1.1	−7.7	35.8	0	0	0	2	1.2	0.7	25	3
328	ALA	106.23	106.1	106.5	352	53.3	52.2	0	0	0	1.4	1.7	1.8	10	6
517	ALO	13.05	12.6	14.4	242.5	0.9	55.9	0.25	0.09	0.36	0.9	0.6	3.7	3.9	16
246	AMO	239.96	237.7	241.4	117.5	0.9	61.8	0.69	−0.1	−0.2	0.8	1.2	7.4	2	50
18	AND	232.21	231.8	232.5	23.1	33.6	16.6	0	0	0	0.6	0.1	2.7	0.8	5
466	AOC	135.15	134.7	135.4	26.7	0.5	66.7	0	0	0	1.7	0.9	1.7	1.1	6
1111	AQI	92.85	92.6	96.1	303.3	−7.8	39.7	0.65	0.22	0.2	1.4	1.8	3	6.7	22
171	ARI	77.18	70.7	83.9	43.7	24.2	40.6	0.72	0.21	0.27	1.4	0.6	2.7	2.1	29
206	AUR	158.17	155.6	160.4	90.7	39	65.9	0.92	−0.1	−0.2	0.9	1	4.5	3	31
21	AVB	28.98	21.5	32.5	201.4	3.8	18.6	0.63	−0.1	−0.4	1.3	0.6	3.8	3.1	56
900	BBO	292.02	291.6	292.4	227.9	44.9	47.6	0	0	0	1.6	0.9	1.8	2.8	9
342	BPI	138.18	128.6	158.9	344.8	1.1	39.6	0.82	0.38	−0.2	1.6	1.8	5.5	2.4	420
411	CAN	110.92	108.6	113.2	34.2	49.1	56.9	1.36	0.32	−0.4	1.6	1.2	3.7	4.9	31
1	CAP	128.87	113.7	135.4	307	−9	21.7	0.52	0.24	−0.2	1.2	0.7	10	7.4	552
20	COM	266.05	251.6	313.5	159.4	31.5	63.3	0.94	−0.4	0	1.2	1.1	10	3.8	1779
388	CTA	222.94	222.7	223.4	69.6	31.1	44.4	0	0	0	1.4	1.3	1.8	1	7
497	DAB	262.91	262.5	265.4	211.3	21.6	59.9	1.16	0.47	−0.3	1.1	0.8	4	0.7	24
334	DAD	254.89	254.5	279.3	209.2	58.4	40.9	1.75	−0.3	0	1.8	2.3	3	0.6	177
994	DBC	276	275.6	276.5	124.7	11	39.3	0	0	0	2	2.9	4.2	2.5	13
885	DEV	275.02	274.7	275.3	196.5	10.8	69.6	0	0	0	0.9	0.9	1.8	1.6	6
824	DEX	267.99	267.8	268.3	158.9	−4	68.5	0	0	0	1.4	1.6	2.9	3.5	14
498	DMH	264.09	261.7	270.4	151.9	−23.9	61.9	1	−0.2	0.05	1.4	1.7	3.3	0.6	84
563	DOU	268.9	268.5	270.5	158	42.9	56.4	1.91	−0.1	0.33	1.2	0.6	5.3	1.8	24
502	DRV	253.03	251.5	264.5	185.3	13.3	68.2	1.11	−0.1	0.03	1.3	1	4.2	0.5	115
221	DSX	188.83	188.8	190.1	158	−2.3	32.5	0.23	−1.2	−0.2	2	1.1	2.7	2.4	8
1120	DUM	267.95	267.8	272.4	219.1	84.3	29.6	−1.2	−0.4	0.06	1.8	0.8	3.3	1.8	54
530	ECV	300.84	300.5	301.2	190.4	−17.9	66.9	0	0	0	0.6	1	1.8	2.5	4
23	EGE	207.95	196.6	216.3	104.2	28.4	68.2	0.9	−0.2	−0.1	1.5	1.2	3.8	2.3	297
529	EHY	261.95	245.9	269.5	136.9	1.4	62.3	0.78	−0.2	−0.1	1.4	1.6	6.9	1.9	571
145	ELY	49.99	46.6	52.5	291	43.4	44.5	−0.5	0.37	−0.1	1.6	1	10	5.5	101
893	EOP	355.06	354.6	356.4	258.2	−16.1	70.8	0.87	−0.4	0.1	0.7	0.5	2.6	2	9
513	EPV	276.93	247.5	288.3	212.7	2.9	66.3	0.81	−0.2	0	1.3	1.1	5.2	1.1	446
191	ERI	134.23	122.5	148.4	40.5	−12.6	64.1	0.98	0.27	−0.1	1.6	1	5.6	1.9	318
1127	ESL	328.08	327.6	328.4	173.8	−4.4	40.4	0	0	0	1.5	2	2.6	5.4	9
31	ETA	45.06	33.8	65.5	337.5	−1.1	65.5	0.66	0.33	0.06	0.9	1	10	27	2054
746	EVE	253.12	246	257.5	132.5	−46.9	42.1	1.12	−0.2	0.18	2.5	1.4	10	0.9	90
11	EVI	356.92	353.7	2.5	186	3	27.9	0.88	−0.4	−0.1	1.6	1.4	3.7	8.7	156
548	FAQ	108.95	107.7	116.3	315.2	−4.2	38	0.95	0.38	0.02	1.7	1.7	2.6	4.2	55
1123	FFH	273.98	273.5	274.5	161.7	−26.3	63.7	0	0	0	2	1.1	3.7	2.6	13
1125	FFL	317.98	317.6	318.4	163	−0.3	40.3	0	0	0	2	1.9	4	4.3	12
1128	FTE	351.88	350.7	352.4	253.5	48.9	35.8	−1.2	0.38	1.76	1.4	1.6	4.2	3.3	17
531	GAQ	51.04	50.5	52.4	307.1	16.7	61.6	1.27	−1.5	1.61	1.3	0.9	3.4	3.2	16
4	GEM	262.02	246.7	265.4	113.5	32.3	33.6	1.02	−0.2	0.1	1.3	1.3	10	48	12764
139	GLI	35.95	35.6	36.5	224.7	−11.1	28.2	0	0	0	1	0.5	3	4.1	6
404	GUM	299	297.6	300.5	227.9	68.5	28.7	0.9	−0.8	0.28	1.3	0.7	5	2.8	29
1124	HTV	293.06	292.5	293.4	226.3	0.6	65.9	0	0	0	1.6	0.9	3	3.8	18
343	HVI	40.04	36.6	42.3	203.3	−11.6	18.1	0.35	−0.3	−0.3	0.8	0.5	5.7	3	45
16	HYD	254.9	241.7	282.5	124.1	2.8	58.7	0.81	−0.2	−0.1	1.4	1.2	10	6.9	2757
458	JEC	82.18	81.9	82.4	314.6	33.5	52.7	0	0	0	0.6	0.5	4	12	10
459	JEO	92.82	92.5	93.4	245.7	−8.1	13	0	0	0	0.8	0.3	3.5	6.8	7
431	JIP	93.77	93.5	95.3	331.5	29.3	58.6	1.2	0.21	0.36	0.6	0.7	4.5	7.6	13
319	JLE	281.82	279.2	286.7	147.2	24	52.5	0.71	−0.2	−0.4	1.5	0.5	4.2	0.5	26
175	JPE	108	106.6	118.4	347.5	10.6	64.2	0.8	0.27	0.04	1.1	0.8	5.7	5.5	99
510	JRC	84.18	83.9	85.5	320.6	43.9	49.9	0.87	0.7	0.16	0.9	0.7	3	7.7	12
829	JSP	108.82	108.5	109.2	354.3	9.5	65.8	0	0	0	0.6	1.6	2.2	3.1	4
344	JUG	125.17	123.7	126.2	280.3	50.3	27.4	0.9	−0.3	0.14	0.8	0.3	5.7	5.1	32
533	JXA	105.03	104.7	107.3	29.6	7.6	68.7	0.81	0.05	0.02	1.2	0.3	3	5.2	14
793	KCA	289.06	288.8	292.3	137.9	8.7	44.6	0.49	−0.6	−1	1.5	3.3	3	2.9	41
12	KCG	136.62	136.5	150.3	283.4	50.2	22.2	−0.7	0.88	−0.1	1.8	0.7	5.1	1.2	119
336	KDR	250.9	249.5	253.4	184.8	70.5	43.9	2.92	0.07	−0.1	1.8	1.6	10	4.8	161
445	KUM	222.92	221.5	228.2	144.3	45.7	65.1	1.25	−0.3	−0.1	0.9	1.1	10	2.4	107
1121	LAD	278.92	278.6	279.3	140.5	33.7	49.6	0	0	0	0.4	0.5	2.7	1.4	4
1119	LAV	259.11	257.8	259.4	133.4	−39.5	49.6	0.76	−1.3	−1.6	0.8	0.5	1.5	0.3	6
13	LEO	236.01	225.5	257.3	154.2	21.7	70.3	0.63	−0.4	0.04	1	1.1	10	8.4	1868
22	LMI	207.85	204.6	215.4	158.7	37.3	61.4	1.13	−0.3	−0.1	1	0.8	10	1.7	158
524	LUM	214.93	212.5	216.3	158.5	49.5	60.3	1.1	−0.6	−0.8	1.3	1.1	3.4	1.3	33
6	LYR	32.14	27.6	35.9	272	33.4	46.7	1.98	−0.3	0.57	1.5	1.2	10	36	607
520	MBC	54.1	53.7	54.4	301.6	−15.6	65.9	0	0	0	0.8	0.9	3.8	4.4	7
559	MCB	238.04	236.7	238.2	94	−20.7	44	−2.4	1.18	−1.5	1.6	0.9	2.7	0.8	10
1118	MLT	258.88	256.6	259.2	152.2	28.7	65.3	0.79	0.2	0.29	1.4	1.1	2.4	0.9	26
19	MON	256.98	247.6	272.4	99.7	8.3	41.4	0.66	−0.1	−0.2	1.1	0.9	10	2.8	875

Table 4 – J14 shower catalog — continued.

iauno	code	lsp	ls1	ls2	ra	de	vg	dra	ddec	dvg	sdr	sdv	sig	ip	ns
318	MVE	264.11	263.7	269.2	148.3	−37.7	54.4	1.88	−0.5	0.48	1.5	1.2	3	0.8	31
1117	NEV	245.9	245.6	246.5	179.8	−4.5	66.8	0	0	0	0.9	0.5	3.1	1	5
1116	NFL	247.07	246.6	248.2	179.8	13.4	68.2	0.29	0.04	−0.1	0.9	1.2	2.7	1	12
245	NHD	226.07	225.6	226.4	123.4	−4.3	65.3	0	0	0	1.7	0.4	1.8	3.1	11
581	NHE	35.76	34.7	36.2	263	37	40.7	2.95	−0.4	0.67	1.4	0.8	4.3	5.9	17
33	NIA	151.86	150.6	158.5	350.5	−2.5	31.9	0.72	0.79	−0.6	1.6	2.7	1	3.7	80
392	NID	222.97	222.6	223.4	191.9	69.2	42.1	0	0	0	2	1.7	2.2	1.7	12
250	NOO	247.91	228.6	260.5	91.4	15.3	42.4	0.7	−0.1	−0.1	1.5	1.9	10	4.1	999
215	NPI	182.12	181.8	184.4	12.7	9.2	28.1	−0.5	0.2	−1.3	1.6	2.3	1.8	4.5	31
488	NSU	241.02	240.6	243.2	147.5	59.8	55.3	1.19	−0.8	−0.2	1	0.9	3.4	2.1	31
17	NTA	232	199.7	276.4	60.4	23.1	27.4	0.84	0.17	−0.1	1.5	1.5	10	6	3880
337	NUE	168.02	160.5	171.5	69	0.8	65.8	0.88	0.36	0.1	1.9	1.4	4.4	7.4	223
1115	NXE	241.88	241.6	243.5	65.2	−3.3	26.1	0.56	−0.6	−0.4	1.6	0.7	2	1.7	18
818	OAG	207.02	206.6	209.4	70.8	35.9	56.7	0.42	−1	0.38	0.7	0.5	2.2	0.3	9
555	OCP	190.9	190.8	191.2	45.7	69	48.8	0	0	0	2	2.2	2.6	8.7	9
281	OCT	192.63	192.5	192.8	168.8	78.5	45.5	0	0	0	0.4	0.9	10	18	19
333	OCU	201.97	200.8	204.4	144	64.5	55.6	1.84	−0.5	0.07	1.5	0.9	10	4.7	77
338	OER	232.98	210.6	237.4	59.9	−1.4	27.5	0.79	−0.2	−0.2	1.8	1.2	5.2	1.7	317
569	OHY	312.06	306.5	312.4	178.8	−34.7	58.3	1.11	−0.3	−0.4	1.6	1.2	3.7	2.6	50
514	OMC	57.97	56.5	58.5	306.5	−32.8	64.3	−0.1	−0.4	−0.3	1	0.9	3.5	3.1	10
873	OMI	152.88	152.6	153.5	40.1	−5.8	62.1	0	0	0	1	1.2	2.7	2.7	9
481	OML	217.34	216.8	221.5	146.8	29.4	67.6	1.04	0.38	−0.1	1.5	0.7	2.4	2.5	80
8	ORI	207.94	194.8	228.5	95.2	15.6	66.3	0.74	0.05	−0.1	1.4	1.5	10	28	5991
860	PAN	72.08	71.7	72.4	355.3	46.5	50.9	0	0	0	1.1	0.1	2.6	3.7	5
183	PAU	135.4	131.1	135.5	352.9	−20.2	44.2	0.44	0.4	−0.2	0.9	1	2.7	0.5	14
642	PCE	158.09	157.9	159.4	6	−5.5	36.2	1.03	0.4	0.91	1.2	0.9	1.8	4.3	15
7	PER	140.03	116.7	156.4	47.7	58	59	1.69	0.14	−0.1	1.7	1.3	10	45	8836
728	PGE	275.9	274.9	277.4	126.6	25.4	39.6	5.12	−1.4	0.02	1.5	1.5	2.2	1.5	23
645	PHC	188.83	188.6	189	121.7	29.9	66.1	0	0	0	0.8	0.3	1.8	2.6	4
372	PPS	96.93	91.7	98.2	11.9	23.1	66.2	1.03	0.7	0.15	1.5	0.7	3.2	10	63
552	PSO	164.85	161	165.3	78.1	−2.9	65.3	1	0.79	0.3	1.4	0.9	1.7	3.3	29
839	PSR	24.98	24.7	26.2	242.3	13.6	45.4	2.27	−0.1	1.32	2	1.2	5.3	7.8	23
339	PSU	252.04	250.6	261.2	169.3	44	61.4	0.68	−0.6	−0.2	1.3	1	5.2	0.9	105
10	QUA	283.1	279.5	289.2	229.8	49.7	40.3	1.26	0	−0.2	1.8	1.7	10	24	1469
876	ROR	183.91	183.6	184.3	84	3.7	65.7	0	0	0	1.2	0.9	1.6	3.8	8
512	RPU	223.79	221.1	232.8	122.5	−25.1	57.1	1.41	−0.2	−0.1	1.4	0.8	1.6	0.8	42
5	SDA	127.93	118.7	153.5	340.6	−16.3	40.1	0.79	0.25	−0.2	1.5	1.3	10	7.3	1345
1114	SGC	202.7	202.5	203.3	131.7	32.1	67.7	0	0	0	2	1	2.6	5	17
1113	SJA	114.87	114.6	118.5	36.8	10.1	68.9	0.69	0.17	−0.3	1.1	0.6	3.1	2.1	15
526	SLD	221.95	220.8	222.4	161	67.7	49	0.97	−1.5	0.38	1.4	1.1	4.6	1.4	21
1126	SOV	312.07	310.7	312.3	199.8	−18.6	68	0.43	0.16	0	1.2	0.8	2.4	3.4	22
208	SPE	167.09	163.1	177.5	47.5	39.4	64.3	1.22	0.06	0.04	1.2	1	10	7.9	320
237	SSA	204.12	203.9	204.5	48.8	23.7	42.9	0	0	0	0.9	2	2.7	1	4
561	SSX	268.98	268.7	269.2	152.3	−3.4	66.3	0	0	0	0.7	0.8	1.9	1	5
2	STA	222.9	181.6	267.4	53.6	14.4	27.7	0.75	0.15	−0.1	1.6	1.5	10	6.8	4408
480	TCA	207.02	200.6	208.1	136.6	29.4	67.8	1.13	0	0	1.4	0.9	3.4	1.4	76
535	THC	131.96	131.8	132.2	19.2	−12	61.8	0	0	0	0.8	0.6	3.5	1.5	6
613	TLY	198.89	198.5	199.5	123.4	42.4	66.5	0	0	0	1.4	1.1	3	2.3	7
593	TOL	224.17	224	224.4	119.0	41.5	65.8	0	0	0	1.2	1.5	2	3.3	9
340	TPY	248.96	247.7	251.1	138.2	−25.7	59.8	1.02	−0.2	0.4	1.1	0.8	5.3	1.6	39
571	TSB	343.02	342.7	343.5	215.7	24.6	49.6	0	0	0	1.4	1.1	4.3	7.9	12
543	TTB	285.11	284.7	285.4	210.8	15.6	64.2	0	0	0	1.1	1.6	1.4	1.2	5
507	UAN	97.07	96.9	97.2	17.7	43.9	57.2	0	0	0	1.4	0.7	3.3	9.8	8
1122	UMN	273.97	273.5	274.4	161.9	42.9	54.8	0	0	0	2	2	4.5	3.3	15
1112	UPI	107.03	105.5	112.2	20.1	28.1	66.5	1.01	−0.4	0.08	1.6	1	3.7	8.7	76
15	URS	270.75	263.9	271.4	219.3	75.4	33	0.89	−0.5	−0.2	1.5	0.9	10	5.5	289
705	UYL	167.91	167.6	171.4	110.0	55.5	58.9	1.63	0.17	0	1.7	1	4.8	2.7	31
346	XHE	351.88	350.6	352.4	252.5	48.9	35.9	−1.2	0.38	1.76	1.4	1.6	4.2	3.3	17
341	XUM	299.02	297.7	300.5	169.7	32.5	41	0.8	−0.5	−0.2	1.2	0.7	10	5.3	53
335	XVI	255.97	252.6	271.2	187.1	−7.8	68.1	0.63	−0.4	0.05	0.8	1	10	0.7	177
444	ZCS	113.99	107.5	116.3	8.1	51.1	57	1.79	0.43	0	1.2	0.9	5.2	6.4	83

lsp: peak (or center) solar longitude (Ls) of the shower (or the cluster). Origin of dra, dde, dvg, degree, decimal
ls1: begin Ls, degree, decimal
ls2: end Ls, degree, decimal
ra: right ascension of radiant, degree, decimal
de: declination of radiant, degree, decimal
vg: geocentric velocity, km/s, decimal
dra: ra component of 2 dimension moving vector of the radiant at lsp, ra degree/day, decimal
dde: de component of 2 dimension moving vector of the radiant at lsp, de degree/day, decimal
dvg: vg difference at lsp, km/s/day, decimal
sdr: standard deviation of the radiant direction distribution (1 sigma of cluster radius on the equatorial coordinate), degree, decimal
sdv: standard deviation of the geocentric velocity, km/s, decimal
sdd: standard deviation of the DD', decimal
sig: significance of the 3 sdr cluster against sporadic meteors, sigma, decimal (Peak cluster sig value for shower)
ip: percentage of shower intensity, ns / all count on ls1–ls2, percentage, decimal
ns: number of the shower meteors in the period of ls1–ls2 (SNMv3Er1Ev5), integer

Orbital and physical properties of η-Virginids from the data of the European Fireball Network

Adam Brček[1], *Jiří Borovička*[2] *and Pavel Spurný*[2]

Meteor activity from February to April is low and the only major source of activity can be linked to the Virginid Meteor Complex. One of its well-known members are the η-Virginids (IAU #11 EVI) and the goal of this work is the study of this particular meteor shower. The detection of ten η-Virginid fireballs from the data of the European Fireball Network allowed us to specify the mean orbital elements and confirm the four year cycle of activity. Significant result of this work is the estimated bulk density for meteoroids, which suggests asteroidal origin of this meteor shower. One detected meteor also suggests the existence of a southern branch of η-Virginids.

Received 2021 August 19

1 Introduction

The η-Virginids (IAU #11 EVI) is a minor meteor shower with maximum activity around the solar longitude of 357° (Jenniskens et al., 2016). They belong to the Virginid Complex, the observations of which come from the 19$^{\text{th}}$ century (Denning, 1899). Jenniskens (2006) remarks that based on the data from Jacchia et al. (1967), Virginids penetrate deeper into the atmosphere than the majority of other showers and are in this way similar to Geminids. It is worth noting that Jacchia et al. (1967) measured only two Virginid meteors. Another observed feature of η-Virginids is their four year cycle of activity (Shiba, 2018). The shower's origin is not known, but Babadzhanov et al. (2015) hypothesized that its parent body is the asteroid 2007CA19 which may be an extinct or dormant Jupiter-family comet.

The main contribution of this work is the insight into physical properties of η-Virginids and the specification of their orbital elements. Data from the IAU Meteor Data Center were used to compare the mean orbital elements. The comparison includes the work of Jenniskens (2006), Lindblad (1971), Jenniskens et al. (2016), and also Shiba (2018).

2 Observational Data

The data was obtained from the European Fireball Network (EN), which consists of 20 stations (as of 2021) using all-sky photographic digital cameras (Spurný et al., 2017). The used data was gathered from 2016 to 2021. First, fireballs which could potentially belong to the Virginid Complex were selected. The period of interest was defined as a solar longitude interval ranging from 310° to 35° (J2000.0). The focus was put on ecliptic showers, therefore meteors with inclination i greater than 15° as well as those with semi-major axis a greater than 5 AU were not taken into account. Simultaneously, to focus on the constellation of Virgo and its surroundings, only geocentric radiants with right ascension α ranging from 80° to 250° and declination δ ranging from −30° to 50° were taken into account.

Applying the above-mentioned conditions led to 158 meteors for further research. The geocentric radiants and velocities were then manually compared and to determine the membership to a meteor shower, D_{SH} (Southworth & Hawkins, 1963) and D_D (Drummond, 1981) criteria were used. The requirement was D_{SH} less than 0.20 and D_D less than 0.10 for a given meteor.

3 Results

In total, there were 10 meteors that could be firmly associated with η-Virginids. All of them fulfill the requirement for D_{SH} and D_D criteria when compared to the mean orbit from Jenniskens et al. (2016). Solar longitude $\lambda_\odot$ of all meteors ranges from 345° to 3°. Positions of geocentric radiants are shown in Figure 1 and Figure 2. Mean orbital elements are given in Table 1, in which $\lambda_\odot$ is the solar longitude, α is the right ascension of geocentric radiant, δ is the declination, v_g is the geocentric velocity, a is the semi-major axis, e is the eccentricity, q is the perihelion distance, ω is the argument of perihelion, Ω is the longitude of ascending node, and i is the inclination of orbit in relation to the ecliptic plane. Computed values for all η-Virginid meteors are shown in Table 2 and Table 3. Drift of radiant position is very well defined (Figure 3 and Figure 4) and the use of linear regression leads to the following results

$$\alpha = 183.1 + 0.93(\lambda_\odot - 354.8),$$
$$\delta = 4.6 - 0.34(\lambda_\odot - 354.8).$$

For comparison, data from the CAMS database[a] were also added to Figure 2, Figure 3, and Figure 4.

Our results very well correspond with the data from Jenniskens et al. (2016). When comparing the mean orbital elements, both D_{SH} and D_D criteria yielded a value of 0.01. Somewhat worse correspondence was with the mean orbit from Shiba (2018). Noticeable discrepancy is especially in the declination of radiant and its drift. It is worth mentioning that Shiba (2018) presents the results divided into four phases based on the activity. The comparison was done with the phase corresponding to the maximum activity.

Despite the small data set, evidence of four year cycle of activity is also apparent. Half of all observed

[1]Charles University, Faculty of Mathematics and Physics, Ke Karlovu 3, CZ-12116 Praha 6, Czech Republic. Email: brcekadam@gmail.com

[2]Astronomical Institute of the Academy of Sciences, Fričova 298, CZ-25165 Ondřejov, Czech Republic. Email: jiri.borovicka@asu.cas.cz

IMO bibcode WGN-494-brcek-evi
NASA-ADS bibcode 2021JIMO...49...98B

[a]http://cams.seti.org

Table 1 – Mean geocentric radiants, velocity and orbital elements (J2000.0) for η-Virginids from the data of the European Fireball Network.

$\lambda_\odot$ [°]	α [°]	δ [°]	v_g [km.s^{-1}]	a [AU]	e	q [AU]	ω [°]	Ω [°]	i [°]
354.8	183.1	4.5	27.1	2.50	0.819	0.451	282.3	354.6	5.3

Table 2 – Geocentric radiants (J2000.0), velocities, and physical properties of all ten observed η-Virginids and two meteors possibly related to η-Virginids.

Code	$\lambda_\odot$ [°]	α [°]	δ [°]	v_g [km.s^{-1}]	Mag.	P_E	Type	m [kg]
EN060319_204604	345.727	176.24	6.98	27.67	−10.9	−4.24	I	7.1E-01
EN100321_191736	350.150	178.19	5.61	26.88	−4.5	−4.39	I	4.3E-03
EN120318_231735	352.079	179.73	6.35	26.46	−5.1	−4.53	I	2.4E-03
EN140317_194345	354.182	181.66	5.31	26.51	−5.8	−4.61	I/II	3.4E-03
EN140321_205321	354.209	179.98	6.43	25.17	−3.7	−4.56	I/II	1.3E-03
EN150321_011020	354.387	182.14	4.76	26.54	−6.7	−4.65	I/II	4.3E-03
EN150317_233402	355.337	186.58	2.25	29.40	−5.3	−4.50	I	2.8E-03
EN190320_201746	359.416	187.51	3.51	27.18	−3.8	−5.44	IIIA	4.3E-04
EN210321_003342	360.332	188.77	2.31	27.64	−9.1	−4.40	I	6.6E-02
EN230321_013723	362.361	190.27	1.45	27.33	−6.4	−4.38	I	1.5E-02
EN280219_020302	338.926	166.08	12.59	25.33	−1.6	−4.84	II	1.53E-04
EN140320_000751	353.603	177.11	−3.77	26.61	−2.5	−4.71	II	2.72E-04

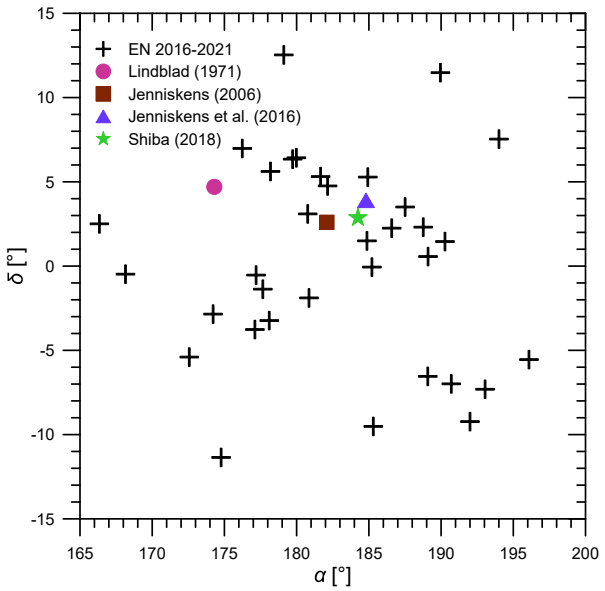

Figure 1 – Distribution of geocentric radiants near the cataloged radiants of η-Virginids for all measured meteors with solar longitude between 340° and 10°.

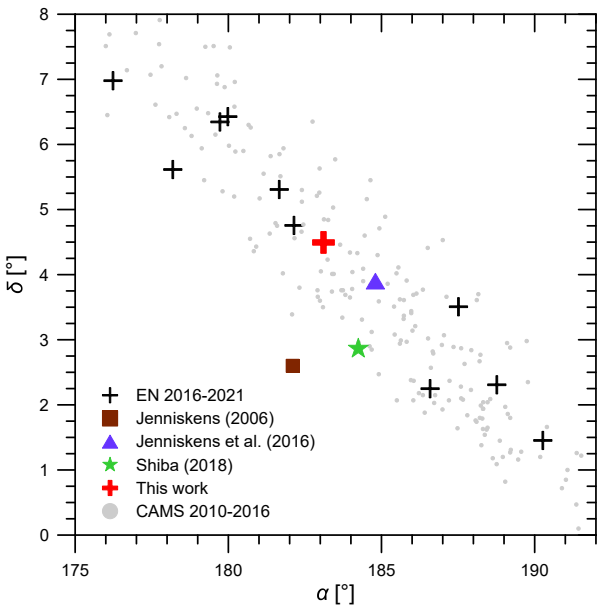

Figure 2 – Distribution of radiants for meteors belonging to η-Virginids. Individual radiants are plotted as black crosses and the mean radiant as red cross. Mean radiants from other sources and individual radiants from the CAMS system are given for comparison.

meteors were from 2021. To check whether this enhancement was not due to better weather conditions or overall increase of network efficiency in 2021, we counted the total number of meteors observed by the network in the η-Virginid activity period (March 5–25) in individual years and compared it to the number of η-Virginids. The total number of meteors in 2016–2021 was 18-35-24-26-62-49. The number of η-Virginids was 0-2-1-1-1-5, i.e. the percentage of η-Virginids was nearly four times larger in 2021 than in 2018–2020. Year 2021 should therefore be the year of maximum activity, which is in agreement with the results from Shiba (2018).

The P_E parameter (Ceplecha & McCrosky, 1976) was used to determine the physical properties of observed meteoroids. Nine out of ten meteors were classified as type I or I/II, which corresponds to compact material and of a high bulk density. One meteor was classified as a type IIIA, however it was a meteor with magnitude −3.5 and P_E parameter might not yield reliable classification for fainter meteors. The brightest meteor had a magnitude of −10.9 and its initial photometric mass was estimated to be 700 g.

Table 3 – Elements of heliocentric orbit (J2000.0) and values of D criteria (the criteria were calculated with respect to the author in the note, the author whose mean orbit yielded the lowest value of D criteria was chosen).

Code	a [AU]	e	q [AU]	ω [°]	Ω [°]	i [°]	D_{SH}	D_D	Note
EN060319_204604	2.356	0.821	0.421	286.10	345.72	5.17	0.08	0.05	J16
	±0.003	0.001	0.001	0.03		0.02			
EN100321_191736	2.498	0.818	0.456	281.72	350.15	4.36	0.07	0.02	J16
	±0.012	0.001	0.001	0.02		0.01			
EN120318_231735	2.514	0.812	0.473	279.78	352.08	5.44	0.07	0.03	J16
	±0.007	0.001	0.001	0.02		0.01			
EN140317_194345	2.507	0.812	0.470	280.13	354.18	5.30	0.04	0.02	J16
	±0.037	0.001	0.001	0.08		0.04			
EN140321_205321	2.462	0.792	0.511	275.67	354.21	5.16	0.11	0.06	J16
	±0.026	0.002	0.001	0.04		0.03			
EN150321_011020	2.439	0.810	0.464	281.07	354.39	5.04	0.02	0.01	J16
	±0.043	0.004	0.002	0.24		0.16			
EN150317_233402	2.532	0.851	0.378	290.40	355.34	5.49	0.13	0.10	Sh18
	±0.055	0.004	0.002	0.11		0.06			
EN190320_201746	2.564	0.823	0.454	281.86	359.42	6.19	0.04	0.02	Sh18
	±0.047	0.004	0.001	0.14		0.10			
EN210321_003342	2.578	0.830	0.438	283.59	360.33	5.77	0.08	0.04	Sh18
	±0.006	0.001	0.001	0.03		0.01			
EN230321_013723	2.532	0.824	0.445	283.03	360.37	5.48	0.07	0.03	Sh18
	±0.018	0.001	0.001	0.03		0.02			
EN280219_020302	2.491	0.796	0.507	275.75	338.92	5.39			
	±0.051	0.005	0.002	0.06		0.06			
EN140320_000751	2.533	0.815	0.468	100.32	173.60	4.44			
	±0.081	0.007	0.002	0.06		0.04			

Note: J16: Jenniskens et al. (2016), Sh18: Shiba (2018).

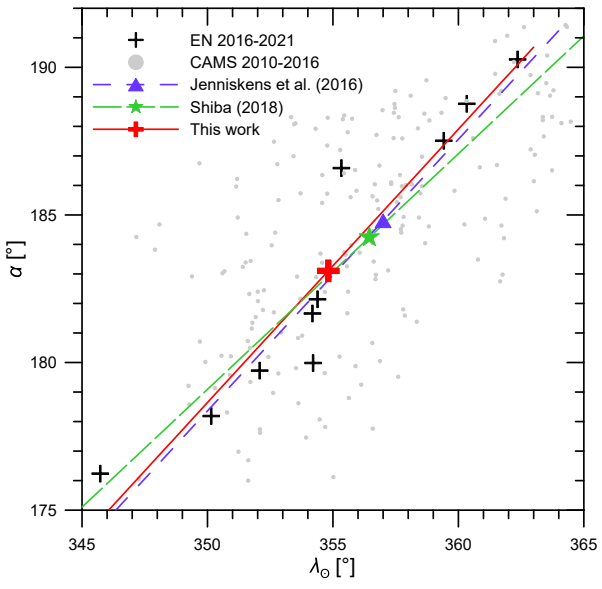

Figure 3 – Drift of right ascension with respect to solar longitude.

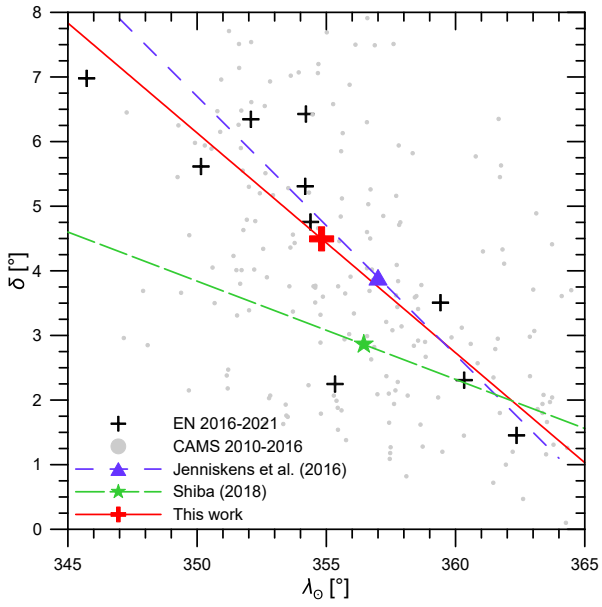

Figure 4 – Drift of declination with respect to solar longitude.

3.1 Fireballs possibly related to η-Virginids

Besides the ten above-mentioned fireballs, more potential η-Virginids were detected. Parameters of the two of them which are worth mentioning are shown at the bottom of Table 2 and Table 3. One fainter detected meteor (EN280219_020302) falls well within the expected trend, but was observed relatively early, indicating that the activity of η-Virginids might start sooner than expected.

Another interesting catch was a meteor labeled EN140320_000751 which seemed similar to other η-Virginids, but its argument of perihelion and longitude of ascending node were shifted by 180°. This result could suggest the presence of a southern branch of η-Virginids, although more data is needed. The possibility of its existence was even mentioned by Shiba (2018). This specific meteor also showed better correspondence with the object 2007CA19 (Babadzhanov et al., 2015) in terms of its orbit.

4 Discussion

Although the data set consists of only 10 meteors, thanks to the accuracy of measurements from the European Fireball Network, it is enough to reach results comparable to the results from the CAMS data, which consists of hundreds of meteors. η-Virginids are well-defined and all of the observed meteors should belong to this meteor shower. The results also indicate the four year cycle of activity with the year 2021 being a year of maximum activity.

The main results of this work are the physical properties of meteoroids forming the η-Virginids. Calculated P_E parameters suggest that meteoroids are composed of compact material. Most of the meteors were classified as type I, which gives an estimate to the bulk density of meteoroids. Type I corresponds with bulk density of around 3500 kg.m^{-3} (Ceplecha & McCrosky, 1976). This indicates that η-Virginids are more likely to be of asteroidal origin. Babadzhanov et al. (2015) links the η-Virginids with a cometary object, however, the results of this work exclude the possibility that the meteoroids are composed of soft cometary material. This is the case of not only small meteoroids, but also of the large ones with masses of hundreds of grams. Physical properties of η-Virginids are therefore very different from those of Taurids (Borovička & Spurný, 2020), even though the orbits of both showers are of similar type.

5 Conclusion

Data gathered from the European Fireball Network specifies the mean orbital elements and radiant position drift of η-Virginids, and also confirms their four year cycle of activity. The data also suggests high strength of material composing its meteoroids and rough estimate for bulk density is around 3500 kg.m^{-3}. Additionally, one detected meteor may indicate the presence of a southern branch of η-Virginids.

Acknowledgements

This work was supported by grant no. 19-26232X from the Czech Science Foundation.

References

Babadzhanov P. B., Kokhirova G. I., and Obrubov Y. V. (2015). "The potentially hazardous asteroid 2007CA19 as the parent of the η-Virginids meteoroid stream". *Astronomy and Astrophysics*, **579**, A119.

Borovička J. and Spurný P. (2020). "Physical properties of Taurid meteoroids of various sizes". *Planetary and Space Science*, **182**, 104849.

Ceplecha Z. and McCrosky R. E. (1976). "Fireball end heights: A diagnostic for the structure of meteoric material". *Journal of Geophysical Research*, **81:B35**, 6257–6275.

Denning W. F. (1899). "General Catalogue of the Radiant Points of Meteoric Showers and of Fireballs and Shooting Stars observed at more than one Station". *Memoirs of the Royal Astronomical Society*, **53**, 203.

Drummond J. D. (1981). "A test of comet and meteor shower associations". *Icarus*, **45:3**, 545–553.

Jacchia L., Verniani F., and Briggs R. E. (1967). "An Analysis of the Atmospheric Trajectories of 413 Precisely Reduced Photographic Meteors". *Smithsonian Contributions to Astrophysics*, **10**, 1–139.

Jenniskens P. (2006). *Meteor showers and their parent comets*. Cambridge University Press, Cambridge [u.a.].

Jenniskens P., Nénon Q., Albers J., Gural P. S., Haberman B., Holman D., Morales R., Grigsby B. J., Samuels D., and Johannink C. (2016). "The established meteor showers as observed by CAMS". *Icarus*, **266**, 331–354.

Lindblad B. A. (1971). "A computerized stream search among 2401 photographic meteor orbits.". *Smithsonian Contributions to Astrophysics*, **12**, 14–24.

Shiba Y. (2018). "Eta Virginids (EVI) four year cycle". *WGN, Journal of the International Meteor Organization*, **46:6**, 184–190.

Southworth R. B. and Hawkins G. S. (1963). "Statistics of meteor streams". *Smithsonian Contributions to Astrophysics*, **7**, 261–285.

Spurný P., Borovička J., Mucke H., and Svoreň J. (2017). "Discovery of a new branch of the Taurid meteoroid stream as a real source of potentially hazardous bodies". *Astronomy & Astrophysics*, **605**, A68.

Handling Editor: David Asher
This paper has been typeset from a LaTeX file prepared by the author.

Radio Meteors

A global network for radio meteors listeners

Lorenzo Barbieri[1] *and Gaetano Brando*[1]

In the amateur's activity, the radio meteors observation has been practiced by very few observers with different and not easy techniques. Starting from the experience of RAMBo, the authors have created a device based on SDR (Software Defined Radio) technology which, by analysing radio meteoric echoes, measures and records the main physical parameters of the radio meteors. The low cost and the construction and management simplicity make it suitable for the creation of a global network of receiving stations capable of producing coherent observational data useful for studying meteor showers.

Received 2021 July 19

1 Observational standards for meteors

Almost everything we know about meteors is due to centuries of visual observations.

If the ancient observational "reports" date back to the 3rd century BC, it is at the beginning of the 20th century that the observation techniques based on a standard were defined. That allows to overcome the individual observers subjectivity and therefore allows to put together a large amount of data from all over the world and recorded at different times.

The advent of cameras with wide-field optics that allows video observation has led to the definition of other observational techniques and standards, for example: Metrec, UFO, CAMS, standards compatible with each other.

The observation of meteors in the amateur radio field has instead been characterized so far by methods and techniques that are always different, depending on the skills or inclinations of the individual observers.

The project that we illustrate here has the ambition to start defining a hypothesis of a common technique and observational standard in this field as well.

2 The radio meteors

When a body (meteoroid or debris), after travelling for millennia in interplanetary space, enters the upper layers of the earth's atmosphere it impacts with the first molecules of the atmosphere it encounters along its path.

The speed of these particles moving within the solar system, with reference to the earth, is very high: from a minimum of 12 to a maximum of 72 kilometres per second.

It follows that, however small the mass of the meteoroid may be (usually a few grams), its kinetic energy, given by: $E_c = {}^1\!/_2 mv^2$ it is definitely high.

With the exception of the rare cases in which the meteoroid is of great mass, the impact after a very rapid increase in temperature usually involves its disintegration.

The effects of this process are the emission of light and the breaking of electrical ties in the atoms, a process that generates a free ions and electrons cylinder settled along the body path.

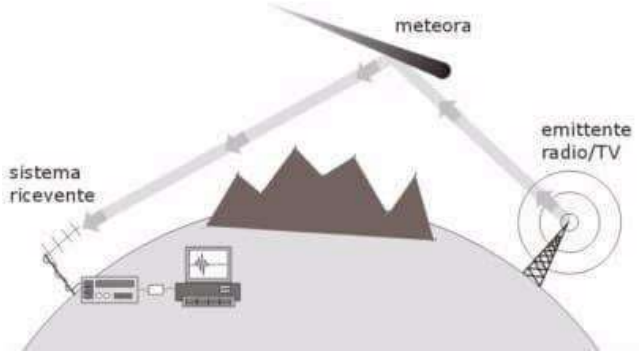

Figure 1 – Radio meteor.

The first phenomenon is commonly known like "meteor".

The cylinder of free ions and electrons can be more or less dense (depending on the kinetic energy of the impact) and more or less persistent, since ions and free electrons immediately tend to recombine.

When free electrons are hit by an oscillating electromagnetic field they are induced to oscillate with the same frequency. This movement in turn involves the re-emission of an electromagnetic field and if this movement is in phase for a large number of electrons there is a radio electric transmission that can be received from distance.

It therefore follows that if a cylinder of free electrons generated by a meteoric phenomenon is hit by a radio electric transmission it behaves (at least in a small part of it) as a reflector of this transmission; reflection that lasts until the moment of dissolution due to the ions and electrons recombination.

The minimum required linear density of a radio meteor is given by Belkovich (1971):

$$\alpha_0 = \frac{U_{eff}}{R_0}\sqrt{\frac{32\pi^2 d_0^3}{\lambda^3 R_i r_e^2 P_T G_T G_R}}$$

Where d is the distance, the parameters U, R, P and G refer to the technical characteristics of the transmitting and receiving equipments (maximum power, antenna gains, input impedance). It is important to note that the lambda wavelength is in the denominator and in the cube.

[1]Associazione Astrofili Bolognesi (AAB)

IMO bibcode WGN-494-barbieri-network
NASA-ADS bibcode 2021JIMO...49..102B

It follows that as the wavelength decreases, the minimum threshold of admissibility of a radio meteor rises making reception more difficult.

This point will be resumed later.

If a VHF transmitter is continuously in power and with an emission pointed upwards, a receiver tuned to the same frequency in a point of the territory not in optical view can receive the transmitted signal in those moments in which a meteor, generating the cylinder of free electrons, creates the reflection conditions.

When the reception of this signal takes place, we therefore speak of a "radio meteor".

As already mentioned, radio meteor is a reflection phenomenon of an electromagnetic signal, and therefore is subject to the physical laws that govern this phenomenon and in especially to the condition for which the incidence angle is equal to the reflection angle.

This consideration is quite interesting and has implications on which we will return at the end of this article.

3 Reception of radio meteors

Unlike meteors which are only nightly visible and whose observation is heavily influenced by lunar illumination, light pollution and weather conditions, radio meteors are continuously detectable. Their listening could only be disturbed by airplanes or satellites echoes or by sporadic E layer reflection.

Since the second post war period, meteoric radars have been built for radio meteors study.

Generally they are divided into two types: "forward scatter" and "back scatter" depending on the position of the receiver with respect to the aiming of the transmitter: in the first case the receiver is placed very far from the transmitter (hundreds of kilometres) and receives reflections generated more or less "halfway" between the two.

In the second case, the receiver is close to the transmitter and receives "backward" reflections.

Among the many examples of meteoric radars we can mention that of Vedrana di Budrio (Bologna) owned by the CNR in operation in the 1990s or, currently, the Canadian CMOR located in Ontario.

Meteoric radars are devices that include transmitters that emit pulse signals and a set of receivers equipped with directional antennas working as interferometers in order to reconstruct speed, position and direction of origin of the meteor.

Figure 2 – Graves.

These data allow to know the orbital parameters of the meteoroid and therefore to "assign" it to the swarm of origin.

Meteoric radars are therefore complex and very expensive devices intended for professional activity and are headed by research institutions or universities.

The amateur world (amateur astronomer and amateur radio) has approached this sector with various experiences, starting from the transmission of communications beyond the earth's curvature, based precisely on the moments in which a reflection induced by a radio meteor allowed it.

Obviously, no amateur can afford the purchase and operation of a powerful transmitting device, consequently amateur activity can only be done using other transmitters, like television transmitting devices, military radars, amateur radio beacons, etc.

Listening is normally done through a normal amateur radio receiver tuned in SSB mode (Single Side Band) about 1000 Herz away from the carrier of the broadcast signal.

This technique allows you to listen to an audio signal at the output of the receiver with a frequency equal to the difference between the received signal and the frequency tuned by the radio.

In the case of the aforementioned 1000 Herz, the audio output generated sounds like a whistle that emerges from the noise from time to time, whenever a radio meteor reflection is received. This whistle has intensity and duration proportional to the size of the free electrons cylinder, and to the ion-electron recombination process duration.

Sometimes dedicated softwares that graphically represent the audio signal creating the so-called "waterfall" are used, usually in false colours, a method that displays the amplitude, frequency and duration of the audio signal on a video monitor.

Amateur activity almost always ends here, with simple listening.

4 Counting and measuring radio meteors

Within the Associazione Astrofili Bolognesi we asked ourselves whether it was possible to go beyond just listening and making measurements capable of investigating the trend of meteor showers even at an amateur level.

Obviously the characteristics of amateur availability impose great limitations.

First of all, the absence of a pulsed signal transmitter prevents both the measurement of position and direction; in other words, even if there were several receivers arranged in various ways on the territory, and even if they could be connected, triangulation would not be possible.

Once the idea of knowing the orbital parameters of the individual meteors has faded, what remains possible is to know the instant of the event, the amplitude of the generated audio signal and the duration of the event of each radio meteor detected.

With these data, it is possible to point to the analysis of the hourly trend (Hourly Rate) and to an evaluation of the kinetic energy of the masses of the recorded meteors.

For this kind of observation it is therefore necessary to listen continuously, to digitize the signal and to record it in view of a physical and statistical analysis.

Given the need for continuous operation for the purposes of digitization and recording, we have discarded the use of personal computers by focusing on dedicated hardware.

5 The RAMBo experience

RAMBo (Radar Astrofilo Meteorico Bolognese) exploits the signal emitted by the military radar transmitter Graves placed in France which continuously transmits in the VHF band at very high power (the frequency is 143.05 MHz).

Its transmission is directed upwards and therefore, both for this reason and for the opposite shielding from the Alps, it is not listenable from Bologna directly.

Our receiver has a 10-element Yagi directive antenna (Figure 3) pointed in azimuth in the direction of the transmitter, and in declination at about 25 degrees, where we calculated to be the reflection point with the upper layers of the atmosphere.

The radio receiver we used is a Yaesu FT 857.

The receiver audio output is amplified with an operational circuit, divided into two outputs and one of the two is squared off to measure its frequency, while the other is detected for an amplitude measurement.

These two signals are sent to a microprocessor (Arduino) programmed by us.

With Arduino, frequency, duration and amplitude are measured, the instant of the event is established and the results are written in a log file consisting of a row of data for each meteoric event.

After a few months of experimentation, we were able to improve both the hardware and the software up to the complete elimination of the many "false positives"

Figure 3 – Vertically polarized Yagi antenna.

that an AM (amplitude modulation) reception normally entails.

For this purpose we used the microprocessor as a frequency meter: if several consecutive samples lie in a narrow window around the tuned frequency we can reasonably assume that it is a meteor.

If the frequencies of consecutive samplings are random, the echo is discarded.

The RAMBo experience was a positive experience: with it we have recorded and measured almost a million meteors every year from 2014 to today.

We have calculated the RZHR of many showers, we have recognized the filaments of some meteor showers, with its data we have taken part in two editions of IMC (the annual congress of the International Meteor Organization) and we wrote a couple of articles (Barbieri, 2016; Brando, 2016; Barbieri & Brando, 2019).

As evidence of the RAMBo potential, we mention the observation concerning the 2016 Perseid swarm: some days before the earth encounter with this well-known meteor shower an astronomical telegram (CBAT) signed by P. Jenniskens (2016), analysing the interactions of the swarm with the major planets, predicted the possible appearance of a filament a few hours before the

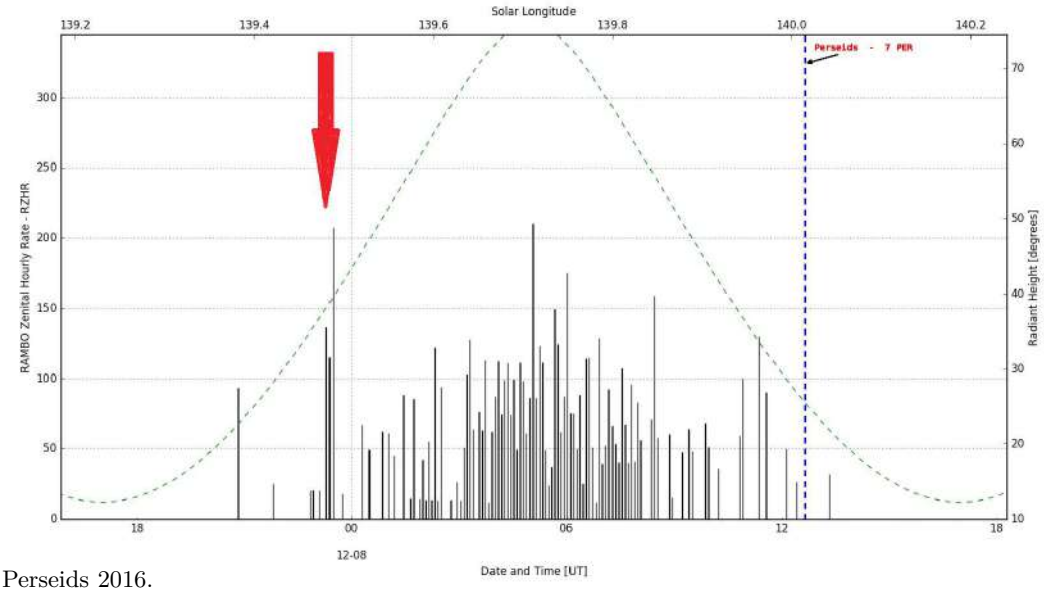

Figure 4 – Perseids 2016.

swarm peak activity around solar longitude 139.5: i.e. around midnight on 2016 August 11.

Indeed, as can be seen from the graph (Figure 4), the filament was detected by RAMBo at 23^h20^m UT on August 11. It should be noted that the duration is about three temporal samplings; since each sampling is 5 minutes long, the overall duration of this meteor shower filament was about 15 minutes.

From this data we can roughly extrapolate the dimensions of the filament: since the earth travels in interplanetary space at about 107 000 km/h, from the: $s = v/t$ we get that the diameter will be $\geq 27\,000$ km, depending on whether the earth has perfectly intersected it in the middle or more or less laterally.

The data collected over time are published dynamically on a page of the website of our Association[a] and archived weekly on `http://www.ramboms.com/`.

6 The limits of the RAMBo experience

Despite having given us various satisfactions, RAMBo has some limitations.

First of all, this experience is difficult to reproduce: the sound card is our prototype, its assembly and its use require electronics knowledge not common for all amateur astronomers. The same should be said for Arduino programming.

Another limit is that equipment isn't cheap: the radio we use is extremely expensive and other similar devices are even more expensive.

Third limit: the measurement is taken from an audio signal generated by the radio; it can be assumed that it could be roughly proportional to the actual radio electric power of the received signal, but we cannot be certain of this at all: if you want to think in terms of radar, you must directly measure the radio electric power received by the antenna.

For these reasons we have tried to develop a receiver that exceeds these three limits, and to do this we have faced the world of SDR.

7 What is SDR (Software Defined Radio)

Radio as we know it historically can be defined as a set of analogue components that each performs a certain function.

For example, if we think of the classical superheterodyne radio we find inside it: an input amplifier, a local oscillator, a mixer, a band filter, an intermediate frequency amplifier, a double half-wave rectifier and a detector.

All these functions, although performed by analogue devices, are actually mathematical functions: to remain with the functions listed above, they are multiplications, divisions, subtractions, generation of trigonometric functions, integrations, etc.

As we known, to multiply, subtract, divide, generate sinusoids or integrate and derivate, today it is much simpler and more efficient to use a computer rather an analogue circuitry.

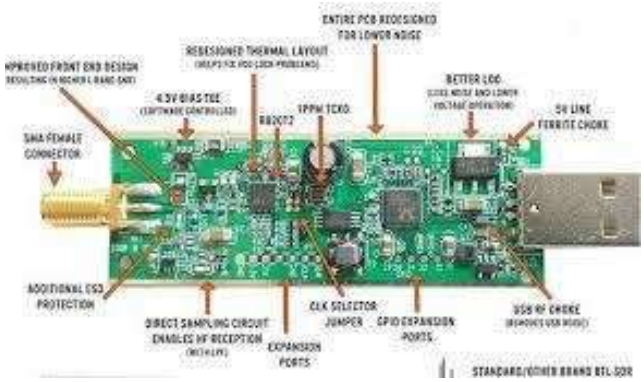

Figure 5 – Dongle.

The SDR (Software Defined Radio) in fact performs this function: once the antenna signal has been digitized, it is computer processed by using dedicated algorithms; in that way the PC works like a radio.

The first studies on SDR go back to 1970 in the USA and the first SDR transceiver was made in Germany in 1988.

Today the SDR devices are in every television, digital radios (DAB) and smartphones.

In the 2000s, the advent of the RTL2832U integrated circuit made it possible also for thousands of amateurs and enthusiasts to access the world of digital radio.

This chip is commonly implemented in the small circuit called "dongle" shown in Figure 5. The connector for the coaxial cable coming from the antenna is visible on one side and the USB connector for connecting to a computer on the other.

We have tried a few, what we though best is the NooElec NESDR Smart v4 SDR, it costs 32 euros, is stable, reliable and is the one with the lowest noise among those we tested.

With this very cheap device, any enthusiast can make a receiver using their personal computer.

8 Receive radio meteors with the SDR

Like all software-based businesses, not all industry development is industrial and patented, but there is an open-source niche (GNU Radio).

Using this environment, after more than a year of attempts we had not been able to build a project that met those characteristics we had in mind and this failure led us to give up.

The turning point that led to the resumption of the study and the realization of the project was the discovery of a Python programming language library specially written to drive the integrated circuits RTL2832U and R820T2, the heart of the "dongle".

We have therefore written a Python application that performs the work of tuning the dongle to the frequency of the transmitter chosen by the user, setting the gain, sampling the signal and performing the FFT (Fast Fourier Transform), thus obtaining the frequency and the amplitude of the received signal.

[a] `https://www.associazioneastrofilibolognesi.it/rambo/`

Figure 6 – CARMELO.

It should be emphasized that in this way we obtain the exact measurement not only of the frequency, but also of the signal radio electric power: unlike all previous experiences, based on the audio output listening, this configuration is actually comparable to a real radar.

Once these two quantities have been obtained, our application is able to recognize the meteoric echo by eliminating false positives both due to satellites or air planes and to weather transients such as lightning and to anthropogenic transients. The output file allows you to see the waveform of the recorded echo and the frequency of each individual sample.

After the first successes obtained using a personal computer, we tried to run this application on a small and cheap microcomputer like Raspberry.

The result was to double the execution speed, further improving the application performance.

We have thus created an extremely economical device, easy to assemble and manage: hence the name CARMELO (Cheap Amateur Radio Meteor Echoes LOgger) – see Figure 6.

CARMELO is extremely solid (after months and months of uninterrupted operation of three units there has never been an interruption or a break).

9 First results

The first months of operation showed us CARMELO's potential.

In the following waveforms you can see the time in the abscissa and the signal to noise ratio (SNR) in the ordinates.

Figure 7 shows a typical example of an "overdense" radio meteor, i.e., an event in which the cylinder of free electrons is sufficiently dense to behave like a solid body. Its reflection shows the very rapid rise, the flat saturation trend and the descent due to the dissolution given by the ion-free electron recombination.

Another type of meteor is the underdense, generated by an impact with lower kinetic energy and therefore characterized by a low-density reflecting cylinder (Figure 8).

Note that the difference between these two cases is not limited to the waveform and duration but the difference in amplitude is evident which in these cases is

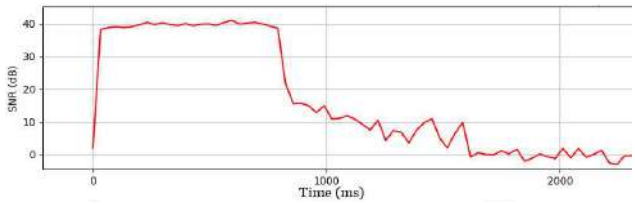

Figure 7 – Waveform of an overdense meteor.

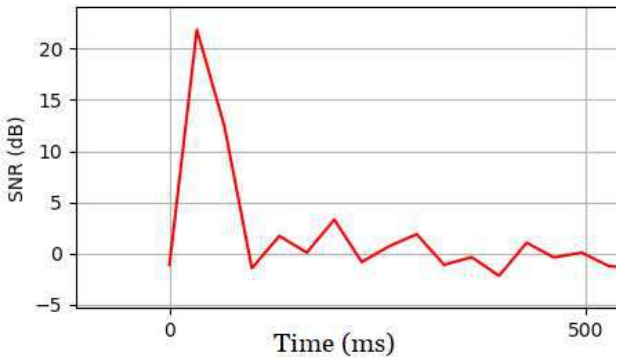

Figure 8 – Waveform of an underdense meteor.

20 dB, that is, about 100 times. The following image instead shows the summary of all the radio meteors recorded in a week; in the abscissa there is always the time, in the ordinate always the SNR while the dimensions of each single event are proportional to the duration.

In the week shown here (Figure 9), three receivers were operational, identifiable by the different symbols that distinguish them. This image is taken from the CARMELO web page.[b]

The page shows in real time the single recordings sent by each receiver in any position on the territory it is located. The only condition is that it is connected to the internet.

Positioning with the mouse on each event, you can read the data relating to each recorded radio meteor (date and time, location, amplitude and duration of the echo), clicking on each event displays its waveform.

Despite the small number of receivers built and put into operation so far, it is already possible to understand the potential of a reception made with a large number of receivers located throughout the area. To show this potential we have created the following graph (Figure 10) which shows the elaboration of the RHR (Radio Hourly Ratio) centred on autumn-winter 2020. The Geminids and the Quadrantids swarms are evident.

The three receivers used so far are tuned to the frequency of the military transmitter Graves, located near Dijon (France).

This transmitter has an advantage and at least two disadvantages:

- the advantage is that it transmits at very high power and this makes it suitable for use also by receivers located hundreds of km away;

[b] http://www.astrofiliabologna.it/graficocarmelo

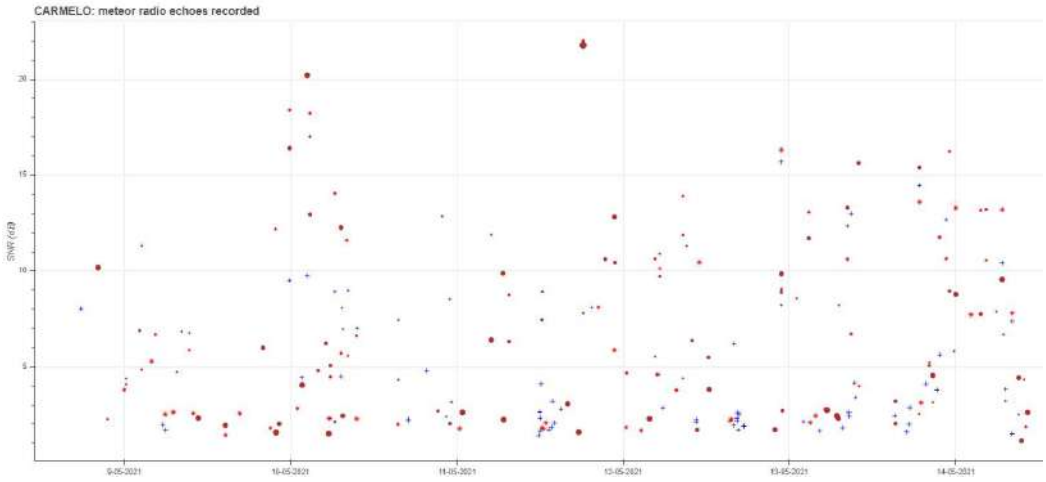

Figure 9 – Meteoric events in a week recorded by three CARMELOs. In the week shown here, three receivers were operational, identifiable by the different symbols that distinguish them.

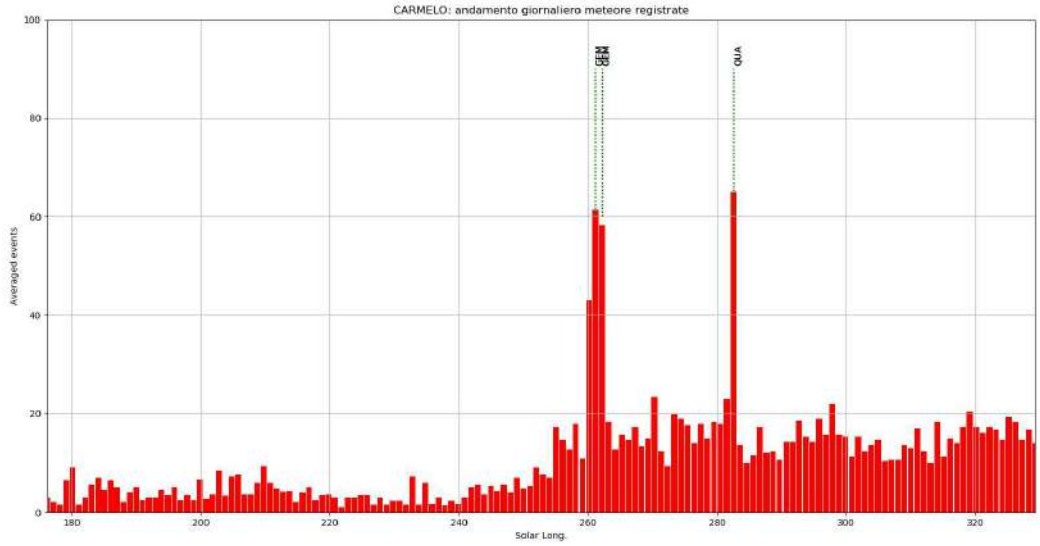

Figure 10 – RHR (Radio Hourly Rate) made with only three observers.

- the first disadvantage is that its frequency (143 MHz) is much higher than the optimal frequencies for receiving radio meteors (at least three times) and this decreases the efficiency of the system, as we have seen in the introduction
- the second significant disadvantage is the fact that, as a radar, its beam scans the sky with a fixed rhythm thus generating an alternation of moments in which the signal is listenable to others of total absence.

Emblematic of this situation is the waveform of a huge meteoric event (2021 April 2) whose duration exceeded half a minute (Figure 11).

During this event the periods of time in which the radio meteor is illuminated and those in which it is not are clearly visible.

As you can see, the transmitting radar sweep period is approximately 4.8 seconds.

This means that if a meteor falls in the period in which Graves does not illuminate that area, it could be lost; in addition, the waveforms we measure, the amplitudes we calculate and also the recorded durations are heavily influenced by the oscillatory behaviour of the transmission.

In this regard, there are two considerations to make.

The first is that only with a reception like that of CARMELO, that is given by the measurement of the radio electric power received and not by listening to the audio of the radio receiver, it was possible to realize this characteristic of Graves, years of experience with RAMBo had not given this perception which instead is so evident from the mere vision of a single waveform generated by CARMELO.

The second consideration is that a transmitter dedicated to the purpose of meteoric observation, also operating at lower power but with a suitable frequency and continuous emission, could lead to excellent results for hundreds of receiving stations. The electronics progress makes this idea much more affordable than in the past.

A next test could be the reception of the Belgian meteoric transmitter BRAMS (Belgian RAdio Meteor Stations) signal to be carried out in north-western Europe. BRAMS transmits at 49.97 MHz.

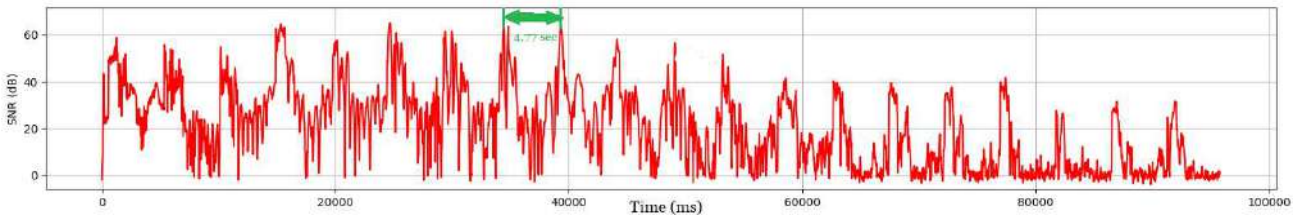

Figure 11 – Radio echo waveform of exceptional duration.

10 A global reception network with CARMELO

There are at least three considerations that lead us to suggest the creation of a receiving stations network based on standard reception and spread throughout the territory.

1. The sensitivity of an SDR dongle is lower than that of an amateur radio receiver. The data in our possession does not allow us to quantify this difference at the moment, but we can assume that it could be considerable.

   Furthermore, the sampling frequency carried out with the mini computer is not particularly high (one sampling every 33 ms), a time greater than the duration of the small underdense meteors.

   It is therefore obvious that we do not expect a quantity of received radio echoes equal to those recorded with the RAMBo experience (about one million radio meteors every year).

   If with RAMBo the underdense radio meteors (about 90%) were the majority, with CARMELO they are drastically reduced, while the overdense ones prevail.

   The result is a lower presence of sporadic meteors and a greater relief of those of greater mass and therefore presumably part of meteor showers.

   More receivers placed at different distances from the transmitter can guarantee better coverage and a high number of received echoes.

2. As already mentioned in the introduction, unlike meteors that can be seen from any position on the territory as long as the light emission is sufficient to be detected, the same condition does not apply to radio meteors.

   As a radio meteor is a phenomenon due to the reflection of an electromagnetic emission, **the principle that the reflected ray must have the same angle AR as the incident one AT applies to it** (Figure 12). It therefore follows that a radio meteor can be received only if the receiver is positioned on the territory in a place that complies with this condition; in another position the reception cannot take place.

   Consequently, receiver stations in different positions will "see" different radio meteors and therefore only a network of observers spread over large portions of space can aspire to receive a considerable share of the radio electric echoes that can be received on that territory.

   Another consideration could be added: the cylindrical shape of the reflecting object makes us hypothesize that the reflected signal with the angle equal to the incident is arranged on a plane.

   The line joining the points Tx and Rx on the earth's surface is orthogonal to the direction of origin of the meteor, that is to the direction of the radiant (Belkovich, 1971). If two receivers detect the same echo simultaneously, they would then identify this line. In this case, therefore, we would be in possession of important information because, knowing the position of the transmitter, we might be able to infer the trajectory of the meteor, a fundamental fact for the attribution to a meteor shower.

   Similarly, but in another way, Jean Marc Wislez (Wislez, 2006) describes the ellipsoid in which the transmitter and receiver are the foci and the meteor's trajectory is tangent at the point p.

   In the case of reception in two different points there will therefore be two ellipsoids intersecting with the point p in common.

   Sasa Nedeljkovic (2006) tackles the geometry of this particular case with the aim of identifying the generating trajectory of the meteor. These considerations make us assume that, with a large

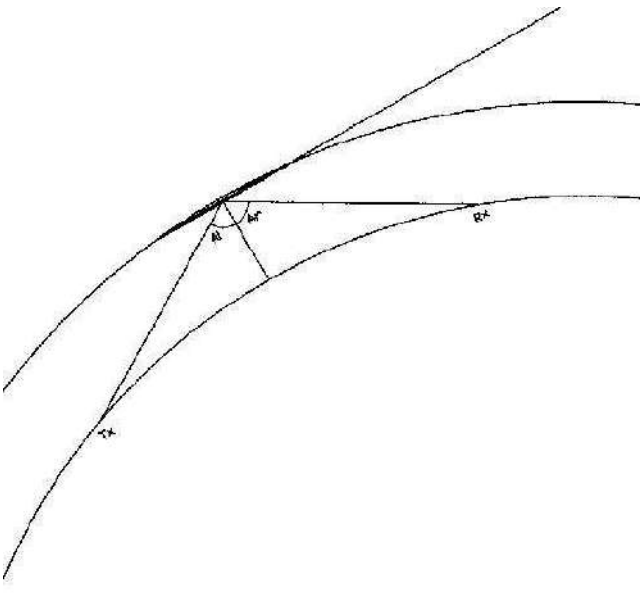

Figure 12 – Reflection geometry.

network of receiving stations scattered throughout the territory, the issue of identifying the trajectory of radio meteors that we had initially excluded from the potential of amateur reception will once again become an intriguing subject of investigation.

These considerations are true only if we consider that the shape of the meteor ionized cylinder does not change over time.

But the shape of the cylinder could be distorted by the high-altitude winds. This could create multiple echoes, consequently the same meteor could be seen by multiple receivers.

3. As mentioned in the introduction, the observation of radio meteors has an undeniable advantage: it is possible continuously regardless of weather conditions and light pollution.

   The only limitation, obviously as for all astronomical observations carried out from the ground, is given by the horizon: each observer can only see meteors or radio meteors whose radiant is above the horizon.

   It follows that some swarms are observable from one hemisphere and not the other or vice versa, but also that the same swarm has observability conditions that change, for a given receiving station, from year to year depending on the time in which they present their peak of activity.

   A global network of receiving stations all over the world that observes with the same standard and continuously, is able to overcome these limitations by ideally approximating the reality of a global terrestrial receiving station travelling in the interplanetary space with a 360 degrees field of view.

   For the three conditions listed above, a global network of receiving stations based on a common standard is therefore highly desirable. Using CARMELO, it is also easily achievable; the data produced today collected, processed and displayed by the site[c] are public and available to the observes community.

   Its eventual realization is based on the availability of individual amateurs, radio amateurs, educational institutions, research institutions or simple curious citizens to host a simple, economical, robust and reliable receiver.

11 What is needed to build a receiving station for radio meteors in the global network

1. First of all, it is necessary to identify a known transmitter that is in continuous operation on the VHF (Very Hight Frequency) radio band. This transmitter must emit on a known frequency and must be tens or hundreds of km away from the receiving station and possibly must not be in sight.

[c] http://www.astrofiliabologna.it/carmelo

Figure 13 – Collinear antenna.

2. It is therefore necessary to have an observation point as free from obstacles as possible.

   Obstacles are essentially manufactured or steep mountains in the immediate proximity that severely obscure the observation horizon.

   So, the best location can be the roof of a building, but it can also be a large garden if there are no buildings close to it. Conversely, the reception made on the lower floors of a high building will evidently lead to the renouncing of global coverage (360°).

3. The choice of the antenna and its correct installation should in no way be underestimated: this is where the effectiveness of the radio meteors detection is decided.

   There are two types of antennas: directional and omnidirectional ones.

   In the first category we mention the Yagi type antennas (see Figure 3), in the second the collinear ones (Figure 13).

   For those who are completely lacking in antennas we can say that if we listen with an omnidirectional antenna, it is as if we were looking at the starry sky with naked eye: we would see many stars in a very wide field of sky, while if we listen with a directional antenna it is as if we were looking at the sky with binoculars or a telescope: we would see a much smaller portion of the sky but we would also see fainter stars than those visible to the naked eye.

   Out of the metaphor: an omnidirectional antenna has a low and fixed gain, while a directive antenna has a higher gain but only towards a certain direction; it is the constructional characteristics of the directional antennas that determine the higher the gain and consequently the smaller the sky investigated area.

   Although most of the radio meteors observations are commonly made with directional antennas generally pointed in the direction of the transmitter and with a certain vertical inclination, we

Figure 14 – "Discone" antenna.

would like to suggest the vertically polarized omnidirectional antennas use for the following reasons.

- First of all, they are easier to assemble: less bulky and less critical in windy areas.
- Furthermore, omnidirectional listening, in the case of a network spread across the territory, allows a better comparison between individual receiving stations because it is independent of the gain in the antenna and gives more comparable results for any triangulation.
- A third reason lies in the cheapness of the antenna. The omnidirectional antennas available on the market can be of various types: ranging from "discone" antennas (Figure 14), whose price is around 80 euros, up to balcony antennas that cost less than 30 euro.

Self-construction should not be underestimated at all. The self-construction of a "ground plane" type antenna (Figure 15) has two advantages: first of all, it is very cheap, since it can be built with a few euros.

Then, it seems absurd but it is not: its efficiency is better than commercial ones.

The explanation of this apparent paradox lies in a simple consideration: commercial antennas are almost never designed to operate on a single frequency but are used to allow radio amateurs to receive (and transmit) on many channels.

An antenna is equivalent to an LC circuit whose electrical characteristics determine the frequency on which it resonates.

A "pure" LC circuit has a narrow and high Gaussian curve of the Q factor (similar to gain) on the central frequency (Figure 16).

A "loaded" LC circuit distributes the gain on a greater basis: the Gaussian is much wider, thus allowing us to tune effectively also on the adjacent frequencies, but also lower and therefore loses gain at the central frequency.

Figure 15 – Self-built ground plane antenna "Carmelina_143".

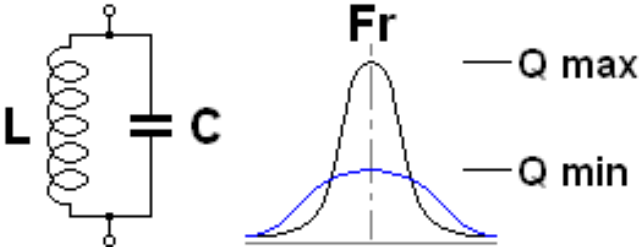

Figure 16 – LC circuit and merit factor (gain).

A final consideration: commercial antennas are also designed to transmit and this is the feature that most affects their price due to the necessary construction accuracy; for simple reception no sophisticated antennas are required. To confirm the aforementioned reasons, an homemade ground plane like the "Carmelina_143" proved to be more performing than all the other commercial omnidirectional systems we have tested.

4. Once the antenna is mounted, the coaxial cable that connects the receiver to it is required: it must be a normal coaxial cable rg 58 type or similar, suitable for VHF. The advice is to use a cable as short as possible, both to save money and to minimize losses and keep the signal to noise ratio (snr) as high as possible. The connectors at its ends must be: on one side a male "SMA" for connection to the dongle and on the other side the connector suitable for the chosen antenna; in most cases it is a male "pls". On the market and

Figure 17 – Testing of the self-built ground plane antenna.

on the internet they can be purchased, including adapter, for a few euros.

5. The dongle must be based on the integrated RTL2832U. We have tried a few, what we recommend is the NooElec NESDR Smart v4 SDR, it costs 32 euros, is stable, reliable and is the one with the lowest noise among those we tested.

   As mentioned, the minicomputer adopted is the famous Raspberry Pi 4 B, 2GB, it works fine: an SD card must be mounted on it: it does not matter that it is large: the software (operating system, program and libraries) takes up only 3 Gigabytes.

6. The minicomputer must be powered with a 5 V power supply with USB-C socket (i.e., that of second-generation smartphones). CARMELO absorbs about 75 milliamps which at 5 V means a power of less than 400 mW. A consumption equal to that of some small LED flash light.

7. Then, you need a LAN network cable that connects the microcomputer with a modem that allows access to the Internet. This cable can also be particularly long, indeed the advice we give is to place CARMELO as close as possible to the antenna and to reach the modem with a network cable of the required length.

   We have not enabled the wireless function on the Raspberry: after all, CARMELO is still a radio receiver and the fewer transmissions there are in the immediate vicinity, the better.

The total of these purchases is less than 200 euros.

12 The software

As seen, the hardware is simple, cheap and common: what transforms this hardware into a real miniature meteoric radar is the software.

What CARMELO needs to work are:

1. the installation of the operating system: the simpler and lighter version of Raspbian is fine.
2. The Python libraries and our program, obviously free.
3. A very small csv type file in which the receiver radio station data are written: location, geographic coordinates, frequency on which the receiver works, the type of antenna used, the symbol and the colour with which the sent observations will appear in the representation overall data received by the system and visible on the appropriate page of the website.

All this will be available writing an email to: `rambometeorgroup@gmail.com`.

References

Barbieri L. (2016). "An antenna, a radio and a microprocessor: which kinds of observation are possible in meteor radio astronomy?". In Roggemans A. and Roggemans P., editors, *International Meteor Conference Egmond, the Netherlands, 2-5 June 2016*. pages 26–30.

Barbieri L. and Brando G. (2019). "Concerning the height of meteors". *WGN, Journal of the IMO*, **47:4**, 108–115.

Belkovich O. I. (1971). *Statistical theory of meteor radar observation*. Kazan University, Russia. (in Russian).

Brando G. (2016). "The 2016 Quadrantids". In Roggemans A. and Roggemans P., editors, *International Meteor Conference Egmond, the Netherlands, 2-5 June 2016*. pages 39–41.

Jenniskens P. (2016). "2016 Perseid meteors". *CBET*, **4293**.

Nedeljkovic S. (2006). "Meteor forward scattering at multiple frequencies". In Verbeeck C. and Wislez J.-M., editors, *Proceedings of the Radio Meteor School, Oostmalle, Belgium, 10-14 September 2005*. International Meteor Organization, pages 108–118.

Wislez J. M. (2006). "Meteor astronomy using a forward scatter set up". In Verbeeck C. and Wislez J.-M., editors, *Proceedings of the Radio Meteor School, Oostmalle, Belgium, 10-14 September 2005*. International Meteor Organization, pages 85–107.

Handling Editor: Jean-Louis Rault

The International Meteor Organization

www.imo.net

Follow us on Facebook
InternationalMeteorOrganization

Follow us on Twitter
@IMOMeteors

Council

President: Cis Verbeeck,
Bogaertsheide 5, 2560 Kessel, Belgium.
e-mail: cis.verbeeck@scarlet.be

Vice-President: Juraj Tóth,
Fac. Math., Phys. & Inf., Comenius Univ.,
Mlynska dolina, 84248 Bratislava, Slovakia.
e-mail: toth@fmph.uniba.sk

Secretary-General: Robert Lunsford,
14884 Quail Valley Way, El Cajon,
CA 92021-2227, USA. tel. +1 619 755 7791
e-mail: lunro.imo.usa@cox.net

Treasurer: Marc Gyssens, Heerbaan 74,
B-2530 Boechout, Belgium.
e-mail: marc.gyssens@uhasselt.be
BIC: GEBABEBB
IBAN: BE30 0014 7327 5911
Bank transfer costs are always at your expense.

Other Council members:
Javor Kac (see details under WGN)
Detlef Koschny, Zeestraat 46,
NL-2211 XH Noordwijkerhout, Netherlands.
e-mail: detlef.koschny@esa.int
Sirko Molau, Abenstalstraße 13b, D-84072
Seysdorf, Germany. e-mail: sirko@molau.de
Francisco Ocaña Gonzalez, C/ Arquitectura, 7.
28005 Madrid, Spain.
e-mail: francisco.ocana.gonzalez@gmail.com
Vincent Perlerin, 16, rue Georges Bernanos,
51100 Reims, France.
e-mail: vperlerin@gmail.com
Jürgen Rendtel, Eschenweg 16, D-14476
Marquardt, Germany. e-mail: jrendtel@aip.de

Commission Directors

Visual Commission: Jürgen Rendtel
Generic e-mail address: visual@imo.net
Electronic visual report form:
http://www.imo.net/visual/report/electronic
Video Commission: Sirko Molau (video@imo.net)
Photographic Commission: Bill Ward
(bill_meteor@yahoo.com)
Generic e-mail address: photo@imo.net
Radio Commission: Chris Steyaert
(radio@imo.net)
Fireballs: Online fireball reports:
http://fireballs.imo.net

Webmaster

Karl Antier, e-mail: webmaster@imo.net

WGN

Editor-in-chief: Javor Kac
Na Ajdov hrib 24, SI-2310 Slovenska Bistrica,
Slovenia. e-mail: wgn@imo.net;
include METEOR in the e-mail subject line

Editorial board: Ž. Andreić, M. Argo, D.J. Asher,
F. Bettonvil, J. Correira, M. Gyssens,
C. Hergenrother, T. Heywood, J.-L. Rault,
J. Rendtel, C. Verbeeck, S. de Vet, D. Vida.

IMO Sales

Available from the Treasurer or the Electronic Shop on the IMO Website	€	$
IMO membership, including subscription to WGN Vol. 49 (2021)		
Surface mail	26	32
Air Mail (outside Europe only)	49	60
Electronic subscription only	21	25
Proceedings of the International Meteor Conference on paper		
1990, 1991, 1993, 1995, 1996, 1999, 2000, 2002, 2003, per year	9	12
2007, 2010, 2011, per year	15	20
2012, 2013, 2014, 2015 per year	25	34
Proceedings of the Meteor Orbit Determination Workshop 2006	15	20
Radio Meteor School Proceedings 2005	15	20
Handbook for Meteor Observers	15	20
Meteor Shower Workbook	12	16
Electronic media		
Meteor Beliefs Project ZIP archive	6	8

2021 Perseids from Canada

Composite image of 282 Perseids captured between $06^{h}50^{m}$ UT (02:50am EDT) and $09^{h}00^{m}$ UT (05:00am EDT) on the night of 2021 August 13/14. The equipment and image details: Canon 6D at ISO 6400, 20 s exposures, Rokinon 14 mm $f/2.8$ lens. Setup was mounted on tripod unguided. 364 continuous exposures were made of which 282 meteors were found, and digitally combined into this image (a few additional Perseids were found but are not included here due to sky rotation). Sporadics and other minor shower meteors are not included. Photographed near Westmeath, Ontario, Canada.
Image courtesy: Pierre Martin.